University of California, Irvine

Targeted Therapies and Associated Biomarkers in Human Cancers

DISSERTATION

Submitted in partial satisfaction of the requirements for the degree of

DOCTOR OF PHILOSOPHY

In Cellular & Molecular Biosciences – Cancer and Cell Biology focus area

by

Luke Nelson

Dissertation Committee:
Professor Olga Razorenova, Chair
Professor David Fruman
Professor Marian Waterman

2019

DEDICATION

This dissertation is dedicated to:

My family, for believing in me and supporting me all these years.

Mom, Dad, Kyle, Angela, Chris, Jessica, and Izzy.

Table of Contents

List of Figures

List of Supplemental Figures and Tables

Acknowledgements

I would like to take this opportunity to thank all the truly wonderful individuals who have helped me along the way through graduate school. It's safe to say that without such loving and supportive people in my life I would have never made it to this point. First and foremost, I want to thank my family. My parents have been the staunchest supporters of my difficult decision to abandon a comfortable 9 to 5 job and head back to grad school. My father, Norman Nelson, is truly an inspiration to me. He is one of the kindest, most genuine, and hardest working people you will ever meet. He taught me that to have success you must be willing to work hard and make sacrifices, but that your life is defined by who you are as a person and how you treat others, rather than your professional success. My mother, Marion Nelson, has been my biggest fan ever since I was a kid and that continues to this day. She's also the smartest person I know and has advised me about so many things throughout the years. I love you both.

I have had the pleasure of working in the lab of Dr. Olga Razorenova. I'm very grateful to Olga for letting me work with her and putting up with all my shortcomings along the way. I'm sure it took a lot of patience to deal with me, especially in the early years when none of the experiments were going as planned! To my lab mates Jordan Thompson and Heather Wright: you are both brilliant scientists, and I am very proud to have worked with you. You deserve all the success that you have achieved, and I wish you even better things in the future. Itsugo "Kevin" Yamayoshi, thanks for bringing some fresh life to the lab, for sharing my love of childish humor, and forcing me to go out and get some exercise instead of staying hunched over my computer every now and then. Binzhi Xu, you have

grown so much as a person and a scientist since you joined the lab. I look forward to seeing you progress even further in the coming years.

I'd like to thank my thesis committee for their continued support throughout the years. Not only are they all terrific and respected scientists, but they are humble, kind and genuinely good people. Dr. David Fruman has a keen scientific mind and always offers great suggestions for experiments. He also advised me whenever I needed it and offered encouragement along the way. Dr. Marian Waterman was always willing to take time out of her insanely busy schedule to chat with me or offer scientific advice or guidance, and for that I am truly grateful.

I had a great experience mentoring and working with many undergraduate students at UCI. Mariel Ma, who has an even weirder sense of humor than me, was truly a joy to work with and reminded me that a failed experiment is not a matter of life and death. I'm excited for your future in medicine and know that you have many great things ahead. Junyi "Chris" Li: your work ethic was incredible and I'm sure that you will take that same drive with you to succeed in grad school. Nguyen Dinh, who was a meticulously organized and hard worker, worked with me when nothing was going according to plan, but kept with it and ultimately made a great contribution to both of my projects.

Finally, I am very grateful to the Institute for Clinical and Translational Sciences at UC Irvine for providing me with funding to support my thesis work and allowing me to be a part of the TL-1 training fellowship for 3 years (Grant UL1 TR001414), through which I received excellent mentorship and extensive scientific training.

Curriculum Vitae

Luke Nelson

EDUCATION **B.S. in Biochemistry**, 2007
Minor in Human Biology
University of California, San Diego

CURRENT POSITION **Dissertation Research**
PhD, expected 2019
UC Irvine, Department of Molecular Biology & Biochemistry
Advisor: Olga Razorenova, PhD

Investigating the use of novel targeted therapies in clear cell renal cell carcinoma (CC-RCC) using patient-derived xenograft tumors in an orthotopic mouse model. Evaluating physiologically relevant PDX culturing and drug screening platforms to better mimic the tumor microenvironment and achieve more robust, reproducible results *in vitro*. Utilizing cell surface markers and RNA sequencing to identify cancer stem cell populations.

RESEARCH TRAINING

Biotechnology

2012-2013 **Research Associate IV**
Hologic, Inc.
Developed a total nucleic acid extraction chemistry for use with diagnostic assays on an automated system. Rigorously optimized the protocol for robust performance across a wide range of human samples such as whole blood, buccal swabs, and stool samples.

2007-2012 **Research Associate I - III**
Gen-Probe, Inc
Designed microRNA detection assays for biomarker discovery in prostate cancer. Worked in a team environment developing and optimizing clinical HLA typing assays and was responsible for writing and implementing SOPs for the product used in the clinic.

UNDERGRADUATE

2006-2007 **Clinical Laboratory Research**
University of California, San Diego
Nory Kamantigue, RN

Acquired and analyzed clinical data investigating the onset of osteoporosis and osteoporotic fractures in male patients.

TEACHING ASSISTANCESHIPS (University of California, Irvine)

2019, Spring Quarter	Bio 99: Molecular Biology
	Bio M116L: Molecular Biology Lab
2017, Winter Quarter	Bio 25: Biology of Cancer
	Bio M125: Molecular Biology of Cancer
2015, Spring Quarter	Bio 99: Molecular Biology
	Bio M116L: Molecular Biology Lab
2015, Winter Quarter	Bio 98: Biochemistry
	Bio M116L: Molecular Biology Lab

PUBLICATIONS

Thompson, J.M., Alvarez, A., Singha, M.K., Pavesic, M.W., Nguyen, Q.H., **Nelson, L.J**., Fruman, D.A., and Razorenova, O.V. (2018). Targeting the Mevalonate Pathway Suppresses VHL-Deficient CC-RCC through an HIF-Dependent Mechanism. Mol Cancer Ther 17, 1781–1792.

Thompson, J.M., Nguyen, Q.H., Singh, M., Pavesic, M.W., Nesterenko, I., **Nelson, L.J**., Liao, A.C., and Razorenova, O.V. (2017). Rho-associated kinase 1 inhibition is synthetically lethal with von Hippel-Lindau deficiency in clear cell renal cell carcinoma. Oncogene 36, 1080–1089.

Wright, H.J., Arulmoli, J., Motazedi, M., **Nelson, L.J**., Heinemann, F.S., Flanagan, L.A., and Razorenova, O.V. (2016). CDCP1 cleavage is necessary for homodimerization-induced migration of triple-negative breast cancer. Oncogene 35, 4762–4772.

Tsai, B.P., Jimenez, J., Lim, S., Fitzgerald, K.D., Zhang, M., Chuah, C.T.H., Axelrod, H., **Nelson, L**., Ong, S.T., Semler, B.L., et al. (2014). A novel Bcr-Abl–mTOR–eIF4A axis regulates IRES-mediated translation of LEF-1. Open Biology 4, 140180.

Siva, A.C., **Nelson, L.J**., Fleischer, C.L., Majlessi, M., Becker, M.M., Vessella, R.L., and Reynolds, M.A. (2009). Molecular assays for the detection of microRNAs in prostate cancer. Mol. Cancer 8, 17.

AWARDS

2016-2019	Institute for Clinical and Translational Sciences, TL-1 Training Fellowship, UC Irvine
2013-2014	Graduate Dean Recruitment Award, UC Irvine

Abstract of the Dissertation

Targeted Therapies and Associated Biomarkers in Human Cancers

By

Luke Nelson

Doctor of Philosophy in Cellular & Molecular Biosciences – Cancer and Cell Biology focus area

University of California, Irvine, 2019

Professor Olga Razorenova, Chair

Targeted therapy represents a class of cancer treatments that interferes with specific cancer-associated molecules and aims to specifically attack reprogrammed cancer cells, leaving normal cells unaffected. In this dissertation, we investigate novel approaches for targeted therapy in Clear Cell-Renal Cell Carcinoma (CC-RCC) and Triple Negative Breast Cancer (TNBC).

In CC-RCC, we uncovered an interaction of the tumor suppressor gene *VHL* with the Rho/ROCK signaling pathway, identifying this pathway as a potential therapeutic target. We found that ROCK inhibition preferentially induces massive mitotic errors in *VHL*-deficient cells and suggest that the induction of mitotic catastrophe represents a novel therapeutic strategy for *VHL*-deficient cancers. We further demonstrate that Cyclin-dependent kinase (CDK) inhibitors show significant cytotoxic activity in *VHL*-deficient CC-

RCC *in vitro* and in a patient-derived xenograft (PDX) orthotopic mouse model. Importantly, we show that these inhibitors do not induce apoptosis in non-transformed cells, or CC-RCC cells engineered to re-express *VHL*. In TNBC, we obtained clinical evidence that the oncogene CUB Domain Containing Protein 1 (CDCP1) is co-activated with the oncogenic kinase c-Src and its downstream target Protein Kinase C δ (PKC-δ) in a subset of patient specimens, and that this class of patients may benefit from the emerging therapeutics targeting this pathway.

Together, these studies contribute to expansion of the targeted therapy library in CC-RCC and TNBC and help to set the stage for more focused preclinical studies to evaluate the efficacy of targeting these pathways.

Chapter 1: Introduction

Opening Statement: Despite great strides in modern medicine, the treatment of cancer remains a daunting challenge to the medical community. Although the mortality rate from most common causes of death such as heart disease, stroke, and diabetes has consistently declined over the past 100 years, the mortality rate from cancer has until recently remained mostly stagnant[1]. It is clear, therefore, that the development of new and improved therapies for cancer is urgently needed. "Targeted therapies" are cancer treatments designed against specific cancer-associated molecules that are meant to accurately target cancer cells, while leaving normal cells unaffected. These differ from conventional treatments like chemotherapy and radiotherapy, which have more broadly toxic effects against all cells. In this dissertation, I will discuss my work on elucidating and targeting relevant signaling pathways in clear-cell renal cell carcinoma (CC-RCC) and triple negative breast cancer (TNBC).

CC-RCC and the Von Hippel-Lindau tumor suppressor.

CC-RCC is the most common form of renal (kidney) cancer. In 2019, there will be approximately 73,000 new cases and 14,000 deaths in the United States, ranking it as the 9th most deadly cancer[2]. About 85% of all cases of CC-RCC involve the inactivation of a gene known as the Von Hippel-Lindau tumor suppressor (*VHL*)[3]. The gene earned its name from the pioneering work of Eugene von Hippel, a German ophthalmologist, and Arvid Lindau, a Swedish pathologist, in describing familial neoplasms of the retina and central nervous system[4,5]. These cases were early examples of what is now known as

VHL disease, an inherited syndrome that predisposes individuals to various cancers due to inherited inactivation of one *VHL* allele[6].

We now know that *VHL* mainly mediates its tumor suppressive function via negative regulation of the hypoxia-inducible factors (HIFs), a family of transcription factors that normally regulates cellular responses to low-oxygen conditions (hypoxia)[7,8]. pVHL (the protein produced by the *VHL* gene) acts as the substrate recognition component of an E3 ubiquitin ligase complex that targets HIFs for proteasomal degradation under normal oxygen tension (normoxia, summarized in Figure 1.2). As a result, CC-RCC tumors that have inactivated *VHL* have high levels of HIF-regulated genes that contribute to tumorigenesis. For example, vascular endothelial growth factor (VEGF) and its associated receptor VEGF-R are direct HIF targets and highly expressed in CC-RCC. Accordingly, these tumors are often highly vascularized, and "anti-angiogenic" therapies are commonly used as treatments, although they are not curative (discussed below). Other HIF targets implicated in CC-RCC tumorigenesis include cyclin D1 (regulation of the cell cycle), Transforming Growth Factor (TGF)-α (stimulation of mitogenic signaling), and Oct4 (regulation of stem cell identity).

History of targeted therapies in CC-RCC.

In general, CC-RCC is highly resistant to traditional chemotherapy and radiation therapy[9]. For this reason, the development of targeted therapeutics for CC-RCC has been and continues to be critical for successful treatment of the disease. Currently, the gold standard for treating CC-RCC remains surgical resection of the primary tumor, via a partial nephrectomy (some of the kidney is saved) or radical nephrectomy (the diseased kidney is completely removed). CC-RCC tumors discovered in early stages have a

A

Estimated New Cases in 2019	73,820
% of All New Cancer Cases	4.2%

Estimated Deaths in 2019	14,770
% of All Cancer Deaths	2.4%

B

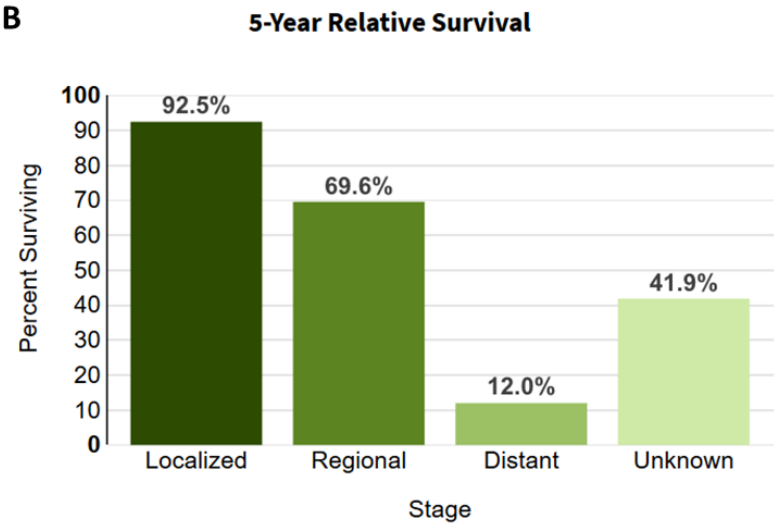

Figure 1.1: Clinical statistics for cancers of the kidney and renal pelvis in the US. **(A)** Incidence data of kidney/renal cancer from the national cancer institute 2019 statistics. **(B)** 5-year survival rate as of 2019. The survival rate of distant (metastatic) disease remains low at 12%. Figure was acquired from the National Cancer Institute, 2019[2]

favorable prognosis, with 5-year survival rates of >90% for localized tumors[2] (Figure 1.1). However, CC-RCC tend to be asymptomatic in early stages, which leads to lack of early detection and patients presenting with late stage or metastatic disease. In this case, the 5-year survival rates drop drastically to ~12%. Thus, survival rates and patient outcomes should be increased by advances in the following areas: 1) improved early detection and 2) advancement and expansion of the therapeutic options for late stage tumors, along with companion diagnostics to better stratify patients and assign the proper treatment regimen. While both arms represent crucial avenues of future research, the work described in this dissertation will focus on the second: discovery and development of new targeted therapies.

Before the advent of targeted therapies, the standard of care for CC-RCC was cytokine treatment using high-dose Interleukin-2 (IL-2) or Interferon (IF)-α[10]. While these therapies produced durable effects in some patients, there was and continues to be a lack of associated biomarkers to predict survival. Furthermore, cytokine treatment has significant toxicity, is restricted to healthy patients with normal organ function, and requires experienced personnel to monitor and manage the side effects. For these reasons, cytokine therapy is not commonly used, although there are still limited examples of its use[10].

Since 2005, three main classes of targeted therapies have emerged for CC-RCC. The first is comprised of Tyrosine Kinase Inhibitors (TKIs) targeting the Vascular Endothelial Growth Factor (VEGF) and Platelet Derived Growth Factor (PDGF) pathway[11–14]. These drugs are “anti-angiogenic” and aim to interfere with the highly vascular nature of CC-RCC tumors. Multiple TKIs targeting VEGF-R and/or PDGF-R have significantly

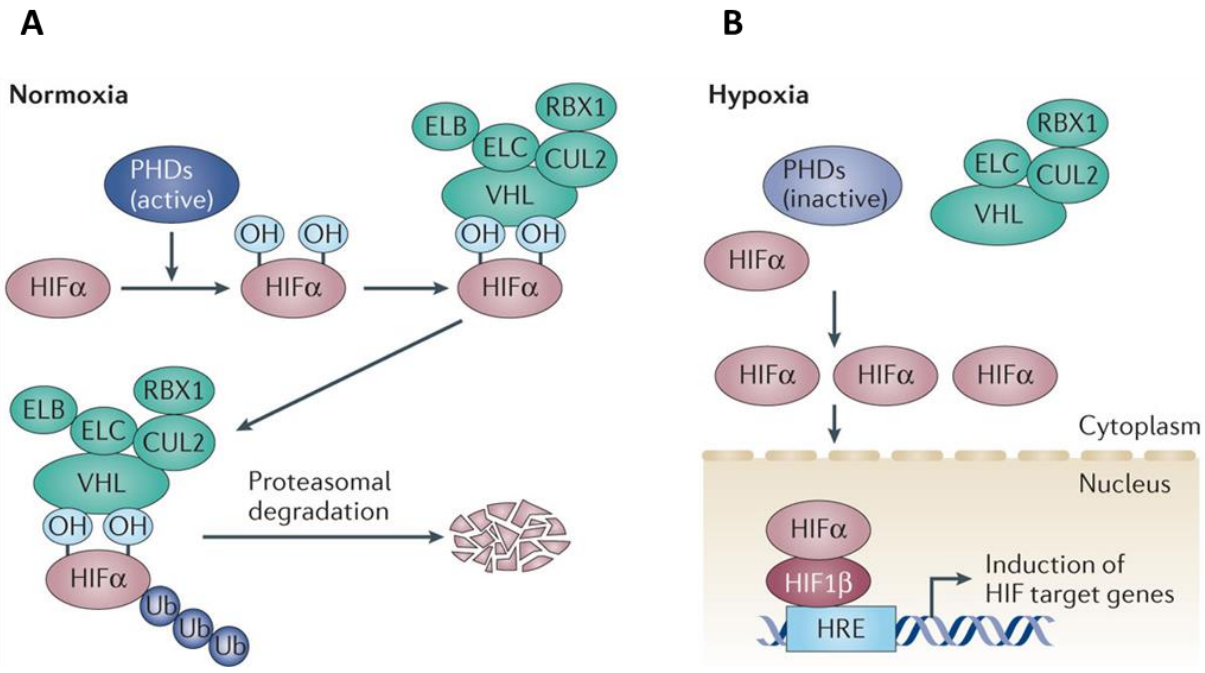

Figure 1.2: Overview of *VHL*/HIF Signaling.

(A) pVHL acts as the substrate recognition arm of an E3 ubiquitin ligase complex. In normoxia, VHL binds hydroxylated HIFα subunits and targets them for ubiquitin-mediated degradation by the proteasome. **(B)** Under hypoxic conditions, HIFα is not hydroxylated, and thus not targeted for degradation by pVHL, allowing HIFα accumulation and activity. In cancer cells that have a lost or inactivated *VHL* gene, lack of the pVHL protein prohibits degradation of HIFα leading to accumulation of HIFα protein levels, even in normoxia. Figure adapted from *Gossage et al*, 2015[15].

improved patient outcomes in randomized clinical trials[12,13,16], with objective response rates (ORR) of up to 33%, and have thus been the most common first-line treatment in recent years. However, despite their effectiveness, these treatments are not curative as patients develop resistance. A second class of inhibitors targets the mammalian target of rapamycin (mTOR)[17,18]. mTOR is a critical node in cellular growth and proliferation pathways[19], and is directly connected to HIF signaling and hypoxic stress via positive regulation of HIF-1α activity[20]. Accordingly, mTOR inhibitors exhibit both anti-proliferative and anti-angiogenic properties[21]. A recent clinical trial showed a 43% ORR with the mTOR inhibitor everolimus in combination with the TKI lenvatinib as a second-line treatment[22], and this therapy was approved in 2016 for patients with failed anti-angiogenic treatment. However, mTOR inhibitors are not currently considered an option for first-line therapy, unless there are clear contra-indications for standard of care first line treatments. A third type of therapy employs *immune checkpoint inhibitors*, a class of drugs that activates the host immune system via repression of inhibitory signaling. While these agents are not discussed at length in this dissertation, they represent an extremely promising emerging family of cancer therapeutics, both for CC-RCC and for other cancers.[1,2] Of note, in 2018 the FDA approved a combination of *nivolumab* (anti programmed death-1 antibody) and *ipilimumab* (anti cytotoxic T-lymphocyte associated protein 4 antibody) as a first-line therapy for intermediate or poor risk CC-RCC patients ("poor risk" refers to patients with the worst prognosis). In a phase 3 clinical trial, this treatment combination had a 43% ORR and a 9% complete response rate (CRR) for previously untreated patients. Although these 3 classes of treatments (TKIs, mTOR inhibitors, and immune checkpoint inhibitors) show some efficacy, the response rates

remain low. Therefore, there is a continued need to identify novel therapeutic options for patients that don't respond to the established treatments.

In summary, the three classes of clinical agents currently in use to treat CC-RCC are: 1)TKIs targeting angiogenesis 2) mTOR inhibitors, and 3) immune checkpoint inhibitors. Although these agents have improved overall patient outcomes, they are not curative in their current state, and the 5-year survival rate for metastatic RCC remains at 12% in 2019 (Figure 1.1). Immune checkpoint inhibitors have significantly changed the landscape of treatment options in the past few years but are not effective against all tumors[23]. Therefore, there is still an urgent need to add to the arsenal of clinical therapeutics available to treat this disease.

The Rho/ROCK signaling pathway in cancer.

Prior work in the Razorenova lab identified rho-associated coiled-coil containing kinase (ROCK) as a promising therapeutic target in *VHL*-deficient CC-RCC. *Thompson et al* showed that the ROCK inhibitor Y-27632 had significant anti-tumor activity *in vitro* and *in vivo* against *VHL*-deficient CC-RCC cells[24]. Re-expression of wild-type pVHL in these cells protected them from the effects of ROCK inhibition, indicating that ROCK inhibitors are specific to *VHL*-deficient cells. This is an example of "synthetic lethality", where simultaneous loss of two genes or signaling pathways (in this case genetic inactivation of *VHL* and pharmacological inhibition of ROCK) causes cell death, whereas loss of only one does not. This is highly desirable in targeted therapies; the ability to accurately target abnormal cancer cells (lacking *VHL*) while sparing non-cancerous cells (expressing *VHL*) is critical to reduce toxicity of the treatment. The study further established that the synthetic lethality was due to pVHL-mediated HIF expression, but did not identify the

downstream mechanisms by which the toxic effect of ROCK inhibitors was taking place. In other words: what function of ROCK is critical for survival in *VHL*-deficient cancer cells, but not in *VHL*-expressing cells?

ROCK functions downstream of the Rho family of small GTPases and phosphorylates various substrates to regulate a host of cellular functions including cytoskeletal function, cellular migration, proliferation and apoptosis[25–28]. ROCK inhibition has shown potent anti-tumor effects in preclinical models of pancreatic cancer[29] and breast cancer[30], among others. ROCK inhibition was also used to disrupt the tumor extracellular matrix in a pancreatic cancer model and "prime" the tumor for treatment with chemotherapy[31]. Since ROCK predominantly regulates force-generating cytoskeletal processes through phosphorylation of substrates like myosin light chain 2 (MLC2) and LIM kinase (LIMK)[32,33], inhibiting ROCK is predicted to counteract tumor invasion and/or metastasis. In support of this, RhoA-mediated ROCK2 activity downstream of VEGF signaling was found to drive the invasive behavior of cervical cancer cells *in vitro*[34]. Another study found that ROCK inhibition decreased bone metastasis in a mouse model of breast cancer[30]. However, the role of ROCK in cancer appears to be context dependent, since ROCK also has some tumor suppressive functions, such as maintenance of adherens junction integrity[35–37]. Therefore, it remains to be seen if ROCK will be a good candidate for targeted therapy in cancer.

Cyclin-dependent kinases and their potential for cancer therapies.

A basic hallmark of cancer is excessive proliferation[38]. Chemotherapeutic agents are thought to derive much of their selectivity due to the fact that cancer cells proliferate more rapidly than normal cells[39]. However, non-targeted chemotherapy has broad off-target

effects (especially to proliferative tissues like the digestive tract, bone marrow and hair). For this reason, targeted therapies aim to directly target aberrant molecules in cancer cells to decrease these side effects. Proliferation of cells is controlled by the cell cycle, a tightly regulated set of events that coordinates cellular growth, replication of DNA, and mitosis of a parent cell into two daughter cells (Figure 1.3). Since this process is so strictly controlled, cancer cells inevitably acquire some type of defect in molecules regulating the cell cycle to progress to malignancy. It is therefore logical that targeted therapies for cancer may aim to target dysregulated portions of the cell cycle machinery.

A core class of molecules regulating progression through the cell cycle are cyclin-dependent kinases (CDKs). For example, CDK4 and CDK6 are largely responsible for phosphorylating Retinablastoma associated Protein 1 (Rb) and releasing E2F transcription factors, which control expression of genes required for entry into the "S" phase of the cell cycle, where cellular genomic DNA is copied in preparation for mitosis[40]. Other CDKs have various roles within the cell cycle (CDK 1, 2, 5), while others are involved in regulation of transcription (CDK 7, 8, 9). As CDKs are master regulators of cell cycle progression, they have long been attractive targets for cancer therapies. However, to date they have not been very effective as treatments in the clinic[41]. Early CDK inhibitors were not very specific to individual CDKs, which are highly similar in their active sites but differ greatly in function[40]. Thus, these pan-CDK inhibitors suffered from broad toxicity[42,43]. More advanced CDK inhibitors have recently been developed, which target several or even individual CDKs[44,45]. Palbociclib, a specific inhibitor of CDK4 and CDK6, significantly delays progression of hormone-receptor positive breast cancer in combination with hormone therapy[46], and received breakthrough approval from the FDA

in 2015. This and other newly developed CDK inhibitors may hold significant promise in improving clinical outcomes in various cancers. As with all targeted therapies, there is a clear need for proper stratification of patients, which remains a daunting challenge. Many clinical trials using CDK inhibitors on unstratified patient cohorts have failed in the past, likely due to a lack of clear predictive biomarkers.

In Chapter 3, I will discuss my work investigating the CDK1/2/5/9 inhibitor Dinaciclib in a patient-derived xenograft (PDX) model of CC-RCC. Although effective as a monotherapy in some preclinical models[47–49], including ours, CDK inhibitors like Dinaciclib are predicted to have the most potential in a combinatorial approach in conjunction with other types of therapy like chemotherapy, other targeted therapies, or immune therapy. Furthermore, the development of even more specific CDK inhibitors targeting a single CDK, coupled with advanced predictive biomarkers, may allow researchers to fully unlock the potential of CDK inhibitors in the clinical setting.

Harnessing "mitotic catastrophe" to treat cancer.

In chapter 4, I will briefly discuss a potential third strategy for targeting CC-RCC cells: the induction of mitotic catastrophe. Mitosis is the process by which a parent cell divides into two daughter cells and is thus crucial for actively proliferating cells such as cancer cells. It has long been observed that cancer cells in general undergo error-prone mitoses, and the German zoologist Theodor Boveri postulated over 100 years ago that aneuploidy (errors in chromosome number) may be a driving force in cancer development[50]. This genomic instability of cancer cells may also contribute to the general "evolution" of tumors, helping cancer cells adapt to evade the immune system or develop resistance to drugs[51]. However, this abnormal and aggressive behavior of cancer cells may also open a

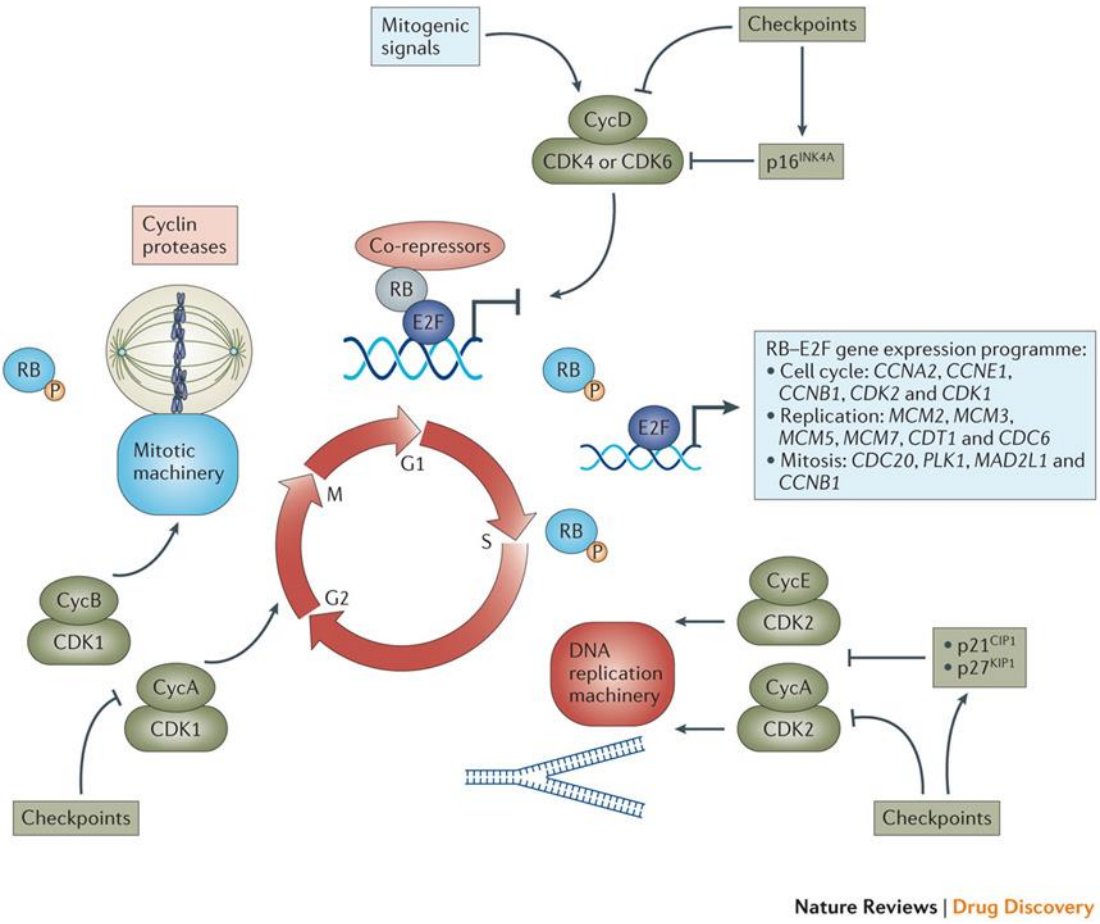

Figure 1.3: Overview of the key components of the mammalian cell cycle.

CDKs function through association with specific Cyclins and phosphorylate various substrates to promote cell cycle progression. CDK2, CDK4, and CDK6 phosphorylate Retinablastoma associated protein 1 (Rb) to promote the release E2F transcription factors and transcription of genes to stimulate G1/S cell cycle progression. CDK1 is involved in stimulation of G2/M progression, as well as assembly of the mitotic machinery. Figure adapted from *Asghar et al*, 2015[41].

therapeutic window. Although a small amount of genomic instability may be beneficial for the evolution of a tumor, gross errors during mitosis will inevitably lead to a lack of viability in daughter cells, leading to cell attrition. Indeed, there are multiple proven safeguards present in normal cells that act to protect against the generation of aneuploidy[52]. For this reason, agents that further increase the genomic instability of cancer cells (which are already unstable) may ultimately push them toward mitotic catastrophe and thus cell death[53]. Microtubular poisons such as the taxanes[54] and Vinca alkaloids[55] have been used in the clinic as anti-cancer treatments for many years. These agents trigger mitotic catastrophe by interfering with microtubule function, which is critical for mitotic fidelity[56,57]. Targeted strategies for inducing mitotic catastrophe, such as inhibition of checkpoint kinase 1 (Chk1)[58] or Aurora Kinase A (AurA)[59], may represent a more refined approach (discussed in more detail in Chapter 4).

As we will see in Chapter 4, mitotic agents may be well suited for treating *VHL*-deficient CC-RCC, since *VHL* functions in the maintenance of mitotic stability through its effect on microtubule function.

Triple Negative Breast Cancer and the need for targeted therapies.

The second type of cancer examined in this dissertation is Triple Negative Breast Cancer (TNBC), the most aggressive and deadly of breast cancers. TNBC is defined clinically by the absence of 3 receptors: human epidermal growth factor receptor 2 (HER2), estrogen receptor (ER), and progesterone receptor (PR). Although seemingly “one disease”, TNBC actually represents a very heterogenous family of tumors. The inherent diversity of TNBC has to date made targeted therapies and precision medicine a challenge in the clinic[60]. Recent studies have attempted to more accurately identify

distinct subtypes of TNBC by characterizing gene expression profiles of patient tumors. These studies have broadly classified TNBC into Luminal Androgen Receptor (LAR), basal-like and mesenchymal subtypes[61,62]. As discussed in chapter 5, these different types of TNBC will likely require drastically different therapeutic approaches. Despite these recent breakthroughs in understanding the genetic basis of TNBC, there is still a dire need for novel targeted therapies and more refined patient stratification criteria to improve the outcomes of TNBC patients.

CDCP1 as a potential target in TNBC.

In the Razorenova lab, we are especially interested in an intriguing oncogene associated with TNBC: CUB domain-containing protein 1 (CDCP1). CDCP1 is a transmembrane glycoprotein that is highly expressed and oncogenic in TNBC[63]. The protein can be extracellularly cleaved, with the cleaved protein displaying enhanced tumorigenic potential. Previous work in the lab by *Wright et al* showed that cleaved CDCP1 forms a homodimer and increases the migratory and invasive properties of TNBC cells *in vitro*[64]. Furthermore, CDCP1 has profound effects on cancer cell metabolism through its regulation of fatty acid oxidation (FAO)[65], which further drives metastatic behavior. These and other recent studies have firmly established CDCP1 as a critical signaling oncoprotein in several types of cancer, including TNBC[66–69].

In chapter 5 I will discuss my work examining CDCP1 activation in clinical specimens of TNBC. CDCP1 activation is tightly linked to activity of the proto-oncogene c-Src and Protein Kinase C (PKC)-δ (Figure 1.4). Activation of this signaling node (Src-CDCP1-PKCδ) likely identifies a subset of TNBC patients that may respond to inhibitors targeting this oncogenic signaling pathway.

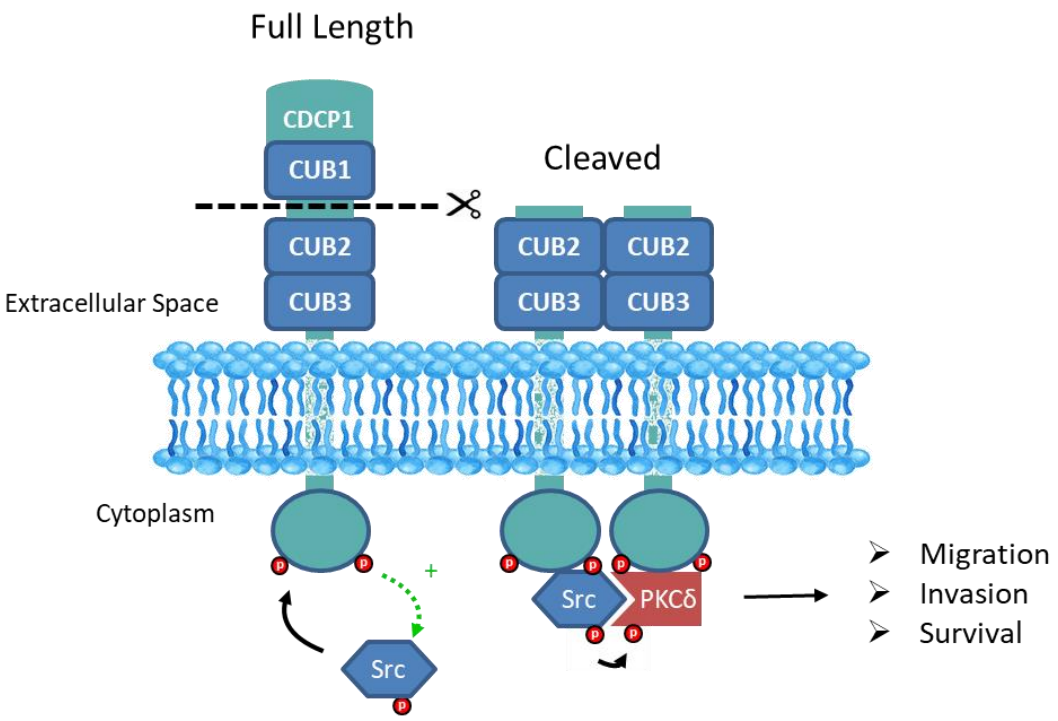

Figure 1.4: Putative CDCP1-Src-PKCδ signaling network

CDCP1 is a transmembrane glycoprotein that can be extracellularly cleaved by a variety of proteases. CDCP1 is both a substrate and activator of the oncogenic tyrosine kinase Src, which phosphorylates CDCP1 at two key residues. Cleaved CDCP1 forms a homodimer and is hypothesized to acta as a "docking site" for Src to phosphorylate its downstream target PKCδ, leading to activation of various pro-survival, pro-invasion cellular phenotypes.

Closing Statement:

The advent of targeted therapies has greatly increased the clinical options for treating various types of cancer. The ability to identify and target dysfunctional molecular pathways in cancer cells allows for the development of more refined pharmaceutical agents with less toxicity to normal cells. However, implementation of treatment strategies and proper stratification of patients remain daunting challenges. As the library of targeted therapies continues to expand moving forward, it will be imperative to develop sophisticated methods for crafting personalized treatment regimens based on each unique patient tumor. This type of "personalized medicine" is finally becoming possible due to recent advances in high throughput genomic and proteomic analysis techniques, although translation to clinical practice remains slow.

In this dissertation, I will look at several emerging targeted therapies applicable to CC-RCC and TNBC. In chapters 3 and 5, I also start to delve into finding predictive biomarkers for drug response or acquired resistance. In chapter 6, I discuss my vision and expectations for moving forward on these projects. Ultimately, future work on targeting new molecular pathways in CC-RCC and TNBC should focus on parallel discovery of companion biomarkers that will predict whether a tumor is likely to respond to a given treatment regimen.

Chapter 2: Crosstalk between *VHL* and the Rho/ROCK signaling pathway in renal cell carcinoma

Introduction

Advanced CC-RCC is a devastating disease with a very poor prognosis and limited treatment options, especially in its metastatic form[2,70]. CC-RCC has historically been very difficult to treat due to its resistance to conventional chemotherapy and radiation therapy[9]. Current options for first-line treatment of metastatic CC-RCC include tyrosine kinase inhibitors targeting the angiogenic vascular endothelial growth factor (VEGF) pathway and immune checkpoint inhibitors[71]. Despite recent advances in therapy options for CC-RCC, the treatments are usually not curative, and the outcome of patients diagnosed with metastatic disease remains poor with a 5-year survival rate of ~12%[2]. Therefore, the discovery and development of novel targeted therapies is crucial to improve the outcome of this deadly cancer.

Rho-associated coiled coil containing kinase (ROCK) is a member of the AGC family of serine/threonine kinases. ROCK functions downstream of Rho small GTPases to regulate a host of cellular functions, including but not limited to cellular migration[32], stress fiber formation[33], cytokinesis[72], and transcription[73] (Supplemental Figure 2.1[74]). ROCK has attracted attention as a potential therapeutic target in cancer due to observations that ROCK activity can contribute to certain aggressive behaviors of tumor cells in both *in vitro* and *in vivo* models[26,30,75,76]. Recently, our research group has shown that multiple ROCK inhibitors specifically target and kills CC-RCC cells lacking the tumor suppressor *VHL*[24], which is lost or deactivated in >80% of CC-RCC cases[3]. We further showed that inhibition

of small GTPase isoprenylation (including Rho) using Fluvastatin was selective for *VHL*-deficient cells[77]. Therefore, *VHL* loss and Rho/ROCK signaling inhibition represent a synthetic lethality pair in CC-RCC. In addition, a clinical study in Japan found that patients with high RhoC or ROCK1 expression had higher grade tumors and poorer overall survival than those with low expression[78]. Together, these studies suggest that targeted inhibition of Rho or ROCK signaling may be a promising therapeutic strategy in CC-RCC. However, the molecular mechanism of sensitivity to Rho/ROCK inhibitors in *VHL*-deficient CC-RCC has not been elucidated. In this chapter, I follow up on the work by *Thompson et al*[24,77] by presenting evidence that the tumor suppressor *VHL* acts as a negative regulator of Rho/ROCK signaling in CC-RCC cells. I then further investigate the mechanisms of the reported synthetic lethality effect of Rho/ROCK inhibition in *VHL*-deficient cells.

Results

pVHL negatively regulates ROCK activity.

Previous work by *Thompson et al.* did not determine if there is a direct regulatory connection between pVHL and the ROCK signaling pathway. To begin addressing this question, we analyzed ROCK signaling in 4 *VHL*-deficient CC-RCC cell lines, with and without exogenous expression of pVHL. Myosin Light Chain 2 (MLC2) phosphorylation was chosen as a readout of ROCK activity since it was the reported ROCK substrate whose phosphorylation sharply decreased after treatment with the ROCK inhibitor Y-27632 (Supplemental Figure 2.2). In 3 out of the 4 cell lines tested, pVHL expression decreased the amount of MLC2 phosphorylation after stimulation with lysophosphatidic acid (LPA), a known activator of ROCK signaling[79] (Figure 2.2A). The pVHL-mediated

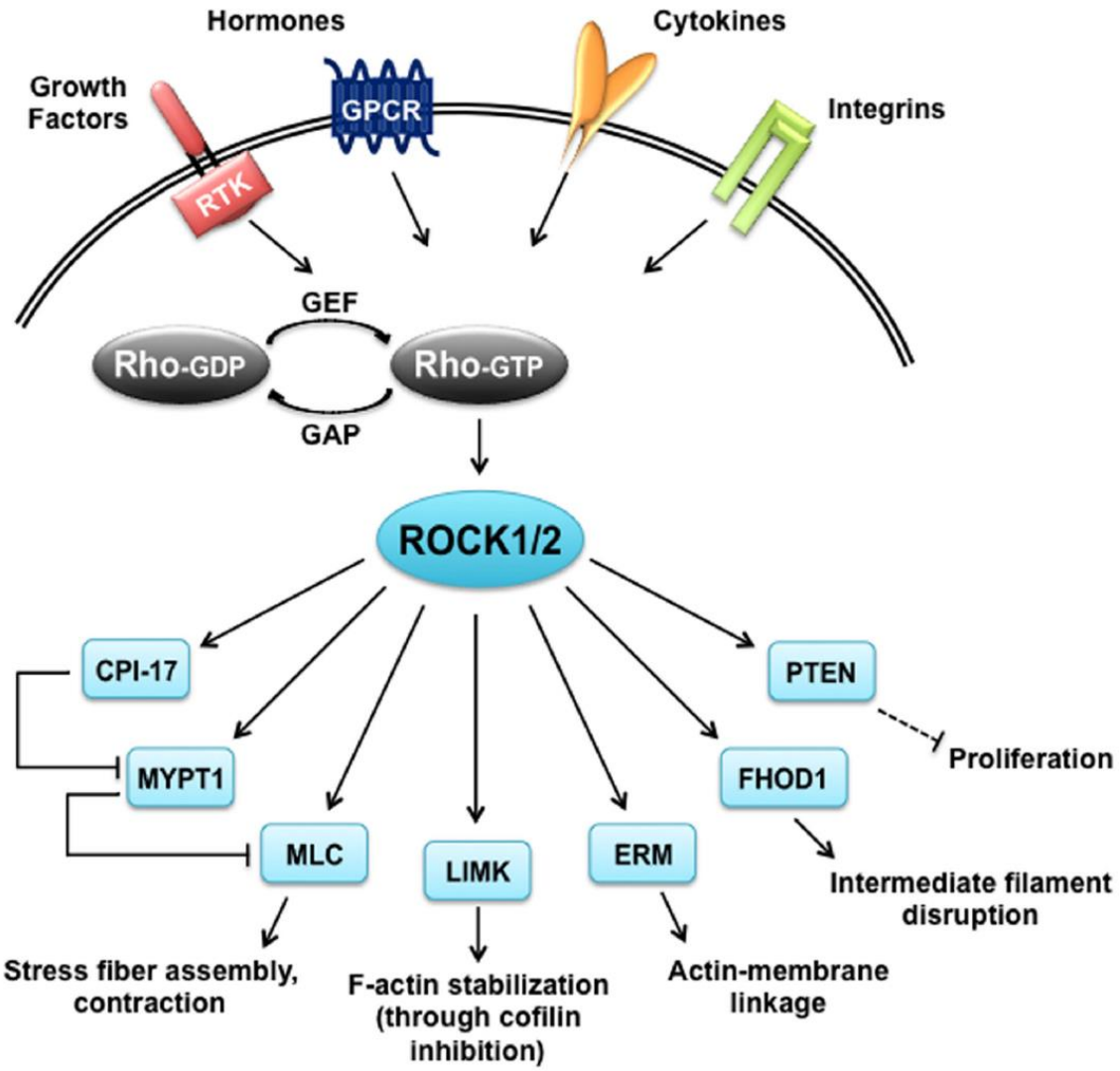

Figure 2.1: Overview of ROCK signaling

ROCK is activated by Rho small GTPases downstream of various stimuli including growth factors, cytokines and integrin signaling. Activated ROCK regulates a host of biological functions through phosphorylation of specific substrates. Figure adapted from *Hartmann et al* 2015[74].

change in MLC2 phosphorylation was tested in at least 4 independent western blots to confirm the reproducibility and significance (Figure 2.2B). In UMRC2 cells, the difference in MLC2 phosphorylation was abrogated by treatment with Y-27632 or siRNA-mediated silencing of both ROCK1 and ROCK2 (Figure 2.2C). In this system, we are taking cell lines that lack pVHL expression and re-expressing the protein exogenously. To confirm that endogenous levels of pVHL are having the same effect, we generated two unique *VHL*-knockout HEK-293 lines using CRISPR/Cas9 (Supplemental Figure 2.2). pVHL depletion led to enhanced MLC2 phosphorylation in both clones tested (Figure 2.2D-2.2E). This increase in phosphorylation was reversed by siRNA silencing of RhoA or RhoC, suggesting that it is dependent on Rho activity. However, while interfering with small GTPase function by treatment with Fluvastatin decreased the overall levels of MLC2 phosphorylation, it did not abrogate the differences between ± pVHL cells (Supplemental Figure 2.4). Taken together, this data shows that pVHL acts as a negative regulator of ROCK activity.

pVHL forms a complex with Rho proteins.

Since pVHL acts as the substrate recognition component of an E3-ubiquitin ligase complex[80], we hypothesized that pVHL may be interacting with relevant proteins in the Rho/ROCK signaling pathway, potentially targeting them for ubiquitin-mediated degradation. We searched the literature for reports of pVHL interacting with proteins involved in Rho/ROCK signaling and found a report of pVHL forming a complex with RhoC[81]. To confirm this result and see if pVHL could interact with Rho family members (Rho A/B/C), we performed immunoprecipitation on HA-tagged pVHL expressed exogenously in HEK-293 cells. We found that pVHL could interact equally well with FLAG-tagged RhoA, RhoB, and RhoC (Figure 2.3A). Since RhoC is known to have a

direct effect on ROCK activity[76] and RhoC knockdown showed the strongest effect on ROCK activity in our own studies (Figure 2.2D), we decided to focus on the RhoC-pVHL interaction. The pVHL mutant C162F harbors a mutation in the elongin binding domain and is thus unable to form the E3-ubiquitin ligase complex[82]. This mutant did not lose the ability to bind RhoC, suggesting that a different pVHL domain is responsible for its interaction with RhoC (Figure 2.3B). To determine the presence of the pVHL/RhoC complex endogenously, we performed a proximity ligation assay (PLA) using antibodies specific for pVHL and RhoC. In pVHL-expressing ACHN cells, we detected the pVHL/RhoC interaction, and the specificity of this signal was confirmed by siRNA knockdown of RhoC (Figure 2.3C, upper panel). Conversely, we did not detect the interaction in pVHL-deficient RCC10 cells, but re-expression of pVHL restored the interaction (Figure 2.3C, lower panel). We next expressed truncated mutants of pVHL to determine the necessary domain responsible for RhoC interaction. pVHL(1-115), which lacks the alpha domain, completely lost the ability to bind RhoC (Supplemental Figure 2.5A). Alpha domain only mutants (116-213) and (167-213) did not express properly in 293T cells and thus we were unable to analyze their binding capacity. This was likely due to the predicted insolubility of these proteins when expressed alone[83]. Since many tumorigenic mutants of pVHL are found in CC-RCC tumors, we hypothesized that some of these disease-associated mutants would also lose the ability to bind RhoC. We tested a panel of clinically identified tumorigenic pVHL mutants and found that all mutants bound RhoC equally well (Supplemental Figure 2.5B). However, many CC-RCC tumors lose pVHL expression entirely, and the result of the loss of the pVHL/RhoC interaction in these

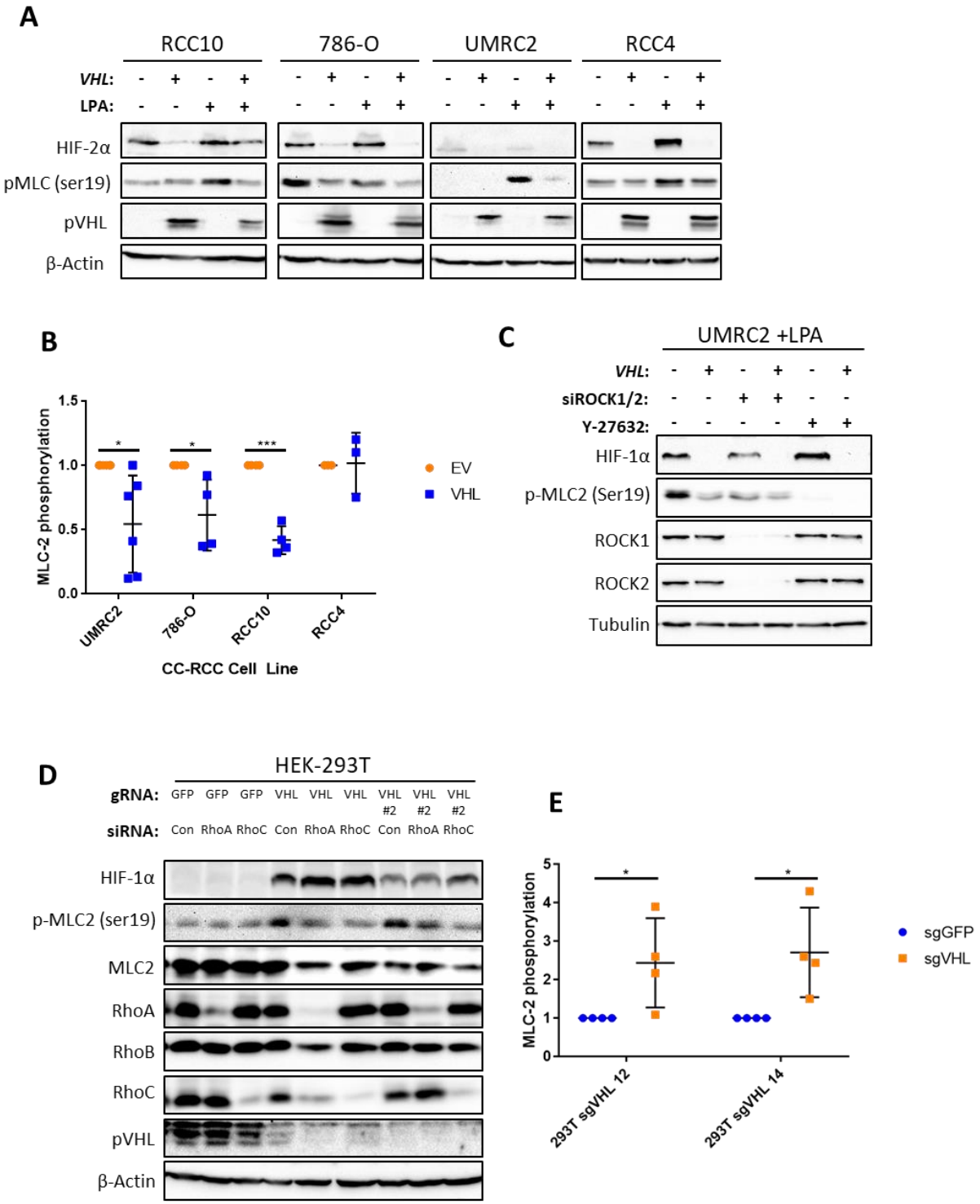
A
RCC10
786-O
UMRC2
RCC4
VHL:
LPA:
HIF-2α
pMLC (ser19)
pVHL
β-Actin
B
MLC-2 phosphorylation
1.5
1.0
0.5
0.0
*
*
***
UMRC2
786-O
RCC10
RCC4
CC-RCC Cell Line
EV
VHL
C
UMRC2 +LPA
VHL:
siROCK1/2:
Y-27632:
HIF-1α
p-MLC2 (Ser19)
ROCK1
ROCK2
Tubulin
D
HEK-293T
gRNA:
GFP GFP GFP VHL VHL VHL VHL #2 VHL #2 VHL #2
siRNA:
Con RhoA RhoC Con RhoA RhoC Con RhoA RhoC
HIF-1α
p-MLC2 (ser19)
MLC2
RhoA
RhoB
RhoC
pVHL
β-Actin
E
MLC-2 phosphorylation
5
4
3
2
1
0
*
*
293T sgVHL 12
293T sgVHL 14
sgGFP
sgVHL

Figure 2.2: pVHL negatively regulates ROCK activity.

(A) pVHL re-expression decreases ROCK target MLC-2 phosphorylation in 3/4 cell lines tested. *VHL*-deficient cells were infected with a lentivirus containing wild type *VHL* and analyzed by western blot. **(B)** Statistical analysis of 4 independent experiments for **(A)**. VHL expression significantly decreases MLC-2 phosphorylation in 3 out of 4 cell lines tested. **(C)** Increased MLC-2 phosphorylation in VHL-deficient UMRC2 cells is reversed by knockdown of ROCK1/2 or ROCK inhibition. UMRC2 matched line was stimulated with LPA in the presence of the ROCK inhibitor Y-27632 or ROCK/ROCK2 siRNA knockdown and analyzed by western blot. **(D)** *VHL* knockout increases Rho-dependent MLC-2 phosphorylation in HEK-293T cells. HEK-293T clones with *VHL* knocked out were generated as described in materials and methods and analyzed by western blot in the presence of RhoA/RhoC siRNA knockdown. **(E)** Statistical analysis of 4 independent experiments showing increased MLC-2 phosphorylation in *VHL*-knockout clones. p values were calculated using unpaired student's t test. *p<0.05, ***p<0.001

cases remains to be investigated. Also, pVHL mutants may lead to altered downstream responses in complex with RhoC compared to wild type pVHL.

Next, we evaluated whether the activation state of RhoC affected its binding to pVHL. RhoC, like other small GTPases, can adopt an “active” and “inactive” conformation when it is bound to GTP or GDP, respectively. The interaction with pVHL was enhanced in the dominant-negative RhoC T19N mutant, indicating that the inactive, GDP-bound form of RhoC is the preferential pVHL binding partner (Figure 2.3D). The activity of each mutant was tested by using a Rho-activity assay (bottom panel of Figure 2.3D, see materials and methods). The dominant-negative T19N mutant had no detectable activity; however, the constitutively active Q63L mutant showed no increase in activity. It is possible that this is due to saturation of the rho activity assay used in this experiment. Interestingly, although more pVHL was pulled down with the T19N RhoC mutant, there was less overall FLAG-RhoC T19N being pulled down by immunoprecipitation with an anti-FLAG antibody. One potential explanation for this phenomenon would be pVHL binding near the N-terminus of Rho near the FLAG tag, thus competing for binding with the FLAG antibody.

pVHL may affect Rho protein levels and activity.

We hypothesized that pVHL may act to decrease the levels of Rho proteins, similar to its regulation of HIF. To test this, we produced four new, low passage ±*VHL* CC-RCC cell lines and tested for RhoA and RhoC expression by western blot. Interestingly, the results were variable between different cell lines tested. RCC10, 786-O, and A498 cells showed a decrease in RhoA expression, while RCC4, RCC10, and A498 cells showed a subtle decrease in RhoC expression (Figure 2.4A). Depleting endogenous pVHL levels in

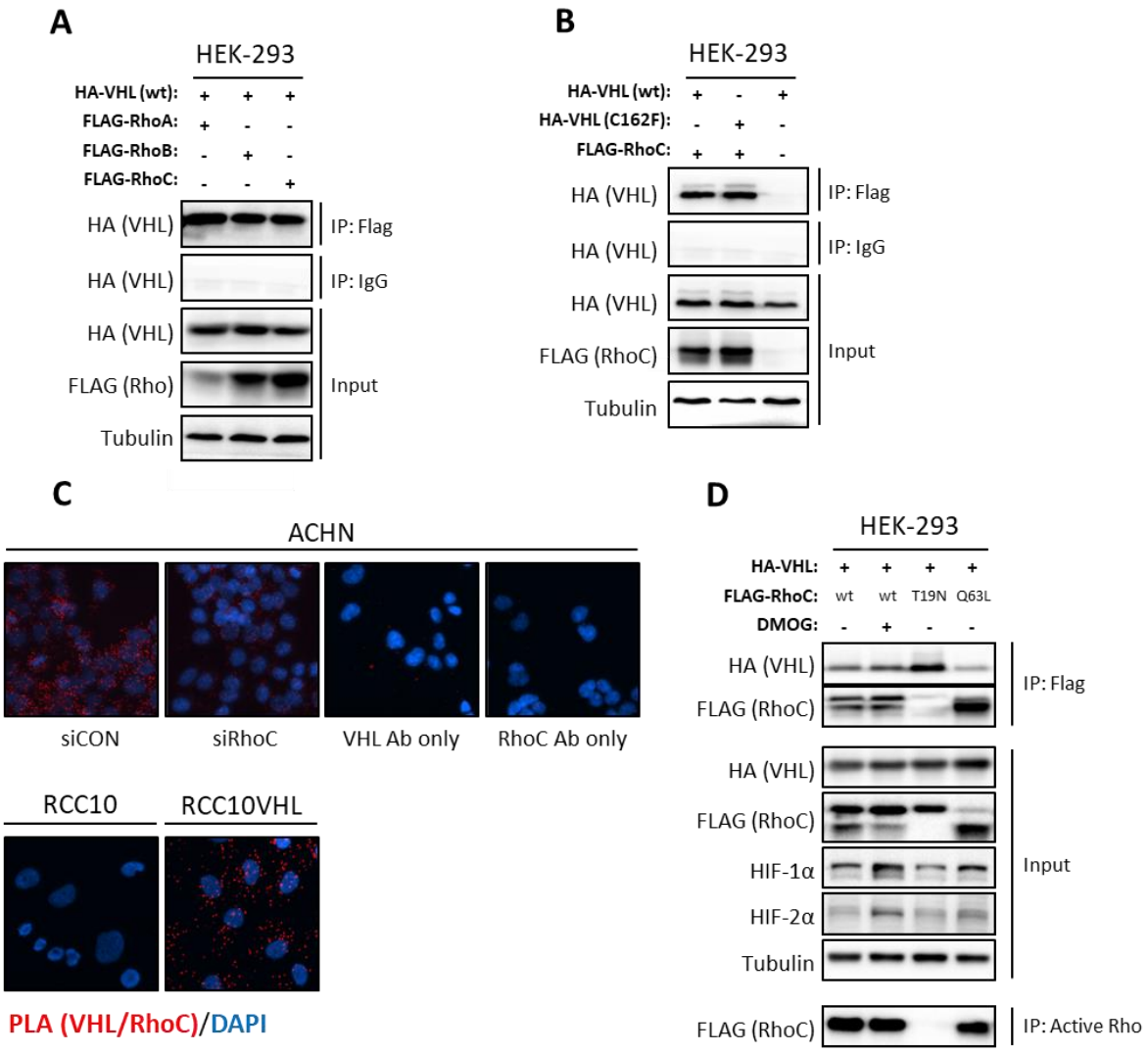

Figure 2.3: pVHL forms a complex with Rho small GTPases

(A) pVHL forms a complex with RhoA, RhoB and RhoC. Tagged constructs encoding pVHL and Rho were co-transfected in HEK-293 cells, then harvested for FLAG co-immunoprecipitation (co-IP). Mouse IgG isotype control was included as a negative control. **(B)** pVHL C162F mutant deficient in E3 ligase complex formation retains the ability to bind RhoC. wt and C162F mutant pVHL were co-transfected with RhoC and analyzed by co-IP as in **(A)**. **(C)** The pVHL/RhoC interaction is detected at endogenous levels. Proximity Ligation Assay (PLA) was used to monitor binding of pVHL and RhoC in ACHN cells and RCC10 cells +/- pVHL. The cells were transfected with an siRNA against RhoC to ensure specificity of the interaction. The assay was performed with each primary antibody individually as a negative control. **(D)** pVHL interacts preferentially with GDP-bound RhoC. Tagged constructs encoding wt VHL and wt, T19N (dominant negative), or Q63L (constitutively active) RhoC mutants were co-transfected in HEK-293 cells, then analyzed by Co-IP as in **(A)**. Activity of the Rho mutants was confirmed by performing an Active Rho pulldown assay (see materials and methods).

ACHN cells (a *VHL*-proficient CC-RCC line) with siRNA produced a subtle increase in RhoA and RhoC protein levels (Figure 2.4B). However, stable knockout of *VHL* in HEK-293 cells with CRISPR/Cas9 showed no difference in RhoA or RhoC expression (Figure 2.2B). To analyze if pVHL expression affects the activation state of Rho proteins, we performed an active Rho pulldown assay on UMRC2 cells with and without pVHL expression. Upon LPA stimulation, the GTP-bound fraction of both RhoA and RhoC increased (Figure 2.4C) and pVHL expression significantly lowered the amounts of LPA-stimulated RhoA activity (Figure 2.4C-2.4D). The activity of RhoC trended toward lower levels with pVHL expression, but the results were not statistically significant. Taken together, these results suggest that pVHL binds Rho in the inactive conformation and restrains its activation upon LPA stimulation.

Rho inhibition is toxic to CC-RCC cells, but "synthetic lethality" with *VHL* deficiency is not consistently achieved.

Previous work in our group established that CC-RCC cells lacking *VHL* are sensitized to cell death by ROCK inhibition, an example of "synthetic lethality"[24]. Since RhoA and RhoC signal directly upstream of ROCK, we hypothesized that inhibition of Rho function would similarly show increased toxicity in *VHL*-deficient cells. To test this hypothesis, we used siRNA to deplete cellular RhoA or RhoC levels in 3 matched cell lines with and without pVHL expression. The results were specific for each cell line: in RCC10 cells, only RhoC knockdown showed an enhanced effect in cells without pVHL, while in RCC4 cells, both RhoA and RhoC knockdown-mediated toxicity were enhanced (Figure 2.5A-2.5B). In 786-O cells, pVHL expression had no differential effect on the toxicity of either RhoA or RhoC knockdown (Figure 2.5A-2.5B). To confirm the effect of Rho inhibition in RCC10 cells, we treated with C3 toxin, a pan-Rho inhibitor. In this case, RCC10 cells

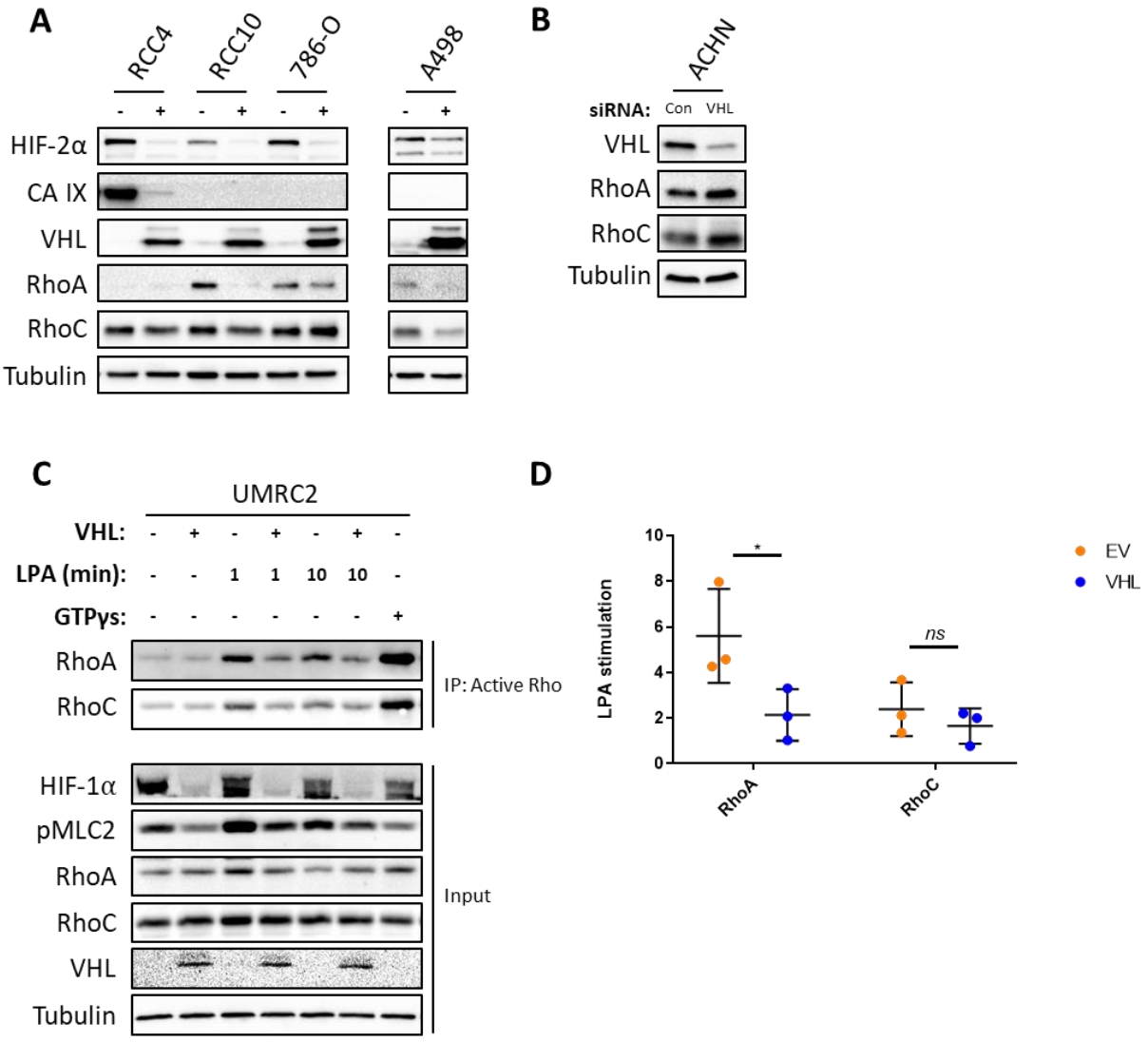

Figure 2.4: VHL may affect Rho expression and activity

(A) pVHL re-expression decreases Rho expression to a varying level in different cell lines tested. Low passage pVHL matched lines were generated by infecting *VHL*-deficient CC-RCC cells with lentivirus encoding wild type pVHL. **(B)** siRNA knockdown of *VHL* in ACHN cells slightly increases RhoA and RhoC expression. **(C)** pVHL expression decreases LPA-stimulated RhoA activity in UMRC2 cells. The cells were serum starved overnight and then stimulated with 1μM lysophosphatidic acid (LPA) for the indicated time points. Control lysate was loaded with GTPγS as a positive control. **(D)** Statistical analysis of western blot analysis in **(C)**. RhoA activity was significantly decreased by pVHL expression, but RhoC activity was not. The experiment was repeated 3 times, and significance was determined using an unpaired student's t test. *p<0.05.

without pVHL were again more sensitive to Rho inhibition (Figure 2.5C). However, this effect was not reproduced in 786-O cells (data not shown). Rho inhibition by C3 toxin was confirmed by a decrease in stress fiber formation (Figure 2.5D). Taken together, this data demonstrates that different CC-RCC cell lines vary in their dependence on Rho isoform expression for survival, with *VHL* loss and Rho depletion being synthetically lethal in certain contexts.

ROCK inhibition with Y-27632 is less toxic to cells with endogenous pVHL expression.

To further explore the effects of ROCK inhibition on cell viability we performed clonogenic colony assays on several *VHL*-deficient CC-RCC cell lines and cell lines endogenously expressing pVHL. On average, cell lines that naturally express endogenous levels of pVHL were more resistant to Y-27632 treatment, although the level of sensitivity varied (Figure 2.6A, “endogenous”). The three *VHL*-deficient CC-RCC cell lines used were all sensitive to Y-27632 but were made resistant after exogenous overexpression of pVHL (Figure 2.6A, “neg” and “exogenous”). Furthermore, the non-transformed renal epithelial cell line RPTEC was mostly resistant to Y-27632 compared to the CC-RCC line RCC10 (Figure 2.6B). These results suggest that on average, ROCK inhibition with Y-27632 preferentially targets cells lacking pVHL expression. However, siRNA-mediated knockdown of pVHL in two resistant cell lines, SN12C (CC-RCC) and MDA-MB-231 (a triple negative breast cancer cell line), did not change the sensitivity to Y-27632 (Figure 2.6C-2.6D). Furthermore, stable overexpression of the pVHL downstream target HIF-1α also had no effect (Figure 2.6E-2.6F). Taken together, these results suggest that while naturally *VHL*-deficient CC-RCC cells are more sensitive to ROCK inhibitors, loss of pVHL

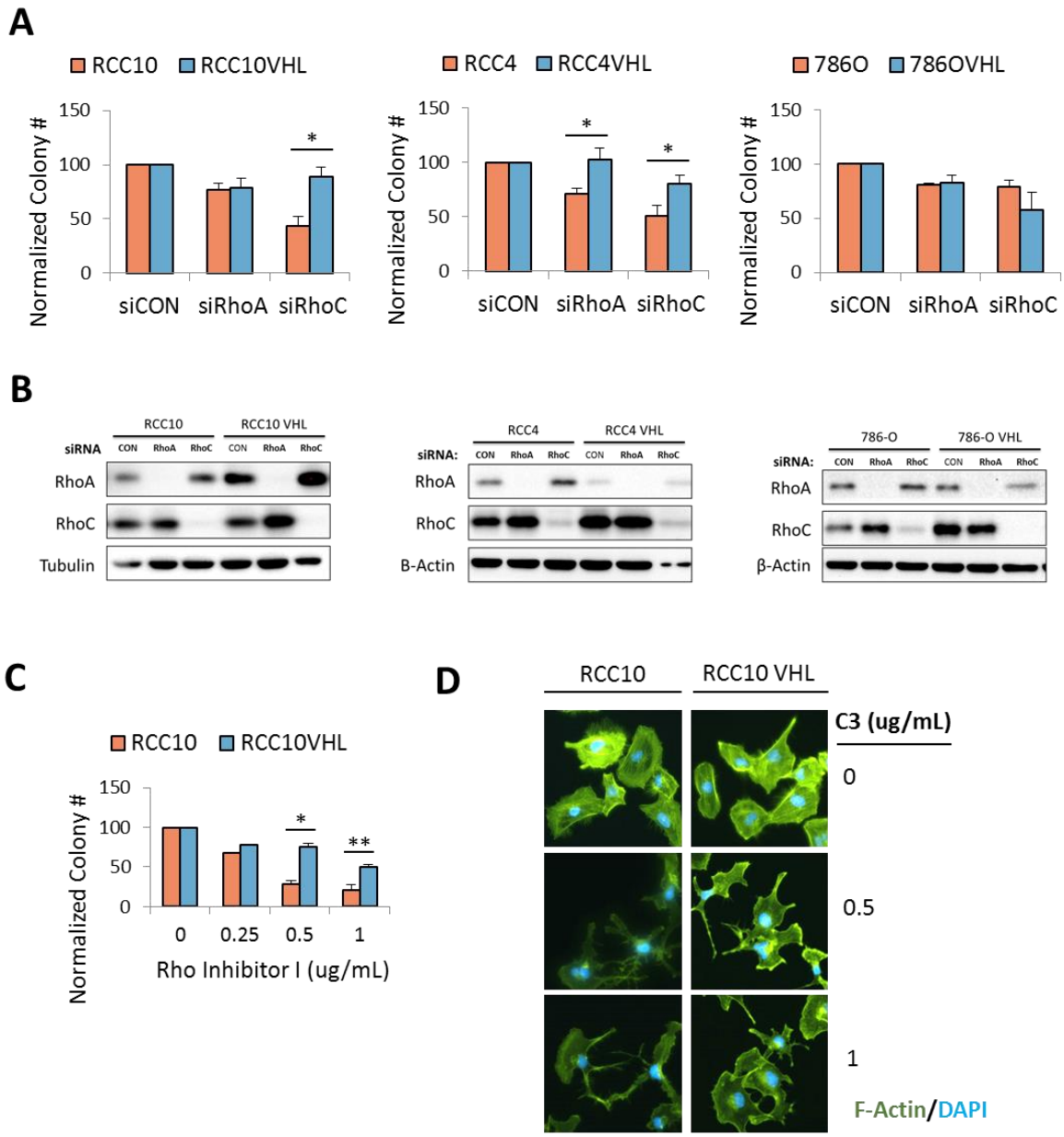

Figure 2.5: siRNA knockdown or chemical inhibition of Rho is toxic to CC-RCC cells
(A) *VHL*-deficient CC-RCC cells vary in their response to RhoA/RhoC knockdown. RhoA is synthetically lethal with pVHL loss in RCC4, and RhoC is synthetically lethal with pVHL loss in RCC4 and RCC10. **(B)** Western blot analysis confirms the efficiency of siRNA knockdown in **(A)**. **(C)** pan-Rho inhibition with C3 toxin is synthetically lethal with pVHL loss in RCC10 cells. Cells were treated with C3 toxin for 24 hours and then plated for colony assays. **(D)** Efficacy of C3 toxin was confirmed by staining treated cells with phalloidin. Error bars represent standard error of the mean. Each experiment was repeated 3 times, and significance was determined using unpaired student's t test. *p<0.05, **p<0.01.

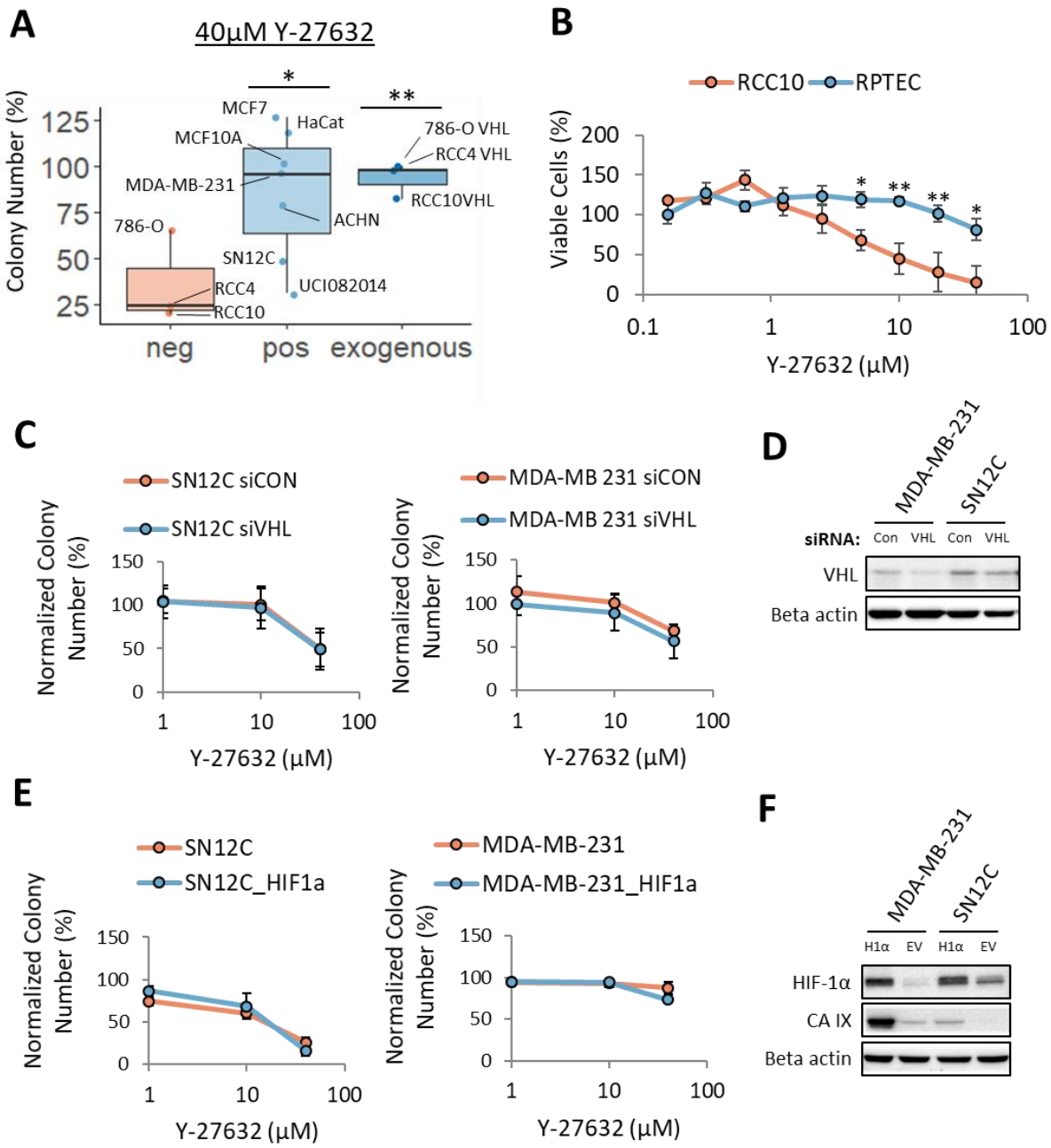
A
40μM Y-27632
Colony Number (%)
125
100
75
50
25
*
**
MCF7
HaCat
MCF10A
786-O VHL
RCC4 VHL
MDA-MB-231
RCC10VHL
ACHN
786-O
SN12C
UCI082014
RCC4
RCC10
neg
pos
exogenous
B
RCC10
RPTEC
Viable Cells (%)
200
150
100
50
0
0.1
1
10
100
Y-27632 (μM)
C
SN12C siCON
SN12C siVHL
Normalized Colony Number (%)
150
100
50
0
1
10
100
Y-27632 (μM)
MDA-MB 231 siCON
MDA-MB 231 siVHL
D
MDA-MB-231
SN12C
siRNA:
Con
VHL
Con
VHL
VHL
Beta actin
E
SN12C
SN12C_HIF1a
MDA-MB-231
MDA-MB-231_HIF1a
F
MDA-MB-231
SN12C
H1α
EV
H1α
EV
HIF-1α
CA IX
Beta actin

Figure 2.6: ROCK inhibition with Y-27632 is preferentially toxic to *VHL*-deficient cells, but pVHL knockdown or HIF-1α expression does not sensitize resistant cells. **(A)** Treatment with 40μM Y-27632 is preferentially toxic to *VHL*-deficient cell lines compared to cell lines endogenously expressing pVHL or expressing VHL through exogenous re-expression. Box and whiskers plot show colony number compared to vehicle-treated controls. **(B)** Non-transformed RPTEC cells are resistant to Y-27632 compared to RCC10 cells in a viability assay. Cells were plated in 96-well plates and treated with the indicated concentration of Y-27632 for five days, then labeled with Calcein AM to quantify viable cells. **(C)**-**(D)** siRNA knockdown of pVHL in Y-27632-resistant cells does not sensitize them to Y-27632 treatment. Cells were transfected with the indicated siRNAs and then plated for colony assays and treated with the indicated concentrations of Y-27632. **(D)** Western blot analysis showing the efficiency of pVHL knockdown in **(C)**. **(E)** Overexpression of pVHL in Y-27632-resistant cells does not sensitize them to Y-27632 treatment. Cells were infected with lentivirus containing HIF-1α and then plated for colony assays and treated with the indicated concentrations of Y-27632. . **(F)** Western blot analysis showing HIF-1α overexpression in **(E)**. Error bars represent standard error of the mean. Each experiment was repeated 3 times, and significance was determined using unpaired student's t test. *$p<0.05$, **$p<0.01$.

alone does not sensitize cells to ROCK inhibition. It is likely that the *VHL*-deficient cells have activated certain signaling pathways over time that render them sensitive to the toxic effects of ROCK inhibitors. However, simply depleting pVHL in short-term assays is not sufficient to recreate this phenomenon.

AGC-family kinase inhibitor AT13148 is more potent than Y-27632, but synthetic lethality with *VHL* loss is limited.

The ROCK inhibitor Y-27632 has relatively low potency, poor pharmacological properties[84], and is thus not well suited for pursuing clinical studies. We therefore chose to investigate the AGC-family kinase inhibitor AT13148, which has enhanced potency and better pharmacological properties compared to Y-27632[85]. It should be noted that while AT13148 inhibits ROCK activity, it is also active against several other AGC-family kinases including AKT, p70S6K, and PKA[85], which may confound the results seen here (discussed further below).

To start, we tested the effect of AT13148 on four *VHL*-deficient CC-RCC cell lines, with and without pVHL expression. Two of these cell lines (RCC4 and RCC10) reproduced the synthetic lethal effect seen with Y-27632 (Figure 2.7A). Interestingly, the other two (786-O and UMRC2) showed no difference in sensitivity based on pVHL expression (Figure 2.7B). These cell lines were in general more resistant to AT-13148, requiring higher concentrations of AT13148 to achieve the IC_{50} in comparison to RCC4 and RCC10, indicating that they probably possess other mechanisms of resistance that are not dependent on pVHL. 786-O was also the *VHL*-deficient line most resistant to Y-27632 (Figure 2.6A), but Y-27632's effect on UMRC2 cells has not been investigated. HEK-293 cells with *VHL* knocked out were also not sensitized to AT13148 treatment (Figure 2.7C). Finally, despite these results we found that AT13148 did show some selectivity toward

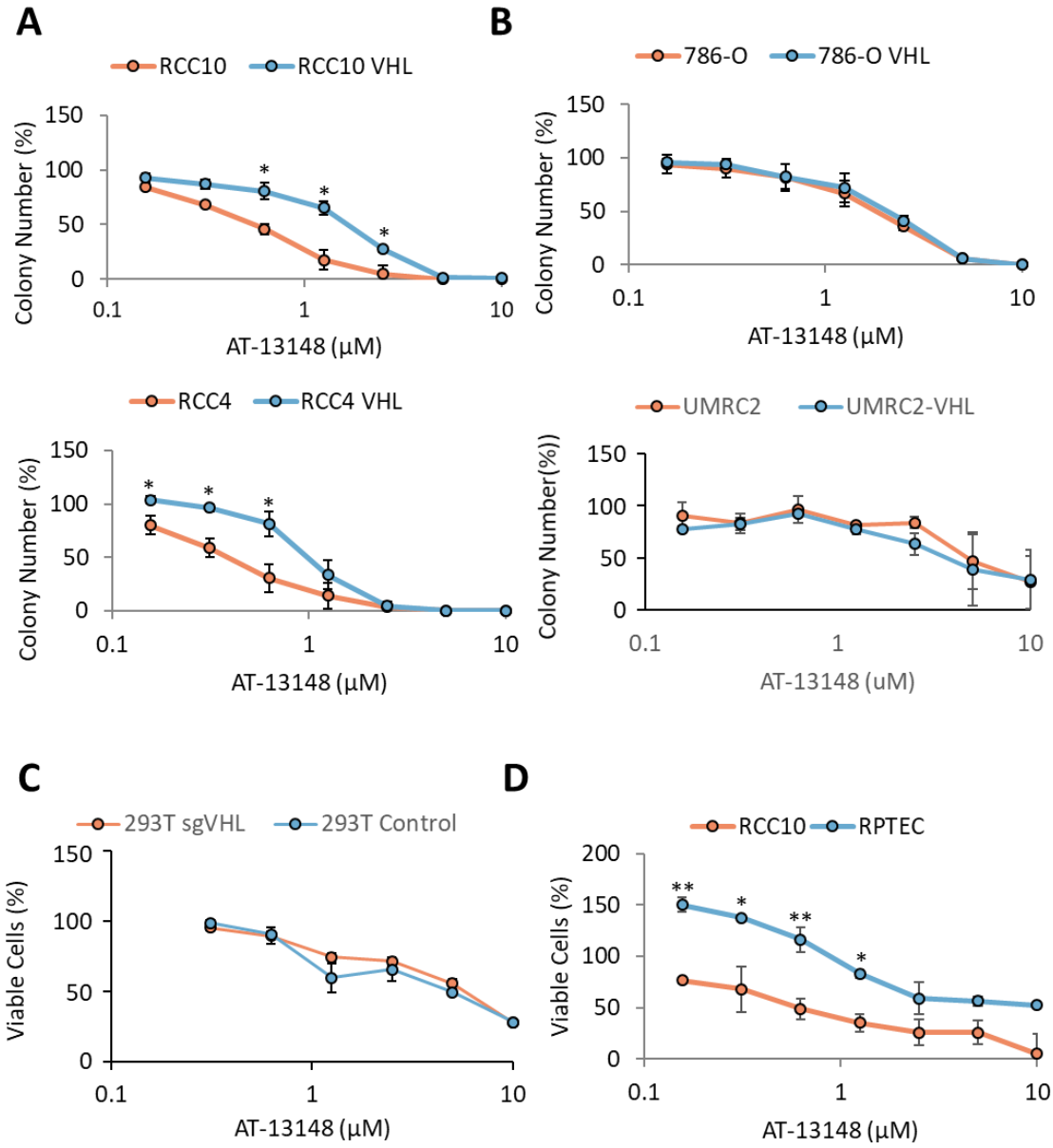

Figure 2.7: AGC-family kinase inhibitor AT-13148 shows a modest preference for *VHL*-deficient cells, but only in some cell lines.

(A)-(B) AT-13148 shows modest synthetic lethality with pVHL loss in RCC4 and RCC10 cells but is not synthetically lethal with pVHL loss in 786-O or UMRC2 cells. *VHL*-deficient cells were infected with a lentivirus containing wild type *VHL* and analyzed by colony assay with the indicated concentrations of Y-27632. **(C) – (D): (C)** Stable knockout of *VHL* in HEK-293T cells does not sensitize them to AT-13148 treatment. **(D)** AT-13148 shows preferential toxicity to *VHL*-deficient CC-RCC cells compared to non-transformed RPTEC cells. Cells were plated in 96-well plates and treated with the indicated concentration of Y-27632 for five days, then labeled with Calcein AM to quantify viable cells. Error bars represent standard error of the mean. Each experiment was repeated 3 times, and significance was determined using unpaired student's t test. *p<0.05, **p<0.01.

RCC10 cells compared to RPTEC cells in a viability assay (Figure 2.7D). In summary, The ROCK/AGC kinase inhibitor AT-13148 was effective at blocking colony formation in CC-RCC cells with IC_{50}'s ranging from 0.5μM - 10μM, but only 2 out of the 5 cell lines tested showed differential sensitivity to AT-13148 based on pVHL expression status.

Discussion

In this study, we showed that the tumor suppressor protein pVHL acts as a negative regulator of ROCK activity in CC-RCC cells. Since ROCK activation has been linked with aggressive behavior of tumors[26,75,86], repression of ROCK may represent a novel mechanism of tumor suppression by pVHL. Although the tumor-suppressive activity of pVHL is thought to rely fully on the regulation of HIFs, there are some examples in the literature of HIF-independent functions of pVHL. pVHL binds directly to microtubules and is a key regulator of microtubule stability[87]. Likewise, pVHL contributes to mitotic fidelity independent of HIF expression via its stabilization of astral microtubules in the mitotic spindle[88]. In the course of this study, we were unable to show definitively if the regulation of ROCK by pVHL was dependent on HIF signaling. However, it should be noted that another study found activation of Rho and ROCK signaling in breast cancer cells under hypoxia[86], supporting the involvement of HIFs in ROCK activation.

Strengthening the connection between pVHL and Rho/ROCK signaling, we found that pVHL was able to form a protein complex with Rho small GTPases, which signal directly upstream of ROCK. Since pVHL acts as the substrate recognition arm of an E3 ubiquitin ligase complex, we analyzed pVHL's effect on Rho ubiquitination and expression. Preliminary data from our collaborators detected no increased ubiquitination of Rho family members upon pVHL overexpression (Supplemental Figure 2.6). pVHL expression

caused a small decrease in Rho expression levels in certain contexts, but the results were inconsistent and in some cases pVHL had no effect on Rho expression. A more likely explanation is that pVHL alters the activity of Rho through a protein-protein interaction. We found that pVHL interacted strongly with Rho mutants locked in the GDP-bound, inactive state. It is therefore possible that pVHL acts to restrain the activation of Rho by locking it in its inactive conformation. In the future, this hypothesis could be tested by analyzing the endogenous interactions of Rho proteins with their downstream substrates like ROCK. Rho activates ROCK by binding directly and causing an allosteric effect[27,89]; it is therefore expected that pVHL expression should decrease the interaction between Rho and ROCK. Importantly, the protein-protein interaction interface between pVHL and Rho should be mapped so that pVHL point mutants can be generated that lose the ability to bind Rho (but not HIFs), to confirm the importance of this interaction.

One Japanese clinical study found that patients with elevated RhoC or ROCK expression had a poor prognosis[78]. This data provides a rationale for studying the role of Rho/ROCK signaling in CC-RCC pathogenesis. RhoA and ROCK signaling was shown to be hyperactivated in breast cancer cells under hypoxia, leading to increased migratory capabilities[86]. Since *VHL*-deficiency causes a “hypoxia-like” effect by upregulation of HIFs, this could be relevant in *VHL*-deficient CC-RCC. ROCK activation is generally considered to be an oncogenic event through its effect on the cytoskeleton, although there are also some potentially tumor-suppressive functions of ROCK such as maintenance of epithelial adherens junctions[36,37,90]. *Thompson et al* did show that treatment with the ROCK inhibitor Y-27632 significantly decreased the tumor formation ability of 786-O cells in a subcutaneous mouse model[24]. Our genetic data knocking down RhoA and RhoC

showed that some CC-RCC cell lines were sensitive to Rho inhibition, further demonstrating the importance of the Rho/ROCK signaling pathway in CC-RCC.

Throughout this study, the function of pVHL was generally assessed by using CC-RCC cell lines that lack a functional *VHL* gene and re-introducing the *VHL* gene exogenously to create a stable cell line. There are several problems with this approach. For instance, we found that the process of re-expressing pVHL was significantly toxic to the target cells; it is likely that these cells have adapted to the absence of pVHL expression and forced re-expression is detrimental in this "re-programmed" state. Because of this, the subpopulation that adapts to exogenous pVHL expression may actually be enriched for more aggressive cells. Indeed, the RCC10-*VHL* cells used in parts of this study are noted to proliferate much more rapidly than the parental RCC10 line (personal observation, data not shown). This type of inherent bias may lead to misinterpretation of results. To address this concern in our study, we acquired low-passage *VHL*-deficient CC-RCC cells and re-introduced *VHL* shortly before doing our experiments to analyze the effects of pVHL expression before long term cellular adaptation to pVHL. Another way to study *VHL* function in CC-RCC is to knock out endogenous expression in normal cells that express VHL. However, *VHL* loss alone does not lead to transformation of cells[91], so this approach does not accurately recapitulate the behavior of cancer cells.

Despite the difficulties in studying pVHL function, our data indicate that cell lines naturally expressing pVHL do tend to be more resistant to the effects of the ROCK inhibitors Y-27632 and AT-13148. Since non-cancerous cells express pVHL, this finding supports the rationale for using ROCK inhibitors to target *VHL*-deficient cancers while minimizing toxicity to normal tissues.

We chose to move forward with the AGC family kinase inhibitor AT-13148, since it is has better pharmacological properties than Y-27632[84,85] and is more potent at lower doses. However, it is interesting to note that the "synthetic lethality" of ROCK inhibition and *VHL* loss is seen more strongly with the ROCK inhibitor Y-27632. Y-27632 was reported to be a highly selective ROCK inhibitor with a K_i of 140nM for ROCK[92], although its off-target effects were not thoroughly investigated in this study and we cannot be sure of its selectivity. AT-13148 is not selective to ROCK and inhibits other AGC-family kinases at a similar efficiency. It is very likely that off-target effects of AT-13148, such as inhibition of AKT, p70S6K, or PKA, do not show preferential toxicity toward *VHL*-deficient cells, and thus decrease the selectivity of this drug.

In summary, we have shown that pVHL acts as a negative regulator of the Rho/ROCK signaling pathway, likely through direct inhibition of Rho activity. Inhibition of Rho activity through siRNA knockdown or chemical inhibition showed synthetic lethality with pVHL depletion in some but not all CC-RCC cell lines tested. Furthermore, the ROCK inhibitor AT-13148 was effective at blocking colony formation of CC-RCC cells and showed moderate preferential toxicity to cells lacking endogenous pVHL expression. While it remains to be seen if ROCK inhibitors hold potential for clinical application in CC-RCC, this study reveals that Rho/ROCK signaling is intimately connected with pVHL expression, and thus represents a potential targetable pathway in *VHL*-deficient CC-RCC.

Materials and Methods

Cell culture, plasmids and chemical treatments

All cancer cell lines used in this study were grown in Dulbecco's Modified Eagle's Medium with 10% Fetal Bovine Serum and 1% Penicillin in a 37°C incubator with 5% CO2. RPTEC

cells were grown in DMEM/F12 medium (Thermo Fisher Scientific) with 5μg/mL insulin, 5μg/mL apo-transferrin, 5ng/mL sodium selenite, 36 ng/mL hydrocortisone, 50 ng/mL human EGF, 1% Penicillin/Streptomycin, and 100 μg/mL G418. Y-27632, AT-13148 and Fluvastatin (Selleck Chemicals, Houston, TX) and C3 Toxin (Rho Inhibitor I, Cytoskeleton Inc.) were diluted in Dimethyl Sulfoxide (DMSO) and serially diluted for each experiment.

The following plasmids were used: pBabe_HA-VHL (addgene #19234), lentiCRIPSR v2 (addgene #52961), pVSV_G, pCMVΔR8.2. The following plasmids were generated by inserting the respective gene into the pLM_CMV_puro vector using EcoRI and XhoI digestion: pLM_CMV_HIF1α, pLM_CMV_HA-VHL, pLM_CMV_FLAG-RhoA, pLM_CMV_FLAG-RhoB, pLM_CMV_FLAG-RhoC, pLM_FLAG-RhoCQ63L, pLM_FLAG-RhoCT19N.

siRNA knockdown

The following siRNAs were used: VHL #L-003936-00-0005, RhoA #L-003860-00-0005, RhoC #M-008555-01-0005, non-targeting siRNA #D-001810-01-05 (Dharmacon, Lafayette, CO). siRNAs were pre-mixed with Dharmafect 1 reagent and added to cells during plating according to the manufacturer's protocol. For colony assays, colonies were counted 7 days after siRNA transfection. For western blot analysis, cells were lysed 72 hours after transfection.

Clonogenic assays

Clonogenic assays were performed by plating 300 cells per 6cm tissue culture plate. The day after plating, tissue culture medium was changed to medium containing experimental compounds. Colonies were counted 7-10 days after plating. All conditions were

performed in duplicate, and each experiment was repeated three times. Results are presented as the mean +/- the standard error of the mean.

Cell Titer Glo viability assay

Cells were plated in 96-well plates and treated with experimental compounds. After 3-4 days, Cell Titer Glo reagent (Promega, Inc) was added to each plate according to the manufacturer's recommendations. Experiments were performed in triplicate and each experiment was repeated three times. Results are shown as the mean +/- the standard error of the mean.

Statistical Analysis

Statistical significance of groups was evaluated by performing two-tailed unpaired student's t-test. p values of <0.05 were considered significant.

Western blot analysis

Cells were lysed in ice-cold lysis buffer (20 mM Tris pH 7.5, 1% Triton X-100, 150 mM NaCl, 1 mM EDTA/EGTA, 10 mM Sodium Pyrophosphate, 10 mM β-glycerophosphate, 1 mM Sodium Orthovanadate, 50 mM Sodium Fluoride) and scraped into chilled tubes, then incubated on ice for 10 minutes with brief vortexing every 2-3 minutes. Samples were centrifuged at 12,000x g for 10 minutes at 4°C to pellet insoluble material. The soluble fraction was mixed with 5x sample buffer (312 mM Tris pH 6.8, 10% SDS, 10% β-mercaptoethanol, 50% glycerol, 0.05% bromophenol blue) and boiled for 5 minutes at 95°C, then cooled on ice. Total protein content of cell line lysates was assessed using BCA assay (Thermo Fisher cat# 23225).

Protein lysates were loaded onto polyacrylamide gels and run for 30 minutes at 90V, then approximately 90 minutes at 120V. Proteins were transferred to 0.2-µM-pore nitrocellulose membranes and blocked for 60 minutes with 5% non-fat milk in PBS/0.05%

Tween-20 (PBS-T). Primary antibodies were diluted in 5% BSA/PBS-T and incubations were performed overnight at 4°C with gentle shaking. Secondary antibodies were diluted in blocking buffer and incubations were performed for 1 hour at room temperature. Images were acquired on the Bio-Rad ChemiDoc XRS+ imaging system.

The following primary antibodies were used: Myosin Light Chain #3672 (1:250), p-Myosin Light Chain Ser19 #3671 (1:250), RhoA #2117 (1:1,000), RhoB #2098 (1:1,000), RhoC #3430 (1:1,000), HA tag #3724 (1:1,000) (Cell Signaling Technologies, Inc, Danvers, MA), HIF-1α #610959 (1:250), VHL #564183 (1:500) (BD biosciences, San Jose, CA), HIF-2α #NB-100122 (1:1,000) (Novus Biologicals LLC, Centennial, CO), ROCK1 #PA522262 (1:500), ROCK2 #PA528774 (1:500) (Thermo Fisher Scientific, Waltham, MA), α-Tubulin #10R-T130A (1:5,000) (Fitzgerald Industries, Acton, MA), β-Actin #A5441 (1:5,000), FLAG tag #F1804 (1:5,000) (Sigma Aldrich, St. Louis, MO), and CA IX #GTX70020 (1:250) (GeneTex, Irvine, CA).

Lentivirus Production and Infection:

HEK-293T cells were transfected with lentiviral plasmid along with packaging plasmids, pVSVG and ΔR8.2. 1.33ug of each plasmid was added to 20uL PLUS reagent in 750uL DMEM and incubated for 15 minutes. The mixture was then mixed with 30uL lipofectamine in 750uL DMEM and incubated for an additional 15 minutes. The complexes were then added to HEK-293T cells at 70-90% confluence. The next day, the medium was changed to DMEM with 10% FBS and 1% Penicillin/Streptomycin. Viral supernatant was collected at 48 and 72 hours after transfection, filtered through a 0.22-μM filter, and stored at -80°C until use. Cells were infected by adding viral supernatant directly to cells in a 6-well plate with 6 μg/mL polybrene. After 2-3 days, the medium was

changed to medium containing 1 μg/mL puromycin for selection of successfully transduced cells. Selection was carried out until all cells in a non-transduced plate were killed.

Generation of VHL-knockout cells

HEK-293T cells were infected with pooled lentivirus from the lentiCRISPR v2 plasmid containing the following gRNAs targeting VHL: #1) CCGAGCGCGCGCGAAGACTA, #2) GTTACAACGGCCTACGGTGC, #3) AACGCGCTCGCGGAAATAGC. As a control, HEK-293T cells were infected in parallel with lentivirus from lentiCRISPR v2 containing a gRNA targeting GFP (targeted sequence: GGGCGAGGAGCTGTTCACCG). After infection, cells were selected for 3 days with 1μg/mL puromycin and then plated at low density to isolate single colonies. Colonies were isolated and expanded before testing by western blot for VHL knockout. Two clones that showed complete loss of VHL and stabilization of HIF protein levels were chosen for downstream analysis.

Immunoprecipitation

400 μg of protein in 200 μL of cell lysis was incubated with 4 μL of anti-Flag antibody (Sigma Aldrich #F1804) for 16 hours at 4°C with gentle agitation. Then 20 μL Protein G Dynabeads (Life Tech #10003D) were added, followed by incubation for 1 hour at 4°C. Immunoprecipitated proteins were collected using magnetic stand, washed 3 times for 5 minutes on ice with cell lysis buffer without protease or phosphatase inhibitors, boiled in 1x sample loading buffer for 5 minutes and then analyzed by western blot.

Proximity Ligation Assay

The assay was performed according to the manufacturer's protocol (Sigma Aldrich #DUO92008, #DUO92009, #DUO92010). Primary antibodies used were VHL #564183 (1:200, BD biosciences, San Jose, CA) and RhoC #3430 (1:100, Cell Signaling

Technologies, Inc, Danvers, MA)) Images were collected as for immunofluorescence staining analysis. 12 mm coverslips were used with 20 µL reaction volumes.

Rho Activity Assay

The assay was performed according to the manufacturer's protocol (#BK036, Cytoskeleton, Inc, Denver, CO). Briefly, Cells were plated at 20% confluence to reach 70-80% confluence after 48hrs. Then, cells were serum starved for 24 hours by washing twice with PBS and replacing medium with serum-free medium. Medium containing lysophosphatidic acid (LPA) was added for the indicated times to stimulate Rho activity. The cells were then lysed and harvested for active Rho pulldown. As a positive control, a fraction of cellular lysate was pre-loaded with GTPγs before performing pulldown. 15uL rhotekin-RBD beads was added to equal total protein amounts from each condition and incubated at 4°C for 1 hour. The beads were washed and boiled in 1X laemmli buffer, and then analyzed by western blot.

Chapter 3: Inhibition of cyclin-dependent kinases with Dinaciclib is effective at reducing tumor growth in an orthotopic PDX model of CC-RCC.

Introduction

Clear cell renal cell carcinoma (CC-RCC) is the most common and deadly form of renal malignancies, which account for 4.2% of cancer cases and 2.4% of cancer deaths yearly in the US[2]. CC-RCC is resistant to conventional chemotherapy[9], and the lack of effective treatment options has been a major detriment to clinical outcomes in advanced CC-RCC tumors. Despite some recent advancements in targeted therapies including tyrosine kinase inhibitors (TKIs) and immune checkpoint inhibitors[23], only ~30-40% of patients respond to treatment, with less than 10% achieving complete responses[16,23,93]. The 5-year survival rate of late stage CC-RCC therefore remains dismal[2], and development of novel targeted therapies remains an urgent clinical need.

Cyclin-dependent kinases (CDKs) are a family of serine/threonine kinases that act as master regulators of the cell cycle and transcription[40]. Since almost all tumors have defects in the regulation of cell cycle and proliferation, CDKs have long been attractive targets for cancer therapy. However, the use of CDK inhibitors in the clinic has so far been limited and the results have been disappointing to date[41]. One problem with early generation CDK inhibitors was the lack of specificity toward individual CDKs. Pan-CDK inhibitors such as Flavopiridol and Roscovitine showed broad toxicity and were ineffective in clinical trials[42,43]. Second generation CDK inhibitors are more selective toward subsets of CDKs. For example, palbociclib is a CDK4/6 inhibitor that was shown to significantly delay progression of hormone-receptor positive breast cancer[46]. Dinaciclib, another second generation CDK inhibitor used in the current study, inhibits CDKs 1, 2, 5 and 9.

Dinaciclib is potent and effective in preclinical models[47,94], but thus far has not been effective in clinical trials of patients with previously treated advanced breast cancer or non-small cell lung cancer, while showing some promising activities in relapsed multiple myeloma[95] and chronic lymphocytic leukemia[96]. Importantly, the failure of these clinical trials may be due in no small part to lack of prognostic biomarkers and patient stratification criteria to accurately select patients who may benefit from treatment with CDK inhibitors. Clinical trials in solid tumors have been limited to treatment-refractory patients and Dinaciclib has not yet been tested in CC-RCC.

Importantly, CDK inhibition has been shown to target MYC-driven tumors. Specific inhibition of CDK1 was selectively lethal to MYC-dependent breast cancer cells[97]. Likewise, CDK9 expression was found to be crucial for the survival of MYC-addicted hepatocellular carcinoma cells[98]. It is therefore possible that specific inhibitors of either CDK1 or CDK9 may be useful targeting tumors with MYC overexpression, which happens in up to 50% of all cancers. In CC-RCC, MYC activation is a common event, providing a solid rationale for testing CDK inhibitors in this cancer type. 25% of CC-RCC tumors have genomic amplification of 8q.24, which harbors the *MYC* oncogene[99]. Furthermore, 80% of CC-RCC have deactivation of the Von-Hippel Lindau tumor suppressor (*VHL*)[100] leading to stabilization of Hypoxia-Inducible Factor (HIF)-2α, which enhances MYC expression and potentiates MYC transcriptional output[101]. While most CDK9 inhibitors to date have shown cross-reactivity with other CDKs, there are currently some promising novel CDK9-specific inhibitors in Phase 1 trials, including BAY1143572 (enrolling patients with both solid and hematological malignancies)[102] and AZD4573 (hematological malignancies only)[103].

In this study, CDK inhibition with Dinaciclib showed potent anti-proliferative and pro-apoptotic effects both *in vitro* and *in vivo* using patient-derived xenograft (PDX) CC-RCC tumors. Furthermore, specific CDK9 inhibition mimicked the effects of dinaciclib *in vitro* and is sufficient to induce apoptosis in CC-RCC cells but not non-transformed epithelial cells. Together, this work supports the strategy of targeting CDKs for treating CC-RCC. In the future, research should be focused on further development of specific CDK inhibitors to reduce off-target effects, and rigorous characterization of companion biomarkers to properly stratify patients that will benefit from CDK inhibitors.

Results

Dinaciclib reduces proliferation of CC-RCC cells in vitro

To assess the effect of CDK inhibition on CC-RCC cell proliferation and viability, we treated a panel of CC-RCC cell lines *in vitro* with Dinaciclib, a CDK inhibitor targeting CDK 1, 2, 5, and 9. Dinaciclib was effective at reducing the proliferation of all 5 CC-RCC cell lines tested, measured by ATP content using the Cell Titer Glo assay (CTG) after 5 days of treatment (Figure 3.1A). To further examine Dinaciclib's effect on CC-RCC, we plated cells freshly harvested from 3 CC-RCC patient derived xenograft (PDX) tumors grown subcutaneously in mice and treated the cells with Dinaciclib. All 3 PDX tumor cell lines were sensitive to Dinaciclib treatment, with a similar sensitivity to established CC-RCC lines (Figure 3.1B). We also tested 3 breast cancer cell lines to compare this effect across different tumor types. In agreement with previous reports[49], the triple-negative breast cancer cell line MDA-MB-231 was sensitive to Dinaciclib, while the ER+ cell lines T-47D and MCF-7 were partially and fully resistant, respectively (Figure 3.1C). The IC_{50} values for all CC-RCC cells ranged from 5 – 13nM, while breast cancer cells had a wider range

(Figure 3.1D, no IC_{50} achieved in MCF-7 cells). To further test the sensitivity of the PDX tumor cell lines in a physiologically relevant 3D environment, we implanted the tumor cells using a 50:50 mixture of Matrigel (a basement membrane extract from the Engelbreth-Holm-Swarm mouse sarcoma) and growth medium. 2 out of the 3 PDX tumors formed robust organoid-like structures when cultured in 3D, and the growth of these organoids (measured using CTG assay) was sharply reduced when cultured in the presence of Dinaciclib, with similar IC_{50}s to 2D culture (Figure 3.1E, 3.1F). In summary, inhibition of CDK 1, 2, 5, and 9 with Dinaciclib was effective at reducing the proliferation of all CC-RCC cell lines tested (5 cell lines, 3 PDX tumor cell lines), and was effective in both 2D and 3D cell culture assays. Dinaciclib inhibits CDK 1, 2, 5 and 9[94]. CDK1 is crucial for G2/M progression[104], while CDK2 and CDK5 are reported to enhance Retinoblastoma associated protein (Rb) phosphorylation to drive G1/S progression[105,106]. CDK9 does not affect the cell cycle and instead promotes RNA pol II-dependent transcription of a range of genes, including the anti-apoptotic gene *MCL1*[107] and the oncogenic master transcription factor *MYC* gene[108]. To ensure Dinaciclib effectively inhibits CDK activity, we performed western blot analysis on cells treated with 40nM Dinaciclib for 24 hours. In all CC-RCC lines, Retinoblastoma associated protein (Rb) phosphorylated at Threonine 821/826 (T821/826) was effectively decreased (Figure 3.2A). A similar effect was seen in renal proximal tubule epithelial cells (RPTEC), a non-transformed kidney epithelial cell line (Figure 3.2A), although these cells are less proliferative and thus have lower basal phosphorylation of Rb. In breast cancer cell lines, the ability of Dinaciclib to decrease cellular viability was directly correlated with its ability to affect Rb phosphorylation; in fully resistant MCF-7 cells Rb phosphorylation was unchanged, and in partially resistant

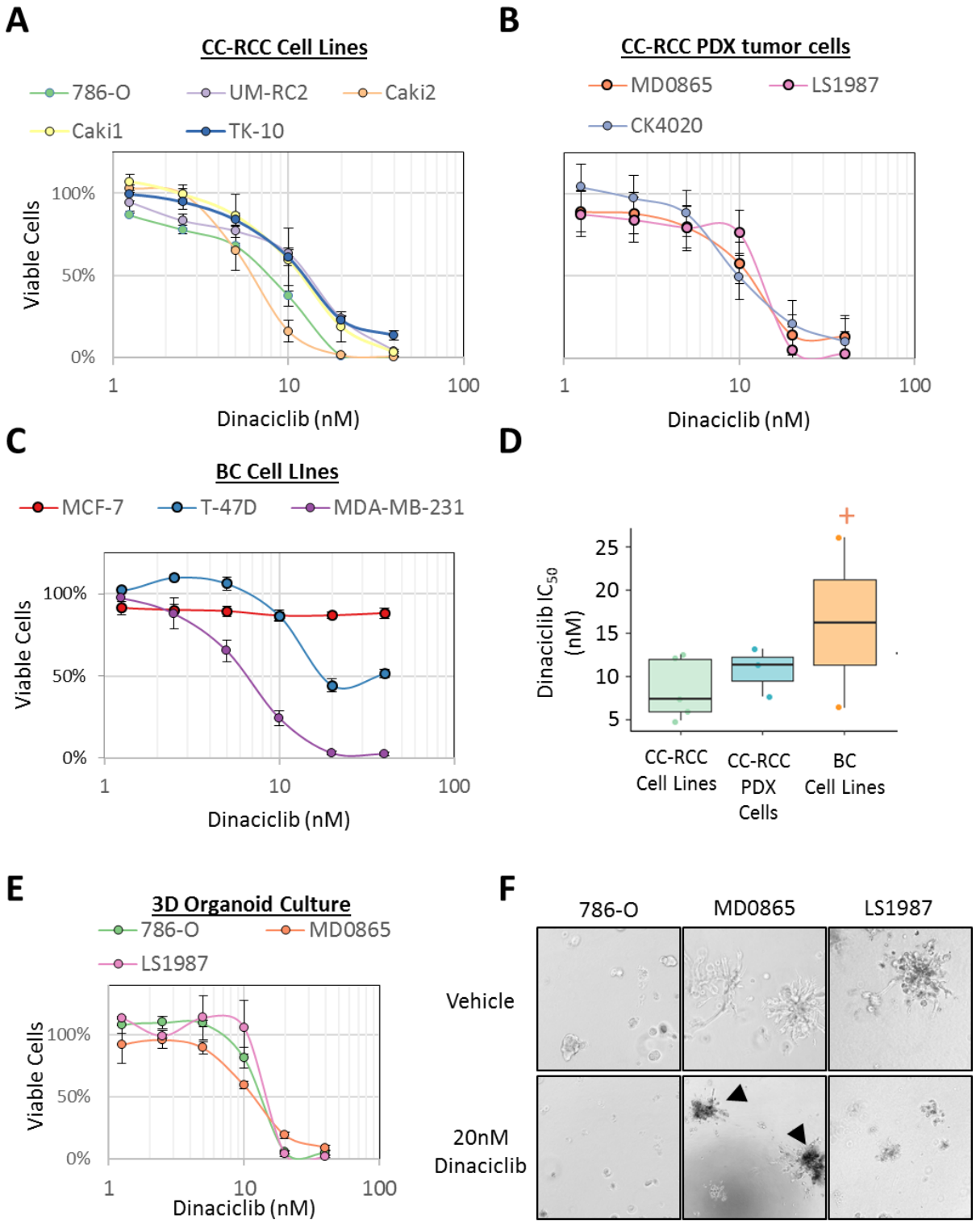
A
CC-RCC Cell Lines
786-O
UM-RC2
Caki2
Caki1
TK-10
Viable Cells
100%
50%
0%
1
10
100
Dinaciclib (nM)
B
CC-RCC PDX tumor cells
MD0865
LS1987
CK4020
Dinaciclib (nM)
C
BC Cell LInes
MCF-7
T-47D
MDA-MB-231
Viable Cells
Dinaciclib (nM)
D
Dinaciclib IC50 (nM)
25
20
15
10
5
CC-RCC Cell Lines
CC-RCC PDX Cells
BC Cell Lines
E
3D Organoid Culture
786-O
MD0865
LS1987
Viable Cells
Dinaciclib (nM)
F
786-O
MD0865
LS1987
Vehicle
20nM Dinaciclib

Figure 3.1: Dinaciclib decreases proliferation *in vitro*.

(A) – **(C) (A)** CC-RCC cell lines, **(B)** CC-RCC PDX tumor cells and **(C)** breast cancer cell lines are sensitive to Dinaciclib, as measured by CTG assay. T-47D cells are partially resistant and MCF-7 cells are fully resistant. Cells were plated in 96 well plates and treated for 5 days with Dinaciclib or vehicle (DMSO), then analyzed using CTG assay. **(D)** IC_{50} values of various cell lines. CC-RCC cell lines, PDX tumor cells and MDA-MB-231 breast cancer cells have IC_{50}s of 5-13nM. T-47D cells have a significantly higher IC_{50}, and MCF-7 cells did not reach an IC_{50} (shown as "+"). **(E)** 786-O cells and 2 PDX tumor cell lines are sensitive to Dinaciclib in 3D. Cells were plated in 50:50 Matrigel:growth medium in ultra-low adhesion 96- well plates and treated as in **(A)-(C),** then analyzed by 3D CTG assay. **(F)** Representative images of organoids from **(E).** Arrowheads mark abnormal organoids that show characteristics of cell death.

T-47D cells, Rb phosphorylation was only partially reduced (Figure 3.2A). Since the CTG assay does not distinguish between inhibition of cellular proliferation and cell death, we assessed the presence of apoptotic markers cleaved caspase 3 and cleaved PARP and found these products in 4 out of 5 CC-RCC cell lines (Figure 3.2A). TK-10 cells, a wild type *VHL* CC-RCC cell line, showed no markers of apoptosis, although the proliferation was still decreased by Dinaciclib (Figure 3.1A). Likewise, RPTEC cells showed no expression of apoptosis markers.

Dinaciclib has been shown to be potent against MYC-driven tumors[109], potentially through a decrease in MYC expression due to CDK9 inhibition[110]. We found that MYC expression was elevated in CC-RCC cell lines compared to RPTEC cells, but MYC protein levels did not decrease in CC-RCC cell lines after 24 hours of Dinaciclib treatment as has been reported in other contexts (Figure 3.2A, left panel)[110,111]. Interestingly, PDX-derived cells did show a decrease in MYC expression after Dinaciclib treatment (Figure 3.2A, right panel), although the total amounts of MYC protein were low compared to RPTEC cells. MCL-1, a key survival protein whose expression is also dependent on CDK9 activity[112], was decreased in all cases. In resistant MCF-7 breast cancer cells, there was no decrease in MCL-1 expression after Dinaciclib treatment (Figure 3.2A).

To determine Dinaciclib's effect on the cell cycle, a panel of cell lines was subjected to cell cycle analysis after 24 hours of dinaciclib treatment. The CC-RCC cell lines 786-O, Caki2, TK-10 and PDX-MD0865 cells were all sensitive to proliferation inhibition by Dinaciclib (Figure 3.1A, 3.1B), but TK-10 and PDX-MD0865 cells did not express apoptosis markers after treatment (Figure 3.2A). In all 3 CC-RCC cell lines tested (786-

O, Caki2, and TK10), there was a significant decrease in S phase cells, indicating a decrease in cells passing through the cell cycle (Figure 3.2B, 3.2C). The appearance of an apoptotic sub-G1 population correlated with the observance of cleaved caspase 3 and cleaved PARP by western blot (Figure 3.2A): 786-O and Caki2 showed induction of apoptosis and sub-G1 cellular content after 24 hours, while TK-10 and PDX-MD0865 did not. PDX-MD0865 had a large amount of sub-G1 cells even without treatment; this is likely because these cells have not fully adapted to cell culture and are experiencing some cell death before treatment. These PDX cells also showed no change in cell cycle distribution after 24 hours, although they were sensitive to Dinaciclib treatment in a 5-day proliferation assay (Figure 3.1B). We observed that freshly isolated PDX cells proliferated much more slowly *in vitro* than the established CC-RCC lines (note the lower basal levels of phosphorylated Rb in Figure 3.2A); therefore, the effects of Dinaciclib may take longer than 24 hours to appear in these cells since they are slowly progressing through the cell cycle. In breast cancer cells, the sensitive MDA-MB-231 cell line showed a decrease in S phase cells and an increase in sub-G1 cells after dinaciclib treatment, while the resistant MCF-7 cells showed no change in cell cycle distribution (Figure 3.2B, 3.2C)

Because some cell lines did not show signs of apoptosis by western blot or cell cycle analysis (Figure 3.2A-3.2C), we investigated the importance of apoptosis on Dinaciclib's inhibition of cellular proliferation seen in Figure 3.1. We treated 786-O cells with Dinaciclib for 5 days (as in Figure 3.1A) in the presence of the pan-caspase inhibitor Q-VD-OPh to inhibit apoptosis. Interestingly, while Q-VD-OPh completely prevented cleavage of caspase 3 and PARP (Supplemental Figure 3.1A, tested 24 hours after treatment), no difference was seen in cellular proliferation in a 5-day assay (Supplemental Figure 3.1B).

This suggests that Dinaciclib's effect on cellular proliferation (Figure 3.1A) is independent of apoptosis, although Dinaciclib does induce apoptosis in some cell lines (Figure 3.2A-3.2C).

Since 80% of CC-RCC tumors lose functionality of the tumor suppressor *VHL*[100] and HIF-2α overexpression (a consequence of *VHL* loss) was reported to enhance MYC activity[101], we next asked if Dinaciclib is selective against *VHL*-deficient cells. To answer this, we generated a 786-O cell line stably expressing pVHL (protein product of the *VHL* gene) and compared its sensitivity to the parental cells. Interestingly, pVHL expression and the accompanying decrease in HIF-2α protein levels did not change the sensitivity of 786-O cells to Dinaciclib treatment in a 5-day viability assay (Supplemental Figure 3.1A). However, we found that pVHL expression completely reversed the induction of Caspase 3 cleavage and PARP cleavage after 24 hours of Dinaciclib treatment (Supplemental Figure 3.1B). These results suggest that pVHL expression does not protect cells from the anti-proliferative effects of Dinaciclib, but pVHL may alter the cellular response to Dinaciclib to inhibit the expression of apoptosis markers.

Dinaciclib preferentially targets actively dividing cells.

CDK inhibitors are thought to be most effective against actively dividing cells, which could create a therapeutic window for targeting the proliferative nature of cancer cells. To determine if Dinaciclib was more potent against cycling cells, we compared the sensitivity of 786-O cells grown in Fetal Bovine Serum (FBS)-containing medium versus cells cultured in medium without FBS (starved). In a 48-hour viability assay, Dinaciclib was effective at decreasing the proliferation of actively dividing cells (Fig 3.3A), while inducing

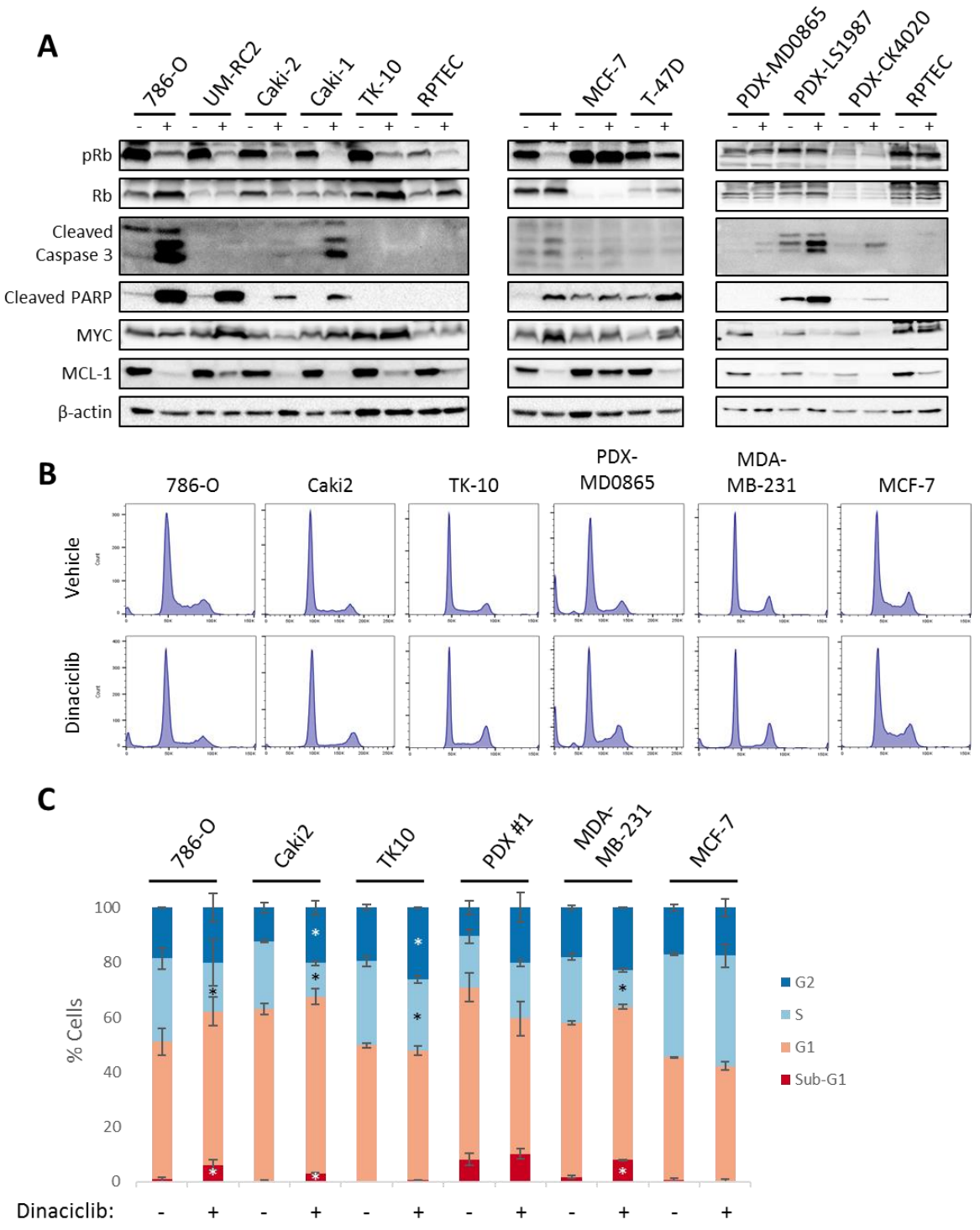
A
786-O
UM-RC2
Caki-2
Caki-1
TK-10
RPTEC
MCF-7
T-47D
PDX-MD0865
PDX-LS1987
PDX-CK4020
RPTEC
pRb
Rb
Cleaved Caspase 3
Cleaved PARP
MYC
MCL-1
β-actin
B
786-O
Caki2
TK-10
PDX-MD0865
MDA-MB-231
MCF-7
Vehicle
Dinaciclib
C
786-O
Caki2
TK10
PDX #1
MDA-MB-231
MCF-7
% Cells
100
80
60
40
20
0
G2
S
G1
Sub-G1
Dinaciclib: - + - + - + - + - + - +

Figure 3.2: Dinaciclib decreases Rb phosphorylation, induces apoptosis, and decreases MCL-1 expression.

(A) Effects of CDK inhibition with Dinaciclib varies across different cell lines. Rb phosphorylation decreases in all CC-RCC cell lines but not in resistant MCF-7 cells. In PDX cells, Rb phosphorylation is low and a non-specific band is present (n.s.). Cleaved Caspase 3 and Cleaved PARP are expressed in some cell lines but not others. MYC expression is unchanged in cell lines but decreased with Dinaciclib treatment in PDX cells (far right panel). MCL-1 expression was decreased with Dinaciclib treatment in all cells except resistant MCF-7 cells. Cells were plated and treated with 40nM Dinaciclib for 24 hours and analyzed by western blot. PDX cells in the far-right panel were plated from freshly harvested xenograft tumors and allowed to establish for several days in culture before treatment. **(B)** Representative cell cycle analysis plots. All sensitive cell lines except PDX-MD0865 showed a decrease in the S phase population, while some cell lines showed an increase in sub-G1 apoptotic population and G2 population upon Dinaciclib treatment. Cells were treated with 40nM Dinaciclib for 24 hours and then stained with propidium iodide and analyzed by flow cytometry. **(C)** Quantitation of cell cycle analysis experiments. Cell cycle distributions were calculated using Dean Jett Fox model on FlowJo version 10. Significant changes upon Dinaciclib treatment are shown as a "*" within the significant cell cycle parameter. Each experiment was repeated 2-3 times, and error bars represent the standard error of the mean. Significance was calculated using unpaired student's t test. *$p<0.05$

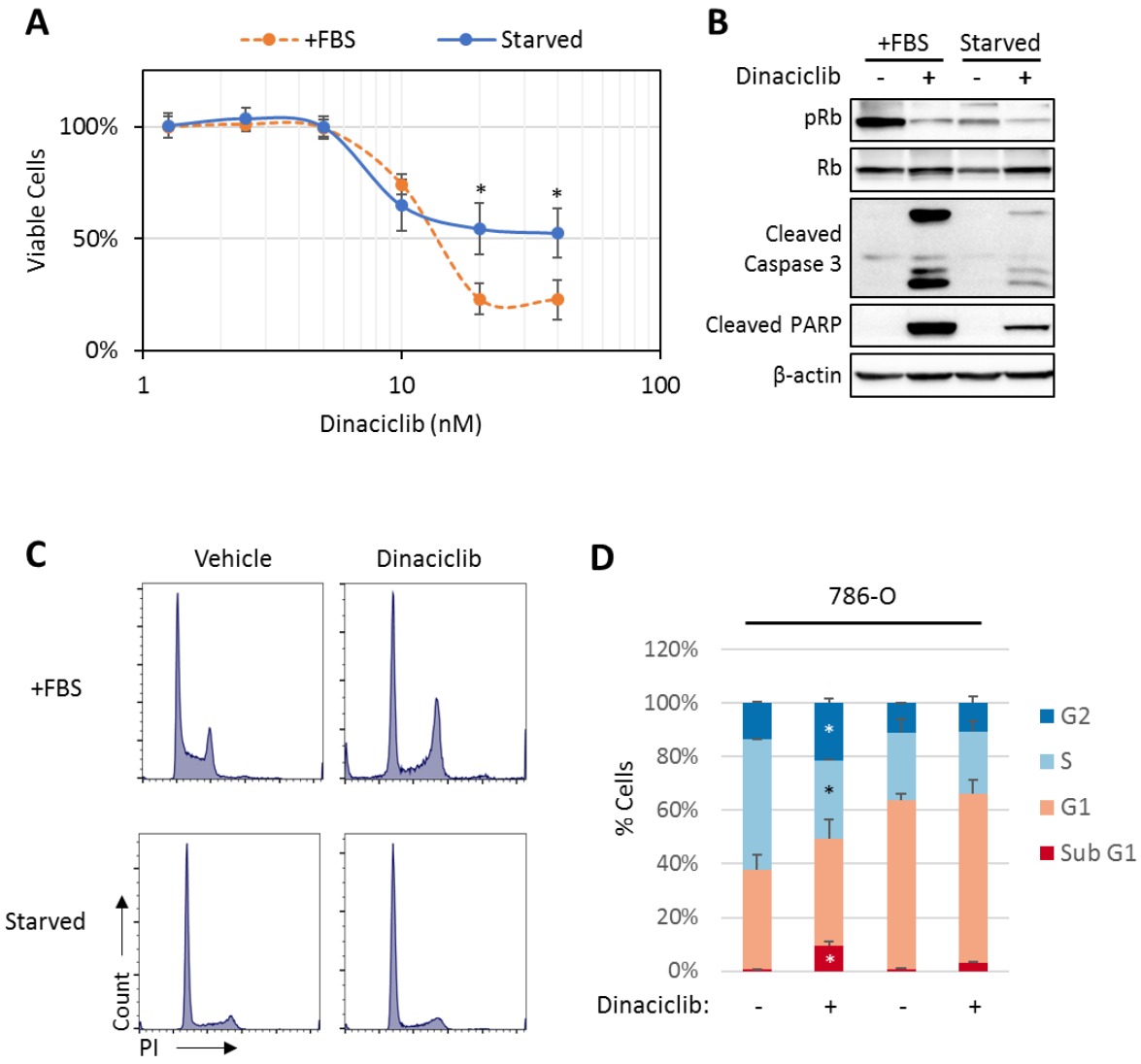

Figure 3.3: Dinaciclib preferentially targets actively dividing cells.

(A) Dinaciclib is more toxic to growing cells than serum starved cells. Cells were grown in growth medium ±FBS for 24 hours, then treated for 48 hours with increasing concentrations of Dinaciclib and analyzed by CTG assay. **(B)** Serum starved cells show less induction of apoptosis markers upon Dinaciclib treatment and less overall Rb phosphorylation. Cells were grown in growth medium ±FBS for 24 hours, then treated with Dinaciclib for 24 hours and analyzed by western blot. **(C)** Dinaciclib affects the cell cycle in growing cells, but not serum starved cells. Cells were grown in growth medium ±FBS for 24 hours, then treated with Dinaciclib for 24 hours and harvested for cell cycle analysis. A representative picture of 2 independent experiments is shown. **(D)** Quantitation of cell cycle analysis experiments in **(C).** Cell cycle distributions were calculated using Dean Jett Fox model on FlowJo version 10. Significant changes upon Dinaciclib treatment are shown as a "*" within the significant cell cycle parameter. Each experiment was repeated 2-3 times, and error bars represent the standard error of the mean. Significance was calculated using unpaired student's t test. *$p<0.05$

apoptosis markers (Figure 3.3B) and arresting cells at G1/S and G2/M checkpoints (Figure 3.3C). The survival of starved 786-O cells was less affected by Dinaciclib treatment (Figure 3.3A). These starved cells had decreased basal Rb phosphorylation (Figure 3.3B) and were mostly dormant at G1/S, with no change in cell cycle distribution after dinaciclib treatment (Figure 3.3C). These cells also showed a weaker induction of apoptosis markers (Figure 3.3B). Taken together, these results show that Dinaciclib has a stronger toxic effect toward actively dividing cells concurrent with arrest at G1/S and G2/M, while being less active against dormant cells. The increased toxicity toward actively dividing cells is likely due to inhibition of CDKs involved in the cell cycle (e.g. CDK 1,2 and 5), while toxicity even in the absence of cell cycle arrest may be the effect of global changes in gene transcription due to CDK9 inhibition.

Dinaciclib inhibits proliferation of non-transformed renal epithelial cells but does not induce cell death.

Although Dinaciclib inhibited the proliferation of all CC-RCC cell lines tested, markers of apoptosis were only detected in some cell lines. Importantly, we showed that non-transformed RPTEC cells did not express cleaved caspase 3 or cleaved PARP after treatment with Dinaciclib. Therefore, we next asked if Dinaciclib was selectively toxic against cancer cells compared to normal renal epithelial cells. To answer this, we compared the sensitivity of 786-O cells to RPTEC cells and Madin Darby Canine Kidney (MDCK) cells, two non-transformed renal epithelial cell lines. RPTEC and MDCK cells were only slightly more resistant to Dinaciclib treatment in 5-day proliferation assays of sparsely plated, actively dividing cells (Figure 3.4A). To compare the sensitivity of these cells at a higher density where cells are not rapidly dividing, 786-O and RPTEC cells were plated and immediately treated with Dinaciclib at a low density or allowed to form a

monolayer before treatment. Dinaciclib was able to inhibit the proliferation of both 786-O and RPTEC cells (Figure 3.4C, rows 1 and 3), but only induced massive cell death in densely plated 786-O cells and not RPTEC cells (Figure 3.4C, rows 2 and 4). Intriguingly, this difference does not appear to be cell cycle dependent, since both cell lines are mostly dormant when plated as a monolayer (Figure 3.4D-3.4E). Although they did die at later time points (Figure 3.4B, 3.4C, 5 days after treatment), 786-O cells plated as a monolayer did not show any change in cell cycle distribution or induction of apoptosis markers by western blot after 24 hours of treatment (Figure 3.4E-3.4F). These results suggest that early induction of apoptosis (<24 hours after treatment) is dependent on the abrupt decrease in Rb phosphorylation and arrest of cells in G1/S and G2/M cell cycle checkpoints, while a delayed induction of apoptosis is not. This is likely due to the differential effects of inhibiting CDK 1 and 2 (involved in G2/M and G1/S progression, respectively) and CDK9, which is not involved in the cell cycle but is important for expression of key survival proteins such as MCL-1. It is likely that inhibition of individual Dinaciclib targets (CDK1, 2, 5, or 9) will have more specific effects that are either completely dependent or independent of cell cycle. Of these, specific inhibitors are only available for CDK1 and CDK9. It is expected that CDK1 inhibition will decrease proliferation and induce cell death in a cell-cycle dependent manner, since the toxic effects of CDK1 inhibition are reported to be dependent on mitosis[113]. Conversely, it is expected that CDK9 inhibition will induce cell death in a cell-cycle independent manner, likely through downregulation of MYC and/or MCL-1 protein levels. Taken together, we found that Dinaciclib exerts two unique and independent effects on cultured cells: inhibition of proliferation and induction of cell death. The anti-proliferative effect is not

selective to cancer cells as both 786-O and RPTEC cells are affected equally, but the induction of cell death was only seen in 786-O cancer cells and not non-transformed RPTEC cells when plated at a high density.

siRNA knockdown of CDK1 or CDK9 is toxic to 786-O cells

Since Dinaciclib inhibits CDK 1, 2, 5 and 9, and displays both anti-proliferative and pro-apoptotic effects, we attempted to elucidate the role of individual CDKs in these processes. We transfected 786-O cells with siRNA pools targeting individual CDKs and investigated the effect on cell growth and induction of apoptosis markers. Knockdown of CDK1 and CDK9 significantly decreased the number of viable cells (Figure 3.5A), with CDK1 knockdown being almost completely effective but CDK9 showing some residual expression (Figure 3.5B). Interestingly, phosphorylated Rb was not decreased in any case, and the total level of Rb was increased in all siRNA conditions (Figure 3.5B). Induction of cleaved PARP expression was seen with CDK1, CDK5 and CDK9 knockdown (Figure 3.5B), but this did not correlate with viability since CDK5 knockdown did not lead to a decrease in viable cell number (Figure 3.5A). Taken together, CDK1 or CDK9 knockdown were the most effective at decreasing the viable cell number in 786-O cells, identifying each as likely effectors of the toxic effects seen with Dinaciclib treatment.

Specific Inhibition of CDK9 shows similar toxicity to Dinaciclib.

CDK9 is an attractive target for cancer therapy due to its seeming requirement for *MYC*-driven tumors[98,109]. CDK9 inhibition induces rapid degradation of certain short-lived proteins such as MYC and MCL-1[108] and induces cell death in hepatocellular carcinoma[98] and B-cell lymphoma[114] models. Since CDK9 does not directly affect the cell cycle, inhibition of CDK9 may more specifically target tumor cells addicted to MYC or MCL-1 expression, decreasing toxicity to normal rapidly dividing cells[115]. Two specific CDK9

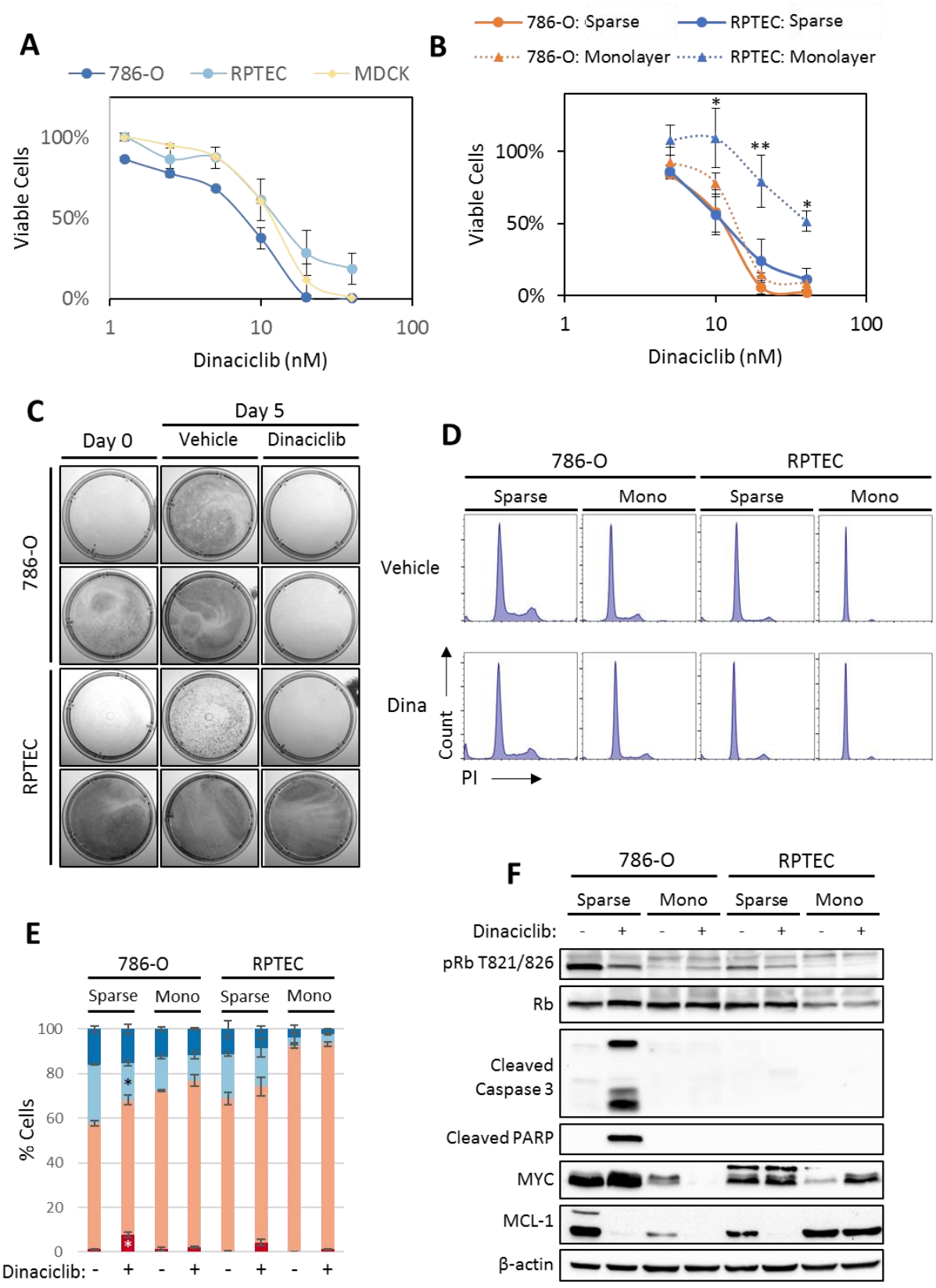
A
786-O
RPTEC
MDCK
Viable Cells
100%
50%
0%
1
10
100
Dinaciclib (nM)
B
786-O: Sparse
RPTEC: Sparse
786-O: Monolayer
RPTEC: Monolayer
Viable Cells
100%
50%
0%
1
10
100
Dinaciclib (nM)
C
Day 5
Day 0
Vehicle
Dinaciclib
786-O
RPTEC
D
786-O
RPTEC
Sparse
Mono
Sparse
Mono
Vehicle
Dina
Count
PI
E
786-O
RPTEC
Sparse
Mono
Sparse
Mono
% Cells
100
80
60
40
20
0
Dinaciclib: - + - + - + - +
F
786-O
RPTEC
Sparse
Mono
Sparse
Mono
Dinaciclib: - + - + - + - +
pRb T821/826
Rb
Cleaved Caspase 3
Cleaved PARP
MYC
MCL-1
β-actin

Figure 3.4: Dinaciclib inhibits proliferation but does not induce cell death in RPTEC cells.

(A) Dinaciclib inhibits proliferation of 786-O cells and non-transformed renal epithelial cells. Cells were plated in 96 well plates and treated for 5 days with Dinaciclib or vehicle (DMSO), then analyzed using CTG assay. **(B)** Dinaciclib is preferentially toxic to 786-0 cells versus RPTEC cells when plated at high density. Cells were plated at low (sparse) or high (monolayer) density in 96-well plates and treated and analyzed as in **(A).** **(C)** Visual representation of results in **(B)**. Cells were plated and treated as in **(B)** on 6cm plates and stained with Crystal Violet at the indicated time points. **(D)** Dinaciclib affects the cell cycle distribution of 786-O cells and induces apoptosis at 24 hours post treatment only when they are plated sparsely and thus are more proliferative. A representative image of 3 independent experiments is shown. **(E)** Quantitation of cell cycle analysis experiments in **(D).** Cell cycle distributions were calculated using Dean Jett Fox model on FlowJo version 10. Significant changes upon Dinaciclib treatment are shown as a "*" within the significant cell cycle parameter. **(F)** Dinaciclib induces expression of apoptosis markers 24 hours post treatment only in sparsely plated 786-O cells. In cells plated as a monolayer, MYC and MCL-1 expression is decreased in 786-O cells but not RPTEC cells. Cells were treated with Dinaciclib for 24 hours and analyzed by western blot. Each experiment was repeated 2-3 times, and error bars represent the standard error of the mean. Significance was calculated using unpaired student's t test. *$p<0.05$, **$p<0.01$

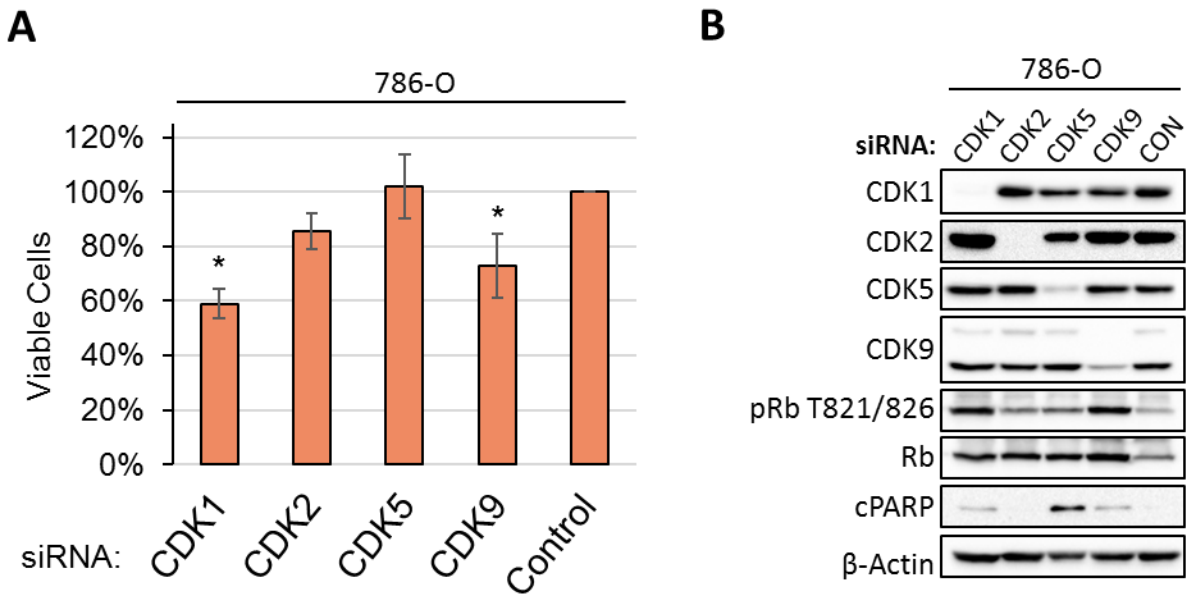

Figure 3.5: siRNA knockdown of CDK1 or CDK9 decreases viable cell number in 786-O cells.

(A) CDK1 or CDK9 siRNA knockdown decreases the total number of viable 786-O cells. Cells were transfected twice with indicated siRNA pools (on Day 1 and Day 4) and analyzed by CTG assay on Day 7. (B) siRNAs are specific to individual CDKs and knock down each target with varying efficiency. Cells were transfected with siRNAs as described in (A) and then analyzed by western blot on Day 6. The experiment was repeated 2 times, and error bars represent the standard error of the mean. Significance was calculated using unpaired student's t test. *$p<0.05$

inhibitors are currently in Phase I trials, being tested in patients with hematological malignancies[103] or a combination of hematological malignancies and solid tumors[102]. To test the effects of CDK9 inhibition in CC-RCC cells, we used the specific CDK9 inhibitor AZD4573[44]. AZD4573 had a similar potency as Dinaciclib in inhibiting the proliferation of sparsely plated 786-O cells (Figure 3.6A). AZD4573 preferentially inhibited the proliferation of 786-O cells compared to non-transformed RPTEC cells at low concentrations, but RPTEC cells were sensitive at higher concentrations (Figure 3.6B). These assays were performed on cells plated at a low density; in the future we will repeat these tests on cells plated as a monolayer to determine if AZD4573 is specifically toxic to densely plated cancer cells versus non-transformed cells. Like Dinaciclib, AZD4573 induced markers of apoptosis and dramatically decreased expression of MCL-1, which is dependent on CDK9 activity (Figure 3.6C)[116]. Because of its unique function, CDK9 does not directly affect Rb phosphorylation; however, we still saw a decrease in Rb phosphorylation upon AZD4573 treatment (Figure 3.6C). AZD4573 induced the expression of apoptosis markers cleaved caspase 3 and cleaved PARP in 2 CC-RCC cancer cell lines and 1 CC-RCC PDX cell line, but not RPTEC cells (Figure 3.6C). These results suggest that AZD4573 will not induce cell death in RPTEC cells (as seen with Dinaciclib in Figure 3.4), but we have not yet tested this. Together, we found that CDK9-specific inhibition mimics the anti-proliferative and pro-apoptotic effects of dinaciclib, and specifically induces expression of apoptosis markers in cancer cells and not normal, non-transformed cells. Further studies are needed to determine if the toxic effects of CDK9 are cell-cycle-dependent.

Dinaciclib reduces tumor growth and induces cell death in an orthotopic PDX model of CC-RCC

To start, we first developed an in-house PDX-based orthotopic mouse model. Low passage (p1 or p2) PDX tumors from CC-RCC patients were obtained from the NIH Patient-Derived Model Repository (PDMR) and implanted subcutaneously in NSG mice. PDX tumors are thought to retain tumor heterogeneity and other clinical features of CC-RCC tumors; as such, all tumors used in animal experiments were never cultured *in vitro*. To label PDX tumor cells for live tracking of tumors, we optimized a cell dissociation and lentiviral infection protocol (total time <4hrs, see materials and methods) and labeled PDX-MD0865 tumor cells with a construct encoding Firefly Luciferase and enhanced GFP (luc2-EGFP). With this method, we were able to transduce ~65% of tumor cells (data not shown). For future experiments and to obtain a pure labeled population, we FACS sorted the GFP+ cells from this tumor and cryobanked labeled tumor pieces for future experiments.

CD105 (Endoglin) is a proposed cancer stem cell (CSC) marker for CC-RCC[117,118]. Early in our study, we analyzed cell surface CD105 expression by flow cytometry and found that 2 out of 3 PDX tumors had a high population of CD105-expressing cells (Supplemental Figure 3.3A). Interestingly, the one tumor that did not express CD105 strongly (PDX-CK4020) grew the slowest *in vivo*, with more than double the time required for palpable tumors to form (data not shown). Although expression of CD105 was reported to be decreased in cultured cells[118], 2 out of 3 CC-RCC cell lines tested (Caki2 and TK-10) also showed high CD105 expression, while 786-O cells were mostly negative (Supplemental Figure 3.3A). Importantly, we confirmed that the $CD105^{hi}$ population from

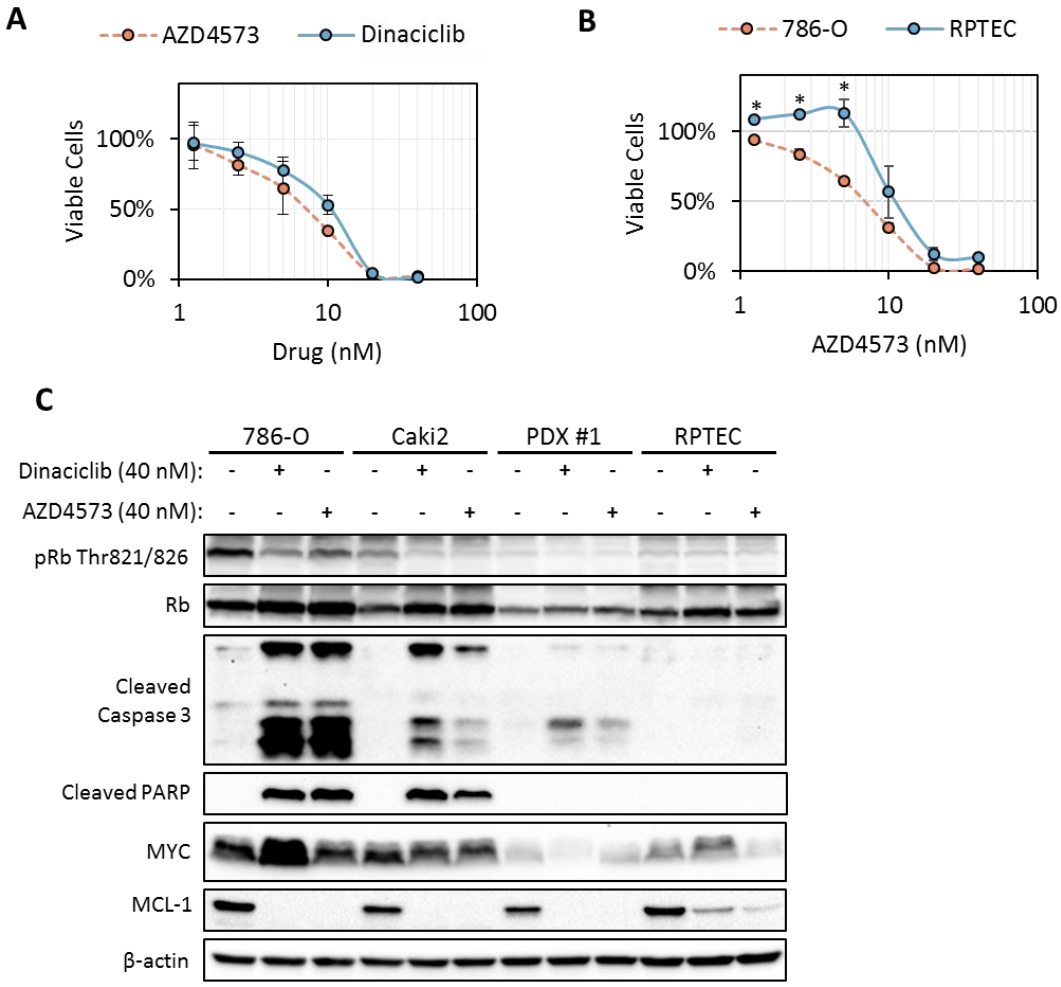

Figure 3.6: CDK9 specific inhibitor AZD4573 decreases proliferation and induces apoptosis markers in CC-RCC cells *in vitro*.

(A)-(B). (A) AZD4573 has a similar potency inhibiting proliferation as Dinaciclib in 786-O cells. **(B)** RPTEC cells are resistant to AZD4573 at low concentrations but sensitive at higher concentrations. Cells were plated in 96 well plates and treated for 5 days with Dinaciclib or vehicle (DMSO), then analyzed using CTG assay. **(C)** AZD4573 and Dinaciclib induce apoptosis markers in 2 CC-RCC cell lines and PDX-MD0865 tumor cells, but not in RPTEC cells. Expression of MYC is higher in CC-RCC cell lines than PDX-MD0865 and RPTEC cells. Dinaciclib and AZD4573 treatment decreases MCL-1 expression in all cell lines, but RPTEC cells retain a low level of MCL-1 expression. Cells were treated with Dinaciclib or AZD4573 for 24 hours and analyzed by western blot. Each experiment was repeated 3 times, and error bars represent the standard error of the mean. Significance was calculated using unpaired student's t test. *$p<0.05$

PDX-MD0865 and PDX-LS1987 had enhanced tumor initiating capabilities by implanting serial dilutions of sorted cells subcutaneously into NSG mice (Supplemental Figure 3.3B).

To evaluate the anti-tumor effects of Dinaciclib in our PDX model, we implanted ~1mm pieces of GFP-luciferase labeled PDX tumors under the renal capsule of NSG mice. Tumor growth was tracked with bioluminescent imaging every week and mice were split into vehicle and treatment groups after 3 weeks. There is significant heterogeneity in these PDX tumor pieces, and we observed that the rate of tumor growth varied widely between tumors. Therefore, we assigned the control and treatment groups to contain a similar distribution of slow and fast-growing tumors (Supplemental Figure 3.4C). Treatment with Dinaciclib for 4 weeks significantly decreased the growth of tumors and decreased the final tumor weight by ~65% (Figure 3.7A, 3.7B). 1 mouse treated with Dinaciclib died early in the study, but it is unclear if this was caused by Dinaciclib treatment or an unknown event. We collected organ tissues for hematoxylin and eosin (H&E) staining and analysis of treatment associated toxicity using terminal deoxynucleotidyl transferase dUTP nick-end labeling (TUNEL) , but this analysis has not yet been completed. Overall, there was no significant difference in body weight changes between mice in the control and treatment groups (Figure 3.7C). Cancer stem cells are generally less proliferative and resistant to chemotherapy[119,120]. Since CDK inhibitors target rapidly cycling cells, CSCs may be insensitive to CDK inhibition. However, $CD105^+$ CSCs in CC-RCC were shown to up-regulate *MYC* expression[118,121], which may render cells more sensitive to CDK1 or CDK9 inhibition. In our model, Dinaciclib treatment did not change the relative amounts of $CD105^+$ cells present in tumors (Figure 3.7D), indicating that Dinaciclib is equally effective against CSCs and non-CSCs.

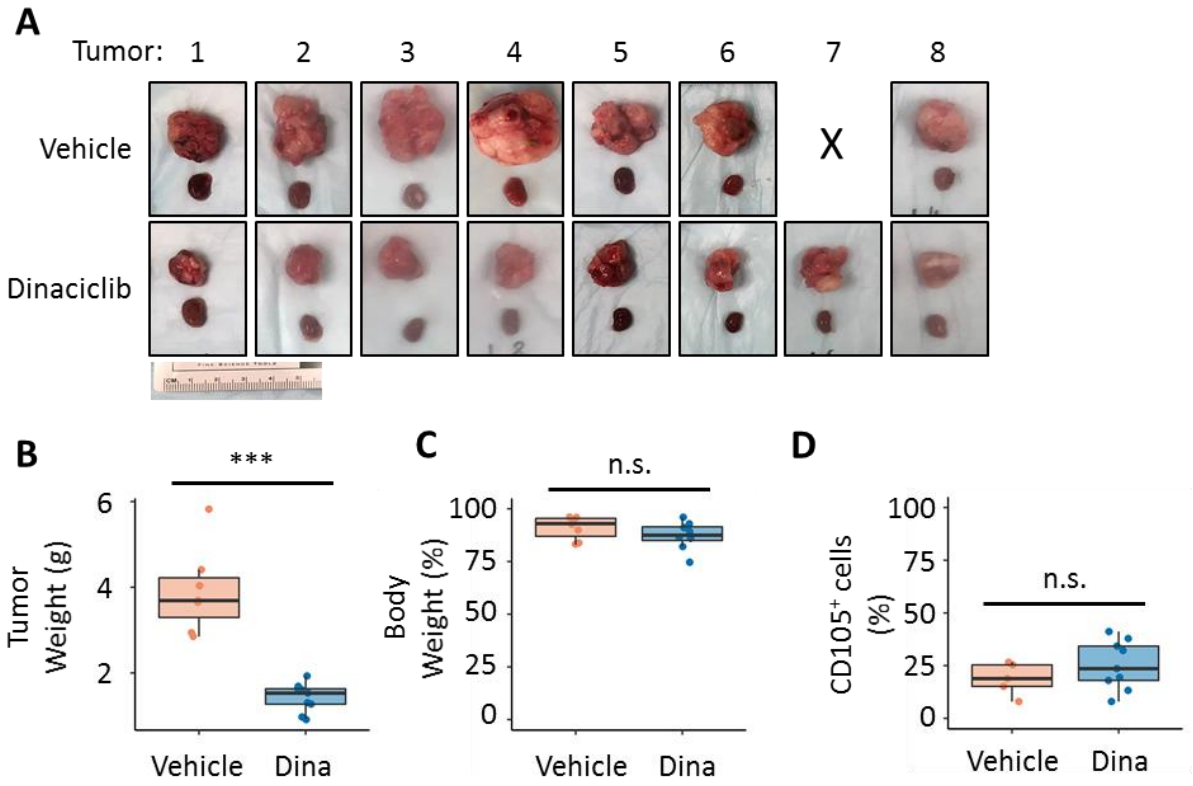

Figure 3.7: Dinaciclib treatment reduces tumor growth in a CC-RCC orthotopic PDX model.

(A) Representative images of paired tumors in vehicle and Dinaciclib treatment groups. Dinaciclib-treated tumors are smaller at time of sacrifice (after 4 weeks of treatment). All tumors were photographed in the same field of few and individual tumors were cropped for presentation purposes. The non-cancerous kidney is shown for reference. **(B)-(D)** Box and whiskers plots: **(B)** Dinaciclib treatment significantly reduces tumor weight. Each point represents a single tumor. **(C)** Dinaciclib-treated group did not show a significant decrease in body weight compared to control group. Mice were weighed each week and the final weight at time of sacrifice was divided by the weight at beginning of treatment. Each point represents a single mouse **(D)** Dinaciclib treatment does not change the total percentage of $CD105^+$ cells in tumors. Tumors were digested to single cells and analyzed for CD105 expression by flow cytometry to quantify CD105+ cells. Each point represents a unique tumor. Significance was calculated using unpaired student's t test. Dina = Dinaciclib, ***p<0.001

Discussion

In this study, we showed that the CDK1/2/5/9 inhibitor Dinaciclib has potent anti-tumor activity in an orthotopic PDX model of CC-RCC. While Dinaciclib has been mostly ineffective as a monotherapy in clinical trials for advanced solid tumors[122,123], there is still significant interest in targeting CDKs in various cancers, and next generation development of novel, more specific CDK inhibitors is ongoing[41,44,102,103].

In CC-RCC, the most common genetic defects involve changes in cellular oxygen sensing (*VHL*), mTOR signaling (MTOR, PIK3CA, PTEN) and chromatin remodeling (PBRM1, BAP1, SETD2)[99]. Loss of *VHL* has been targeted indirectly by anti-VEGF pathway TKIs, which along with immunotherapy represent current standard first line treatments for CC-RCC. mTOR inhibitors are effective in some cases as second line treatment but patient response rate is low (<10%)[17,18,22]. Due to the limited number of targeted therapies available, an expansion of targetable pathways in CC-RCC will likely lead to more effective therapies in the future.

One potential approach for targeted therapy in CC-RCC investigated in this study is to target CDKs. Both CDK1 and CDK9 have been identified as “synthetic lethality” partners with *MYC* overexpression in other cancers such as B-cell lymphoma and hepatocellular carcinoma[97,98]. Since *MYC* amplification is a common event in CC-RCC[99], CDK1 or CDK9 may represent actionable therapeutic targets. Furthermore, CDK1 and CDK9 expression were identified in separate studies as being upregulated in CC-RCC tumors and negatively correlating with patient prognosis[124,125]. These studies, coupled with the fact that *MYC* activity is enhanced through HIF-2α overexpression[101] (a consequence of *VHL* loss in CC-RCC), support the further investigation of targeted CDK1 or CDK9

inhibition in CC-RCC. Recently, CDK2 was shown to negatively correlate with patient survival in CC-RCC patients[126] and CC-RCC cells that developed resistance to mTOR inhibitors (one of the currently available second-line targeted therapies for CC-RCC) upregulated CDK2 and Cyclin A expression[127], highlighting the possibility of applying CDK2 inhibitors as part of combination therapy approaches. However, there is currently no available drug that is fully specific for CDK2[128]. Although not investigated in this study, it should be noted that another potential treatment strategy for CC-RCC is inhibition of CDK4 and CDK6, which are crucial mediators of Rb phosphorylation and G1/S progression. CDK4 and CDK6 are activated by Cyclin D1, which is upregulated as a consequence of pVHL loss in CC-RCC cells[129]. Palbocilib is a CDK4/6 inhibitor that has shown clinical activity and is currently approved for hormone-receptor breast cancer treatment[46]. In the future, it will be beneficial to compare the effects of CDK1 or CDK9 inhibition with CDK4/6 inhibition, especially in the context of biomarker discovery to accurately predict cellular responses to different targeted therapies.

Dinaciclib inhibits CDKs 1, 2, 5, and 9. To narrow down which CDKs may be most important for CC-RCC cellular survival, we knocked down each CDK targeted by Dinaciclib in 786-O cells and found that CDK1 or CDK9 knockdown had the strongest toxic effect. Out of the 4 CDKs targeted by Dinaciclib, CDK1 and CDK9 overexpression are the most negatively correlated with patient survival in CC-RCC in the Cancer Genome Atlas (TCGA) database[130,131] (Supplemental Figure 3.5), and thus may represent actionable targets in the most aggressive tumors. CDK1 has been shown to be synthetically lethal with *MYC* addiction in breast cancer cells[97]. However, due to CDK1's absolute necessity for mitotic progression in non-transformed cells[113] , it is currently

unclear if there is an adequate therapeutic window for targeting CDK1 in cancer cells. CDK9 inhibition may represent a more specific way to target tumor cells dependent on expression of short-lived proteins like MCL-1 and MYC[108,112,114], and two CDK9-specific inhibitors are currently in clinical trials for hematological malignancies[103] and solid tumors[102] . In our *in vitro* studies, Inhibition of CDK9 with the specific CDK9 inhibitor AZD4573 showed very potent effects and was more selective against 786-O cells over RPTEC cells (compared to Dinaciclib), even when the cells were actively dividing (Figure 3.6B). Taken together, these studies suggest that specific inhibition of CDK9 (and potentially CDK1) may represent a novel and promising therapeutic approach in CC-RCC.

The “Cancer Stem Cell” hypothesis postulates that a small sub-population of tumor cells contains the tumor-initiating and tumor-sustaining potential[119]. These CSCs may have very different gene expression programs and behave differently than other cancer cells. For example, *Bussolati et al.* showed in CC-RCC that the $CD105^+$ population had putative tumor-initiating cell properties by sorting patient tumors and implanting the cells at limiting dilutions in mice[117]. The $CD105^+$ population was also found to be enriched in stem cell markers and displayed stem cell behavior *in vitro* and *in vivo*[118,121]. In our study, we confirmed these results by sorting $CD105^+$ cells from two PDX tumors and showing that this CSC population had a significant increase in tumor-initiating potential (Supplemental Figure 3.3). The maintenance of CSCs is thought to drive tumor recurrence and acquired drug resistance; in fact, it has been postulated that chemotherapy enriches for CSCs and may even enhance the formation of a novel CSC population[132,133]. To test how Dinaciclib affects the ratio of CD105+ cells in our CC-RCC PDX tumors, we compared the ratio of $CD105^+$ cells in tumors treated with Dinaciclib or vehicle. We found that while CDK

inhibition with Dinaciclib did not preferentially target CSCs, there was no enrichment after treatment (Figure 3.7D). This result is important since it suggests that Dinaciclib treatment will not lead to expansion of the CSC population as has been reported in other contexts[132,133].

This study shows preclinical efficacy of Dinaciclib in CC-RCC and further supports the rationale for targeting CDK1 or CDK9 due to their importance for survival in CC-RCC cells. Novel, very specific CDK9 inhibitors are currently being developed[44,102] that may hold potential for treating CC-RCC, especially in tumors with MYC overexpression or HIF-2α activation. Finally, if CDK inhibitors are to be successfully applied in the clinic, future research must rigorously characterize companion biomarkers in order to precisely identify patients whose tumors are likely to respond to treatment.

Materials and Methods

Cell culture, plasmids, and reagents

Cancer cell lines used in this study were grown in Dulbecco's Modified Eagle's Medium (786-O, UM-RC2, MDA-MB-231, MCF-7, PDX-MD0865, PDX-LS1987, PDX-CK4020), RPMI 1640 (TK-10, T-47D), or McCoy's 5A (Caki-1, Caki-2) supplemented with 10% Fetal Bovine Serum and 1% Penicillin in a 37°C incubator with 5% CO_2. RPTEC cells were grown in DMEM/F12 medium (Thermo Fisher Scientific) with 5μg/mL insulin, 5μg/mL apo-transferrin, 5ng/mL sodium selenite, 36 ng/mL hydrocortisone, 50 ng/mL human EGF, 1% Penicillin/Streptomycin, and 100 μg/mL G418. Dinaciclib, AZD4573 and Q-VD-OPh (MedChemExpress, LLC) were diluted in Dimethyl Sulfoxide (DMSO) and serially diluted for each experiment.

The following plasmids were used: pBabe_HA-VHL (addgene #19234), pCMV_VSV-G, pCMVΔR8.2, and pFUluc2-EGFP (a gift from Dr. Jennifer Prescher).

Cell Titer Glo Viability Assays

Cells were plated at low density in 96-well tissue culture plates (cell number dependent on cell line), and serial dilutions of experimental compounds were added the next day. After 4-5 days, Cell Titer Glo reagent was added to the plate according to the manufacturer's protocol (Promega, Inc), and luminescence was detected on a Synergy Biotek HT plate reader. For viability assays under serum starvation, cells were pre-starved for 24 hrs before plating in drug-containing serum free medium, and Cell Titer Glo was added after 48 hrs. For 3D viability assays, cells were embedded in 50% Matrigel (Corning)/50% culture medium on ice or in Cultrex PathClear Basement Membrane Extract, Type 2 (Thermo Fisher Scientific) in 96-well plates. The matrix was allowed to harden at 37C for 30 minutes, and experimental compounds were added in culture medium to the appropriate final concentration. After 5 days, Cell Titer Glo 3D reagent was added to the plate according to the manufacturer's protocol.

Western Blotting

Cells were lysed in ice-cold lysis buffer (20 mM Tris pH 7.5, 1% Triton X-100, 150 mM NaCl, 1 mM EDTA/EGTA, 10 mM Sodium Pyrophosphate, 10 mM β-glycerophosphate, 1 mM Sodium Orthovanadate, 50 mM Sodium Fluoride) and scraped into chilled tubes, then incubated on ice for 10 minutes with brief vortexing every 2-3 minutes. Samples were centrifuged at 12,000x g for 10 minutes at 4°C to pellet insoluble material. The soluble fraction was mixed with 5x sample buffer (312 mM Tris pH 6.8, 10% SDS, 10% β-mercaptoethanol, 50% glycerol, 0.05% bromophenol blue) and boiled for 5 minutes at

95°C, then cooled on ice. Total protein content of cell line lysates was assessed using BCA assay (Thermo Fisher cat# 23225).

Protein lysates were loaded onto polyacrylamide gels and run for 30 minutes at 90V, then approximately 90 minutes at 120V. Proteins were transferred to 0.2-µM-pore nitrocellulose membranes and blocked for 60 minutes with 5% non-fat milk in PBS/0.05% Tween-20 (PBS-T). Primary antibodies were diluted in 5% BSA/PBS-T and incubations were performed overnight at 4°C with gentle shaking. Secondary antibodies were diluted in blocking buffer and incubations were performed for 1 hour at room temperature. Images were acquired on the Bio-Rad ChemiDoc XRS+ imaging system.

The following primary antibodies were used: p-Rb T821/T826 #271930 (1:200), Rb #73598(1:200), CDK2 #6248 (1:200), CDK5 #6247 (1:200), CDK9 #13130 (1:200) (Santa Cruz Biotechnology), Cleaved Caspase 3 #9661 (1:1000), Cleaved PARP #5625 (1:1,000), cMyc #5605 (1:1,000), Mcl-1 #4572 (1:1,000), CDK1 #9116 (1:1,000) (Cell Signaling Technology), HIF-1α #610959 (1:250), VHL #564183 (1:500) (BD Biosciences), HIF-2α #NB100122 (1:1,000, Novus Biologicals), and β-Actin #A5441 (1:5,000, Sigma Aldrich).

Cell Cycle Analysis

Cells were plated and treated as described in the text, then dissociated with TrypLE reagent (Thermo Fisher). Cells were collected and centrifuged at 200x g for 5 minutes, washed twice with PBS, and then fixed with ice cold 70% ethanol for 30 minutes at 4°C. Fixed cells were washed once with PBS and the pellet was resuspended in 25 µg/mL propidium iodide + 10µg/mL RNase A in 1% BSA/PBS. Cells were analyzed on a BD

Fortessa flow cytometer. Dean Jett Fox modeling of cell cycle distribution was performed in FlowJo version 10.

Crystal Violet Staining

Adherent cells were rinsed twice with PBS, then fixed and stained in 0.1% Crystal Violet in 0.3% Acetic Acid/95% Ethanol for 15 minutes. Fixed cells were then washed once with PBS and allowed to air dry before acquiring images.

siRNA transfection

The following siRNAs were used: CDK1 #L-003224-00-0005, CDK2 #L-003236-00-0005, CDK5 #L-003239-00-0005, CDK9 #L-003243-00-0005, Non-Targeting siRNA #1 D-001810-01-05 (Dharmacon, Lafayette, CO). siRNAs were pre-mixed with Dharmafect 1 reagent and added to cells during plating on 6cm tissue culture plates according to the manufacturer's protocol. After 3 days, cells were re-plated and re-transfected with siRNAs. After 2 more days, cells were plated on 96-well plates and allowed to incubate for 2 more days before assessing viability with Cell Titer Glo assay (7 days after initial transfection). Cells were collected for western blot analysis 6 days after initial transfection.

Lentivirus Production and Infection

HEK-293T cells were transfected with lentiviral plasmid along with packaging plasmids, pVSVG and ΔR8.2. 1.33ug of each plasmid was added to 20uL PLUS reagent in 750uL DMEM and incubated for 15 minutes. The mixture was then mixed with 30uL lipofectamine in 750uL DMEM and incubated for an additional 15 minutes. The complexes were then added to HEK-293T cells at 70-90% confluence. The next day, the medium was changed to DMEM with 10% FBS and 1% Penicillin/Streptomycin. Viral supernatant was collected at 48 and 72 hours after transfection, filtered through a 0.22-

μM filter, and stored at -80°C until use. Cells were infected by adding viral supernatant directly to cells in a 6-well plate with 6 μg/mL polybrene. After 2-3 days, the medium was changed to medium containing 1 μg/mL puromycin for selection of successfully transduced cells. Selection was carried out until all cells in a non-transduced plate were killed.

For infection of PDX tumor cells with luc2-EGFP virus, a freshly harvested single cell suspension was infected with a 1:1 lentivirus:culture medium with 6 μg/mL polybrene added. The cell/virus mixture was plated on ultra-low adhesion 96-well tissue culture plates and centrifuged at 1,000x g for 90 minutes at 32°C. The cells were then washed twice with PBS and re-implanted in NSG mice subcutaneously for further expansion.

Flow Cytometry and Cell Sorting

Freshly extracted tumors were minced thoroughly and digested in 2mg/mL Collagenase Type IV (Sigma Aldrich, St. Louis, MO) in DMEM/F12 Medium (Thermo Fisher Scientific, Waltham, MA) for 60 minutes at 37°C in a shaking incubator. The resulting suspension was then centrifuged for 5 minutes at 400x g, then washed once with DMEM/F12 and centrifuged again. The pellet was resuspended in 10mL of TrypLE and incubated at 37°C for 10 minutes. The cells were washed once with DMEM/F12 and then resuspended in 1mL DNAse I (20U/mL in DMEM/F12) and incubated for 5 minutes at room temperature. The cells were washed once in DMEM/F12, then filtered through a 70-μM cell strainer and washed once more before resuspending in FACS buffer (1% BSA in PBS).

The cells were stained by resuspending 1,000,000 cells in Zombie NiR viability dye (1:1,000, Biolegend #423105) for 15 minutes at room temperature, followed by one wash in PBS. Then the cells were resuspended in an antibody mixture containing CD105-APC

(1:40, Biolegend #323207), and CD298-PE (1:40, Biolegend #341704) in FACS buffer and incubated for 30 minutes at 4°C. The cells were then washed once with FACS buffer and analyzed in a BD Fortessa Flow Cytometer (BD Biosciences).

For cell sorting, staining was performed as described above, and the cells were sorted on a FACSAria Fusion flow cytometer (BD Biosciences). To separate $CD105^{hi}$ and $CD105^{lo}$ cells, all cells were first gated on CD298-positive cells (denoting cells of human origin) and Zombie NiR-negative cells (viable cells). Then $CD105^{hi}$ cells were gated as the top ~10% of CD105 expressing cells, separated by >1 log fluorescent intensity from the $CD105^{lo}$ population representing the bottom ~20% of CD105 expressing cells. The cells were sorted into DMEM containing 10% FBS, then washed once and resuspended in a 1:1 matrigel:PBS mixture at the appropriate cell concentration and injected subcutaneously into NSG mice.

Animal Experiments

PDX tumor pieces were obtained from the NIH Patient-Derived Models Repository (PDMR) and passaged subcutaneously in NSG mice (NOD.Cg-PrkdcscidIl2-rgtm1Wjl/SzJ, The Jackson Laboratory). Freshly harvested, low-passage tumors labeled with GFP and luciferase (labeled as described in “Lentivirus Production and Infection” section) were minced to pieces of ~1mm diameter and subsequently implanted under the renal capsule of 18 NSG mice. After 3 weeks, mice were injected i.p. with 150 mg/kg D-Luciferin (GoldBio, St. Louis, MO) and bioluminescent images were acquired on a Xenogen IVIS Lumina system. Mice were separated into vehicle and Dinaciclib treatment to equally distribute small and large tumors between the groups (see supplemental figure 3.4). Mice were injected i.p. 3 times a week for four weeks with 30 mg/kg Dinaciclib or

vehicle (20% hydroxypropyl-β-cyclodextrin). Bioluminescent imaging was performed once a week to track tumor growth. After 4 weeks, mice were sacrificed and the tumors were weighed and subjected to downstream analysis including western blot, IHC, and CD105 cell surface staining (see “Flow Cytometry” section).

Chapter 4: Mitotic catastrophe: A potential strategy to target *VHL*-deficient cells

Introduction

Mitosis, the process by which a parent cell divides into two daughter cells, is a crucial and tightly regulated cellular process. It has long been observed that cancer cells in general display mitotic abnormalities[50,53,134]. For example, cancer cells go through error-prone mitoses, leading to loss or gain of chromosomes and aneuploidy generation[135]. This aneuploidy has been suggested to be a driving force of cancer evolution towards a more malignant phenotype caused by general dysregulation of mitotic or proliferation pathways[136]. In this sense, the genomic instability of cancer cells may present a therapeutic window for mitotic agents, a family of drugs that interferes with the ability of cells to undergo mitosis. An example of this would be chemotherapeutic agents targeting microtubules, which have been used in the clinic for many years for various cancers including metastatic breast cancer, ovarian cancer and non-small-cell lung cancer[55,137,138]. Microtubule polymerizing agents like taxanes act by hyperstabilizing microtubules and preventing microtubule shortening[54]. Conversely, microtubule destabilizers like the Vinka alkaloids act in the opposite fashion by stimulating microtubule depolymerization[137]. Interestingly, at low but clinically relevant concentrations, both agents seem to act by decreasing the overall rate of microtubule dynamics, rather than inducing a gross increase or decrease in polymerized microtubule mass, respectively[56,57], underscoring the crucial dynamic regulation of microtubules in normal cell function.

“Mitotic catastrophe” refers to a form of cell death that is a direct consequence of errors during mitosis. Improper segregation of chromosomes during mitosis can lead to aneuploidy and genetic instability[135] (hallmarks of cancer[38]), and the induction of mitotic

catastrophe represents a built-in tumor suppressive safeguard for cells to protect against these effects. Additionally, as described for microtubule poisons, mitotic catastrophe can be caused by a variety of stimuli targeting the mitotic apparatus and thus be induced as a therapeutic endpoint. Although all cells go through mitosis, mitotic agents in the clinic do show some selectivity toward cancer cells. The reason for this may be twofold: 1) Since cancer cells have lost proper regulation of one or more cell cycle checkpoints, they are constantly dividing, and thus going through mitosis. Therefore, mitotic agents may preferentially kill these fast-growing cells. 2) The error-prone mitosis of cancer cells, which may contribute to their aggressive behavior, can also present a therapeutic window, since they may be more sensitive to further perturbations in mitosis and thus mitotic catastrophe.

The tumor suppressor pVHL (the protein product of the *VHL* gene) has been shown to be a key regulator of microtubule dynamics through direct binding to microtubules[87,139]. Furthermore, pVHL was demonstrated to actively contribute to mitotic fidelity, and loss of *VHL* sensitizes cells to the induction of aneuploidy[87]. It is therefore logical that cells lacking pVHL may be hypersensitive to mitotic agents and thus mitotic catastrophe. Since inactivation of the *VHL* gene occurs in >80% of clear cell renal cell carcinoma (CC-RCC), this represents a potential therapeutic strategy for treating CC-RCC.

Rho-associated coiled-coil containing kinase (ROCK) is a key regulator of the cytoskeleton, including microtubules, and ROCK inhibitors have been shown to induce mitotic catastrophe in T cell leukemia cells[140]. In this chapter, I present preliminary results suggesting that induction of mitotic catastrophe with ROCK inhibition may be highly effective in *VHL*-deficient cells. Treatment with the ROCK inhibitor Y-27632 induced

gross mitotic defects in CC-RCC cells that were reversed by pVHL expression in 3 independent cell lines. Moving forward, I outline my plans for further testing this hypothesis, and evaluating novel, targeted mitotic agents in *VHL*-deficient CC-RCC.

Results

ROCK inhibitors induce mitotic catastrophe in *VHL*-deficient cells.

ROCK inhibitors have been reported to induce mitotic catastrophe in T cell leukemia cells by causing centrosome fragmentation and overriding the spindle assembly checkpoint (SAC)[140]. To determine if ROCK inhibition induced mitotic catastrophe in *VHL*-deficient CC-RCC cells, we analyzed the DNA and microtubule patterns in mitotic cells after treatment with Y-27632. Mitotic catastrophe can be caused by the presence of lagging chromosomes that are not attached properly to the spindle pole and may be lost or incorrectly distributed after mitosis[141,142]. Multipolar spindles can arise from defects in centrosome clustering and may also give rise to mitotic catastrophe[143]. Without Y-27632 treatment, the cells showed very little presence of either of these errors. However, after treatment with Y-27632, there was a significant increase in the number of cells with either lagging chromosomes or multipolar spindles, indicating the induction of mitotic catastrophe (Figure 4.1A, 4.1B). As expected, re-expression of pVHL led to a significantly decreased induction of both lagging chromosomes and multipolar spindles, especially after Y-27632 treatment (Figure 4.1A, 4.1B). This effect was repeated in 3 unique cell lines, strongly suggesting that this is indeed due to pVHL expression.

pVHL is a microtubule stabilizer[87], and this effect is likely important for the mitotic effects seen in Figure 4.1A, since microtubule function is critical for assembly of the mitotic spindle. To investigate gross microtubule structure, we performed immunofluorescent

staining of α-tubulin in RCC4 and RCC4-VHL cells expressing pVHL. There was no discernable difference in untreated cells, with both RCC4 and RCC4-VHL cells showing similar microtubule distribution. However, after Y-27632 treatment, RCC4 cells showed a severe disorganization of the microtubule network and seeming loss of a clear microtubule-organizing center, while RCC4-VHL cells did not (Figure 4.1C). These results suggest that loss of pVHL sensitizes the cells to the microtubule disrupting effects of ROCK inhibition.

VHL expression does not alter aneuploidy in RCC10 cells.

RCC10 cells expressing pVHL (RCC10-VHL) had a much lower occurrence of lagging chromosomes and multipolar spindles compared to parental RCC10 cells, both before and after ROCK inhibition. Since mitotic errors can lead to aneuploidy[52], we ran a pilot study investigating the ploidy of RCC10 cells. Chromosome spreads revealed that RCC10 cells are roughly triploid with an average chromosome number of ~70 (Figure 4.2A, B). In untreated cells, pVHL expression did not alter the ploidy of RCC10 cells. However, it is possible that after treatment with a mitotic agent such as Y-27632, significant aneuploidy will be generated in RCC10 but not RCC10-VHL cells, due to the large difference in mitotic defects seen in Figure 4.1. This was not tested in the pilot study but should be tested in the future.

Discussion

In this chapter, we presented preliminary findings that ROCK inhibitors induce mitotic defects specifically in *VHL*-deficient CC-RCC cells, which could be rescued by expression of pVHL. These findings suggest that mitotic catastrophe is important for the toxic effects

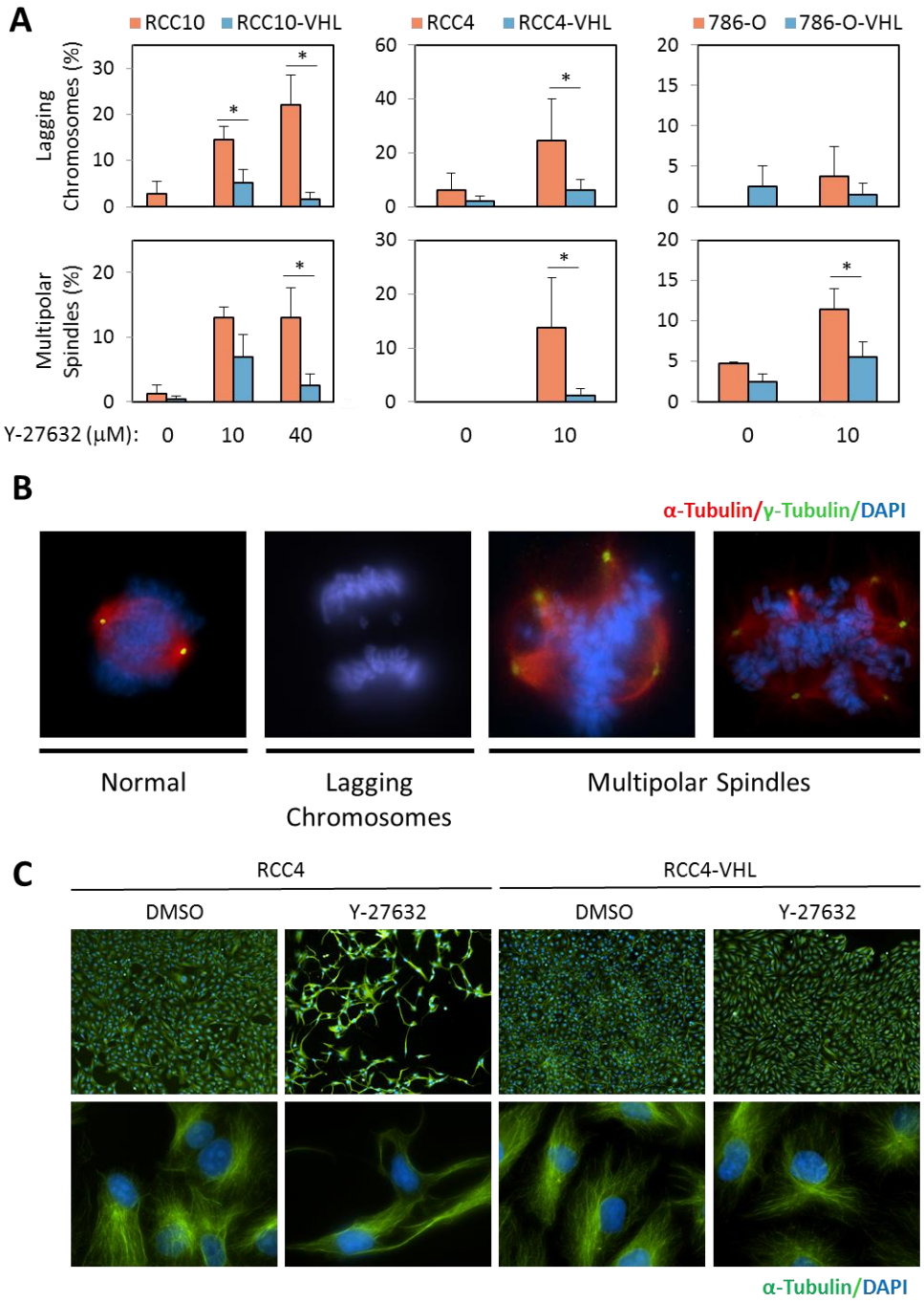
A
RCC10
RCC10-VHL
RCC4
RCC4-VHL
786-O
786-O-VHL
Lagging Chromosomes (%)
Multipolar Spindles (%)
Y-27632 (μM): 0 10 40 0 10 0 10
B
α-Tubulin/γ-Tubulin/DAPI
Normal
Lagging Chromosomes
Multipolar Spindles
C
RCC4
RCC4-VHL
DMSO
Y-27632
DMSO
Y-27632
α-Tubulin/DAPI

Figure 4.1: ROCK inhibition induces mitotic catastrophe specifically in *VHL*-deficient cells.

(A) Expression of pVHL in 3 *VHL*-deficient CC-RCC cell lines decreases the induction of mitotic errors upon Y-27632 treatment. Cells were plated and treated with the indicated concentration of Y-27632 for 24 hours, then fixed and imaged (see materials and methods). Bar graphs show the percentage of total mitotic cells presenting with lagging chromosomes or multipolar spindles. The experiment was repeated 3 times, and at least 50 mitotic figures were analyzed per condition, per experiment. **(B)** Representative images of a normal mitotic apparatus, lagging chromosomes, and multipolar spindles that were quantified in **(A)**. **(C)** Expression of pVHL in *VHL*-deficient RCC4 cells reverses gross microtubule deformation after Y-27632 treatment. Cells were plated and treated with DMSO or Y-27632 for 24 hours, then stained for α-tubulin to visualize microtubules. Top panel: 10X objective, Bottom panel: 40X objective. Statistical significance was determined by unpaired student's t test. *$p<0.05$

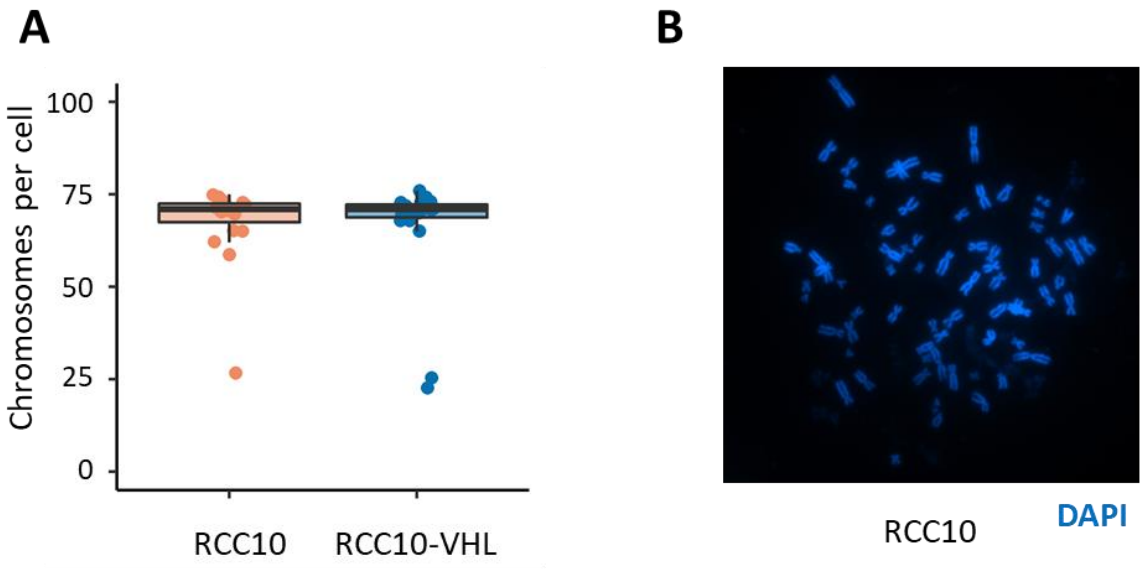

Figure 4.2: pVHL expression does not alter the ploidy of RCC10 cells.
(A) RCC10 and RCC10-VHL cells have a similar, roughly triploid chromosome number. Chromosomes were analyzed by chromosome spread analysis, and each data point represents the chromosome count from a single cell. **(B)** Representative image of chromosomes from a single cell in **(A).**

seen with ROCK inhibitors, although we have not definitively shown this. It will be necessary in the future to determine how ROCK inhibition disrupts the mitotic apparatus in *VHL*-deficient cells. ROCK has a multitude of functions in regulating the cytoskeleton, including microtubule dynamics[144], which is crucial for mitotic spindle assembly. Furthermore, ROCK regulates the actin cytoskeleton, and was shown to be necessary for proper formation of the actomyosin cleavage furrow[145]. It is therefore possible that inhibition of ROCK acts through disruption of gross cytoskeletal dynamics, leading to the mitotic errors seen in Figure 4.1. Alternatively, it is interesting to note that ROCK can function downstream of RhoA and RhoC to promote centrosome duplication, and overactive Rho/ROCK signaling leads to centrosome amplification and chromosomal instability (CIN)[146,147]. Cancer cells often show the presence of supernumerary centrosomes, but are able to execute a successful mitosis by clustering centrosomes to form a normal bipolar spindle[148]. This could explain the results in Figure 4.1A, where CC-RCC cells show minimal mitotic errors in untreated cells. It is possible that ROCK inhibition interferes with centrosomal clustering to cause the observed mitotic defects and cell death, as has been shown for other mitotic kinases including Aurora Kinase A (AurA)[149]. Another report found that ROCK and LIMK inhibitors induced mitotic catastrophe through fragmentation of centrosomes[140]. If pVHL acts to restrain centrosomal amplification through inhibition of Rho/ROCK signaling (as discovered in Chapter 2), this could explain why pVHL-expressing cells are insensitive to the induction of mitotic catastrophe with ROCK inhibitors, since cells *without* supernumerary chromosomes are not sensitive to inhibition of centrosome clustering[150]. Another

possibility is that pVHL-mediated microtubule stabilization protects against the mitotic effects of ROCK inhibition through an unknown mechanism.

Moving forward, it will be beneficial to further characterize the mitotic effects of ROCK inhibitors and expand our studies to include other targeted inducers of mitotic catastrophe. We should determine if pVHL expression represses centrosome amplification in CC-RCC cells, and further determine if this effect is dependent on inhibition of ROCK activity. As mentioned earlier, the mitotic kinase AurA is an emerging cancer therapeutic target in cancer, including breast cancer and KRAS-driven lung cancer[151,152] and induces mitotic catastrophe in acute myeloid leukemia cells[149]. Interestingly, a recent study found that lack of pVHL expression predicted response of CC-RCC cells to AurA inhibition, both *in vitro* and *in vivo*[153], but the role of mitotic catastrophe or centrosome clustering was not investigated. However, these results, combined with the findings in this chapter that *VHL*-deficient CC-RCC cells are sensitive to the induction of mitotic errors, support the further investigation of other mitotic agents in *VHL*-deficient CC-RCC.

Materials and Methods

Cell culture and plasmids

All cancer cell lines used in this study were grown in Dulbecco's Modified Eagle's Medium with 10% Fetal Bovine Serum and 1% Penicillin in a 37°C incubator with 5% CO2. Y-27632 (Selleck Chemicals) was diluted in Dimethyl Sulfoxide (DMSO) and serially diluted for each experiment.

For lentiviral infection and selection of *VHL*-expressing lines, see **Chapter 2: Materials and Methods.**

Analysis of lagging chromosomes and multipolar spindles

Cells were plated onto glass coverslips in 24-well tissue culture plates and treated with Y-27632 or DMSO at roughly 50% confluence. After 24 hours, cells were fixed in ice cold methanol for 15 minutes at -20°C, then washed three times with PBS for 5 minutes each wash. Cells were permeabilized in 0.1% Triton X-100/PBS for 10 minutes at room temperature, then washed three times with PBS. Coverslips were transferred to a humidified chamber and blocked for 1 hour with 10% Normal Goat Serum/1% BSA/0.1% Triton X-100 in PBS, then stained with antibodies against alpha-tubulin (Fitzgerald 10R-T130a, 1:500) and gamma tubulin (Sigma-Aldrich T3559, 1:4,000) overnight at 4°C. Coverslips were then washed 3 times with 0.1% Triton X-100/PBS and incubated for 1 hour with Alexa Fluor 488 goat anti-rabbit IgG and Alexa Fluor 594 goat anti-mouse IgG secondary antibodies (Thermo Fisher) at room temperature. Cells were washed 3 times in PBS, then incubated in 300nM DAPI/PBS for 5 minutes at room temperature. Cells were then rinsed 3x with PBS and mounted onto microscope slides with Vectashield mounting medium (Vector Laboratories).

Lagging chromosomes were observed and the total number of mitotic figures in the appropriate phase (anaphase, telophase, cytokinesis) displaying lagging chromosomes was recorded. The same procedure was performed for quantification of multipolar spindles. At least 50 mitotic figures were counted per condition, per experiment, and each

experiment was repeated at least 3 times. Statistical significance was analyzed using unpaired student's t test. p values less than 0.05 were considered significant.

Chromosome Spreads

Cells were treated with 1ug/mL Colcemid (Sigma) and incubated at 37°C for 1 hour. The cells were then trypsinized and centrifuged at 200x g for 5 minutes. The supernatant was removed and 5mL of ice cold 0.56% KCl was added to the cell pellet followed by gentle inverting to mix, incubated at room temperature for 6 minutes, and centrifuged at 200xg for 5 minutes to pellet. The supernatant was removed and the pellet gently dispersed in the remaining liquid by tapping the bottom of the tube. The pellet was then resuspended in 3:1 methanol:glacial acetic acid dropwise with continuous mixing, then centrifuged at 200x g for 5 minutes. The supernatant was removed, and the pellet resuspended in 1mL of fixative. Slides were prepared by releasing 3 drops of fixed cell solution per slide and allowed to air dry for 1 hour before mounting with Vectashield mounting medium with DAPI (Vector Laboratories). Coverslips were added and sealed with nail polish, then analyzed on a Nikon Ti-E inverted microscope using a 63X oil immersion objective. Only chromosome spreads clearly from single cells were counted.

Chapter 5: The Src/CDCP1/PKCδ pathway is active in a subset of triple negative breast cancer primary tumor specimens

Introduction

Triple negative breast cancer (TNBC) is a heterogeneous group of malignant neoplasms defined by the absence of estrogen receptor (ER), human epidermal growth factor 2 receptor (HER2), and progesterone receptor (PR)[154,155]. Most TNBC are classified histologically as invasive ductal carcinoma of no special type. Recent studies characterizing gene expression profiles of TNBC have broadly classified TNBC into Luminal Androgen Receptor (LAR), basal-like and mesenchymal subtypes[61,62]. The LAR subtype of TNBC expresses androgen receptor (AR) and several other genes involved in androgen and estrogen signalling[61,156]. LAR-TNBC are genetically distinct from other TNBC and have frequent mutations affecting the PI3K signaling pathway[157,158]. In contrast, non-LAR TNBC contain a highly heterogeneous and overlapping set of genomic alterations. Basal-like TNBC are characterized by genomic instability mediated by loss of DNA repair mechanisms controlled by BRCA and a high proliferation rate mediated by loss of cell cycle checkpoint regulation, whereas mesenchymal TNBC are enriched for markers of epithelial-mesenchymal transition (EMT) and cancer stem cells[157–163]. Despite progress in understanding the biologic heterogeneity of TNBC, there remains a clear need for development of new targeted molecular therapies and companion biomarkers for each subtype of these aggressive neoplasms.

The proto-oncogene c-Src is a membrane bound cytoplasmic tyrosine kinase, the cellular form of the transforming protein of Rous sarcoma virus, and the first protein tyrosine

kinase to be discovered[164]. c-Src is the prototypical member of the Src family of non-receptor tyrosine kinases (SFK), which has 9 members. Activation of c-Src and other SFK ("SFK" and "Src" are used interchangeably in this report) has been implicated in the progression of multiple solid tumors, including breast cancer[165–170]. Src activity is increased in breast cancer tissue relative to normal breast tissue and is particularly elevated in subsets of triple negative and HER2+ carcinoma[171]. Early biochemical studies concluded that Src activation in solid tumors was the result of increased enzyme activity and/or increased expression[172–175]. Recent large-scale genomic sequencing studies have not identified Src gene amplification or activating Src mutations in solid tumors[176–178]. This has confirmed the concept that dysregulation of allosteric control mechanisms and/or dysregulated expression contribute to activation of Src in human cancer, but the relative contributions to cancer progression of these two possible mechanisms for Src activation is unknown. Similar to most protein kinases, Src activity is tightly regulated by phosphorylation of several key residues[179,180]. Src is negatively regulated via phosphorylation by C-Terminal Src Kinase (Csk) at a conserved C-terminal tyrosine (Y527 in chicken Src, Y530 in human Src; the chicken protein sequence numbering is commonly used in literature and in this paper). This locks Src in an inactive conformation through an intramolecular interaction between phosphorylated Y527 and the Src SH2 domain[181]. Dephosphorylation at Y527, which disassembles the autoinhibited conformation and promotes autophosphorylation of Src at Y416, is the first step in the canonical pathway of Src activation. Full activation of Src requires phosphorylation of Y416 at the activation loop, locking the catalytic domain of Src in an active conformation[182]. Biophysical analysis of free energy landscapes of the Src kinase domain

indicate the dephosphorylated enzyme can adopt a broad range of conformations, consistent with experimental observations that the kinase domain displays some catalytic activity when the activation loop is not phosphorylated[183]. It is not clear how stable dephosphorylated Src is in vivo or precisely how autophosphorylation of Y416 is regulated, but phosphorylation of Src at Y416 is known to occur in the context of dimerized and activated receptor tyrosine kinases (RTKs) and αβ-integrin complexes[184,185]. Activated Src controls a host of cellular functions, including proliferation, differentiation, and cell migration/invasion, through multiple downstream effectors[185,186].

CUB-domain containing protein 1 (CDCP1) is a transmembrane glycoprotein that is both a Src kinase substrate[187,188] and activator, regulating phosphorylation of some Src substrates, including Protein Kinase C delta (PKCδ)[189,190]. CDCP1 is expressed in embryonic stem cells and many cancer cell types[191]. We and others have shown that CDCP1 is highly expressed and activated in TNBC[63,64], driving tumor progression and metastasis in animal models. CDCP1 can be expressed at the cell membrane as a full-length ~140 kDa form (flCDCP1) and/or a cleaved ~70-80 kDa form (cCDCP1)[192]. Several reports have suggested that cleavage of CDCP1 promotes Src activation *in vitro*, CDCP1 downstream pro-metastatic signalling[66,67], and also allows CDCP1 dimerization necessary for its activity in TNBC[64]. The pro-tumorigenic effects of CDCP1 depend on co-expression of Src, which is capable of phosphorylating CDCP1 at multiple cytoplasmic tyrosine residues[68,69,187,189]. Accordingly, in this branch of oncogenic Src signaling, phosphorylation of CDCP1 at Y734 by Src generates a high affinity binding site for the SH2 domain of Src[190,192], which is critical for CDCP1 phosphorylation at other residues (including Y743) and for CDCP1 downstream signaling[187,189]. PKCδ binding to CDCP1

stimulates PKCδ phosphorylation at Y311 by Src[190,193] and increases cell migration and invasion[194]. PKCδ signaling has been implicated in several types of cancer and appears to have a role both in regulation of cell proliferation and apoptosis, as well as the migratory behavior of cancer cells[194–197]. However, the role of PKCδ in TNBC pathogenesis remains unclear. Nevertheless, the Src/CDCP1/PKCδ signaling pathway appears to be clinically relevant since CDCP1 tyrosine phosphorylation has been correlated with the phosphorylation of SFKs and PKCδ in non-small cell lung cell (NSCLC) tumor samples[198] and breast tumor samples[68]. Although the Src/CDCP1/PKCδ pathway was shown to be active in TNBC cell lines and cell-line-based animal models, there is a lack of studies directly analyzing this signaling pathway in a cohort of TNBC patient samples.

To study Src/CDCP1/PKCδ signaling in TNBC, we first evaluated the expression of specific phosphorylated isoforms of Src, CDCP1, and PKCδ by immunohistochemistry (IHC). Since CDCP1 cleavage cannot be assessed by IHC due to the lack of antibodies exclusively recognizing the cleaved isoform, we developed a method to extract protein from formalin fixed paraffin embedded tissue samples to conduct western blots. The ability to perform western blots enabled the analysis of several phosphoproteins that we were unable to detect by IHC using standard automated immunostainer protocols. The results were evaluated in the context of luminal differentiation and EMT by subgrouping TNBC according to expression of FOXA1 and vimentin. Our results reveal a pattern of Src, CDCP1, and PKCδ phosphorylation that suggests this signaling pathway is active in a subset of TNBC. Lastly, in silico analysis indicated that Src Y416 phosphorylation in TNBC is associated with expression of immunomodulatory genes.

Results

Clinical and pathologic analysis of TNBC data set

To characterize the set of 56 formalin fixed paraffin embedded (FFPE) TNBC patient samples analyzed in this study we first performed IHC staining for several markers distinguishing LAR-TNBC from basal-like and mesenchymal TNBC, the largest subgroups of TNBC with distinct clinical and pathologic features. Forkhead Box Protein A1 (FOXA1) acts upstream of AR and was reported to be overexpressed in LAR-TNBC5. FOXA1 was expressed by tumor cells in 24 out of the 56 TNBC foci (43%). FOXA1 expression was focal (range 20%-90% of tumor cells; median 50%) in 7 foci and complete (100% of tumor cells) in 17 foci, with all positive tumor cells displaying nuclear staining. Tumor foci with >20% FOXA1 positive tumor nuclei were considered FOXA1-positive (FOXA1+). The clinical and pathologic features of the TNBC cohort analyzed in this study are shown in Supplemental Table 5.1 in relation to expression of FOXA1. Patients with FOXA1+ tumors were on average nearly 20 years older than those with FOXA1-negative (FOXA1-) tumors (p=0.0008). All patients who presented with locally advanced disease (T3 or T4, 5 out of 56 patients) had FOXA1- tumors. FOXA1 expression was not significantly associated with nodal stage; however, FOXA1- tumors were more likely to be histologically high grade (p=0.03) and to have a Ki67 proliferation index greater than 30% (p=0.006). These findings indicate that FOXA1 expression identifies a clinically and pathologically distinct subset of TNBC. Since FOXA1 is differentially expressed by LAR-TNBC, FOXA1+ TNBC are expected to overlap extensively with tumors designated LAR based on published gene expression profiles[61,156]. Mesenchymal TNBC subtype was reported to be enriched for markers of epithelial-mesenchymal transition (EMT)[61,161]; accordingly, we assessed the EMT status in our TNBC cohort based on expression of a

classical EMT marker—vimentin[199]. FOXA1 expression was inversely associated with expression of vimentin suggesting that LAR-TNBC are less likely to undergo EMT (Supplemental Table 5.1). Basal TNBC subtype was reported to express SOX10, a neural crest transcription factor[200]; accordingly, we assessed SOX10 expression in our TNBC cohort. FOXA1 expression was inversely related to SOX10 expression, but some FOXA1+ tumors expressed both SOX10 and vimentin (data not shown), suggesting the existence of a TNBC subset with a hybrid luminal-basal phenotype. Surprisingly, CK5/6 (another proposed marker of basal TNBC[201]), was detected in both FOXA1+ and FOXA1- tumors. This may reflect previous observations that CK5/6 staining alone is not sufficient to classify all basal-like tumors[202].

Src is phosphorylated at Y416 in a subset of TNBC samples

To identify TNBC foci with active Src signaling, tissue sections were stained with an antibody recognizing Src phosphorylated at Y416, which is considered to be the classic Src "activation" marker[203]. Of note, the phospho-specific Src_pY416 antibody used in this study (Cell Signaling Technologies #2101) may recognize the activated form of multiple Src family kinases (SFK), including Src, Fyn, Yes, Lyn, Lck, and Hck. By established convention, the term "Src" is used to indicate "SFK" in this report. Src_pY416 was detected in 23 (41%) of the 56 TNBC foci in this cohort. The staining pattern was almost entirely membranous: no nuclear or diffuse cytoplasmic staining was observed (Figure 5.1A; Figure 5.1B shows an example of a negative sample). This finding is consistent with reports indicating that Src activation occurs predominantly at the cell membrane[184]. A similar staining pattern was reported by Anbalagan et al. for their cohort of TNBC breast cancer samples[204]. One exception in our cohort was a tumor that lacked membrane staining and had cytoplasmic granular staining of Src_pY416 (Figure 5.1C). The

percentage of Src_pY416+ tumor cells ranged from 5% to 100% (median 50%). Minor non-tumor cell staining, predominantly in lymphocytes, was present in some tumor foci.

We next examined the clinical and pathologic variables of this TNBC cohort in relation to Src_pY416 expression (Supplemental Table 5.2). There was no association between Src_pY416 expression and patient age, tumor stage, nodal stage, histologic grade or Ki67 proliferation index. Expression of Src_pY416 was detected more often in FOXA1-samples, suggesting a trend toward higher Src activation in non-LAR subtypes (Supplemental Table 5.2), but this trend did not reach statistical significance. However, there was a significant association between high levels of Src_pY416 expression and expression of the EMT marker vimentin. Of the 13 tumors in which >20% of tumor cells expressed Src_pY416, 12 also expressed vimentin ($p = 0.03$). The association between Src_pY416 expression and vimentin was not observed in tumors with weak (<20%) expression of Src_pY416. A subset of the TNBC foci in this cohort was evaluated for expression of additional markers associated with EMT, including Slug and N-cadherin, and no clear association with Src_pY416 was identified (data not shown). Together, our IHC analysis identified a subset of TNBC samples with positive Src_pY416 staining that significantly correlates with expression of the EMT marker vimentin.

Phosphorylation of Src at Y416 is associated with phosphorylation of CDCP1 at Y743 and PKCδ at Y311

To confirm that positive Src_pY416 staining corresponds to active Src, we evaluated the phosphorylation of two Src substrates, CDCP1 and PKCδ[188,193], by IHC. Like Src_pY416, the staining pattern of CDCP1 phosphorylated at Y743 (CDCP1_pY743) and PKCδ phosphorylated at Y311 (PKCδ_pY311) was almost entirely membranous: no nuclear or diffuse cytoplasmic staining was observed (Figure 5.1A). 24 foci (43%) were

CDCP1_pY743+ and 17 foci (30%) were PKCδ_pY311+. CDCP1_pY743 and PKCδ_pY311 staining was detected focally in some tumor foci and diffusely in others. The one sample with “granular” Src_pY416 staining also showed granular CDCP1_pY743 staining but was PKCδ_pY311- (Figure 5.1C). The percentage of CDCP1_pY743+ tumor cells ranged from 5% to 100% (median 55%); the percentage of PKCδ_pY311+ tumor cells ranged from 20% to 100% (median 60%). Positive staining of all three phospho-proteins was highly correlated, indicating coactivation in a subset of TNBC samples (Figure 5.1E and Supplemental Table 5.2). Furthermore, CDCP1_pY743 and PKCδ_pY311 staining colocalized with Src_pY416 in samples with focal expression of Src_pY416 (Figure 5.1D, magnified inset shows area of Src/CDCP1/PKCδ co-phosphorylation). Together, these results show that Src_pY416 staining is a valid marker for Src activation in TNBC, which is accompanied by phosphorylation of the Src substrates CDCP1 and PKCδ.

In silico analysis of The Cancer Genome Atlas data suggests that Src is co-phosphorylated at Y416 and Y527 in TNBC and active in that state

To validate our IHC findings, we compiled a list of proteins whose expression and/or phosphorylation correlates with expression of Src_pY416+ in TNBC by analyzing public data from the Cancer Proteome Atlas (TCPA), an arm of the Cancer Genome Atlas (TCGA) that utilized reverse phase protein array (RPPA) to quantify protein-level expression data[205]. Surprisingly, out of 224 proteins analyzed in TNBC (Figure 5.2A), the TCPA marker that most strongly correlated with Src_pY416 was Src_pY527, the canonical marker of inactive Src[203,206]. Other highly correlated protein markers included phosphorylated SHP2, phosphorylated EGFR, and phosphorylated STAT3, all of which are known to be associated with increased Src activity[186,207,208]. CDCP1 and PKCδ

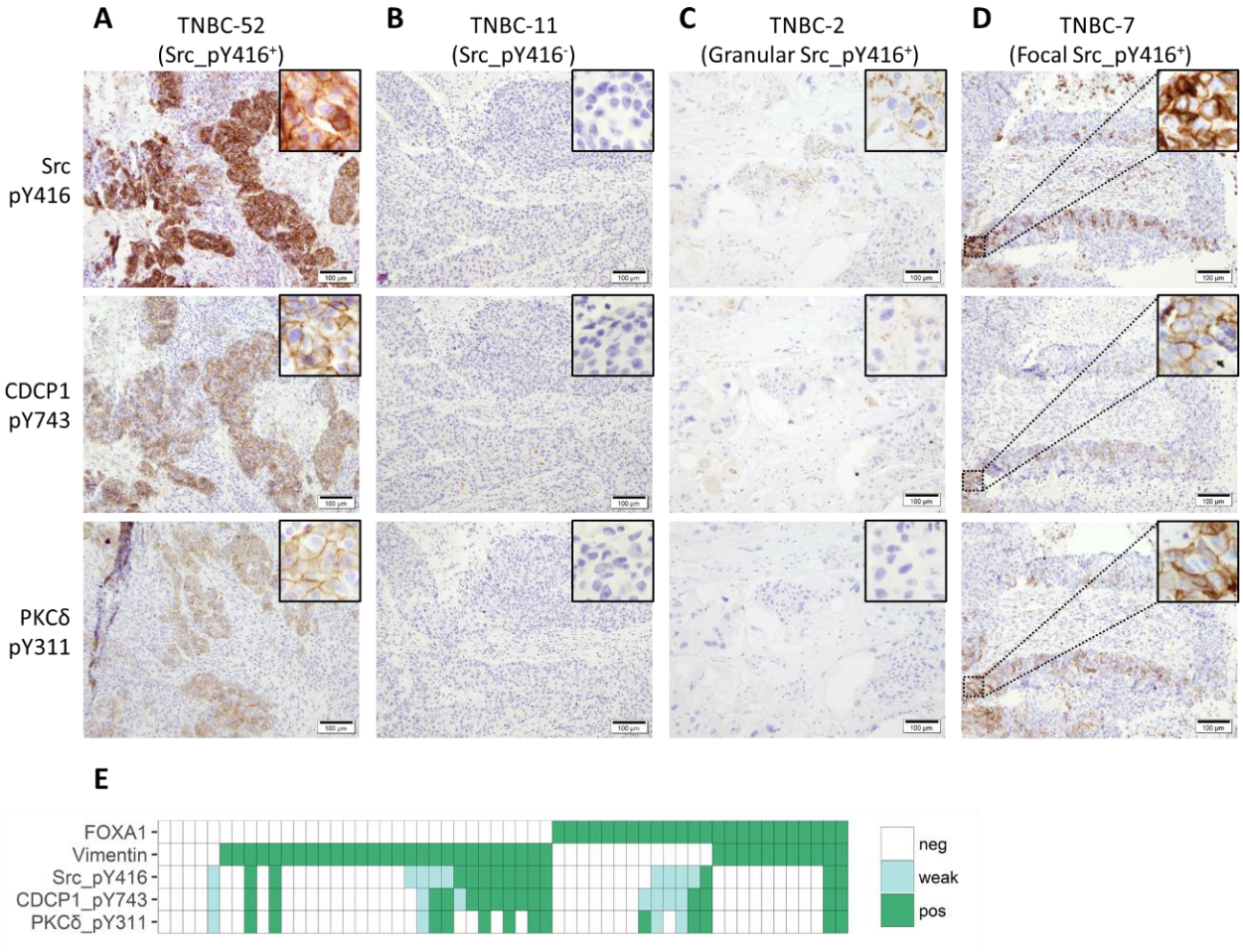

Figure 5.1: Immunohistochemical analysis of Src pathway in TNBC samples.

(A) Representative patient sample with positive staining for Src_pY416, CDCP1_pY743, and PKCδ_pY311. Staining for each marker was detected primarily on the cell membrane. **(B)** Representative patient sample with negative staining. **(C)** One patient sample with a unique "granular" staining pattern for Src_pY416. This sample also showed granular staining for CDCP1_pY743 but was negative for PKCδ_pY311. **(D)** Representative patient sample with positive focal (non-uniform) pattern of staining for Src_pY416, CDCP1_pY743, and PKCδ_pY311 in tumor cells. **(E)** Summary of staining results in panel of 56 TNBC samples. "weak" indicates <20% positive tumor cell staining. Images were acquired using a 10X objective, and insets using a 40X objective.

phosphorylation were not evaluated in this 224-protein dataset. Scatter plot analysis shows a positive correlation between Src_pY416 and Src_pY527, in both TNBC and non-TNBC breast cancer samples (Figure 5.2B). TNBC samples had a higher level of Src_pY416 compared to non-TNBC samples (Figure 5.2C). The level of Src_pY527 did not show the same trend and was similar in TNBC and non-TNBC, suggesting that Src may be regulated differently by phosphorylation and dephosphorylation in different subgroups of breast cancer. Finally, we also examined the TCGA database for mRNA expression levels of Src, CDCP1, and PKCδ in the context of Src_pY416 expression. Src and CDCP1 mRNA expression was elevated in TNBC compared to non-TNBC, while PKCδ expression was decreased (Figure 5.2D). A significant correlation between mRNA expression and Src_pY416 phosphorylation was found for CDCP1, but not for Src or PKCδ (Supplemental Figure 5.1A-C). Together, these data indicate that Src is co-phosphorylated at Y416 and Y527 in a subset of TNBC and is active in this state since phosphorylated SHP2, EGFR, and STAT3 correlate with Src_pY416/ Src_pY527.

Western blot analysis reveals unique Src phosphorylation patterns associated with Src activity and FOXA1 expression in TNBC samples

To further characterize Src and CDCP1 activation status in TNBC, we complemented our IHC data and in silico analysis with western blot analysis of protein lysates extracted from the FFPE tissue samples. Western blotting was crucial to investigate the CDCP1 cleavage pattern associated with Src activation (discussed in the next section), as the two CDCP1 isoforms cannot be distinguished by IHC due to the lack of antibodies that specifically recognize the cleaved isoform. Importantly, western blot analysis of Src_pY416 matched our IHC results: all samples that tested positive for Src_pY416 by IHC also showed a specific band at 60 kDa for Src_pY416 (Figure 5.3A, lanes 4, 8-13).

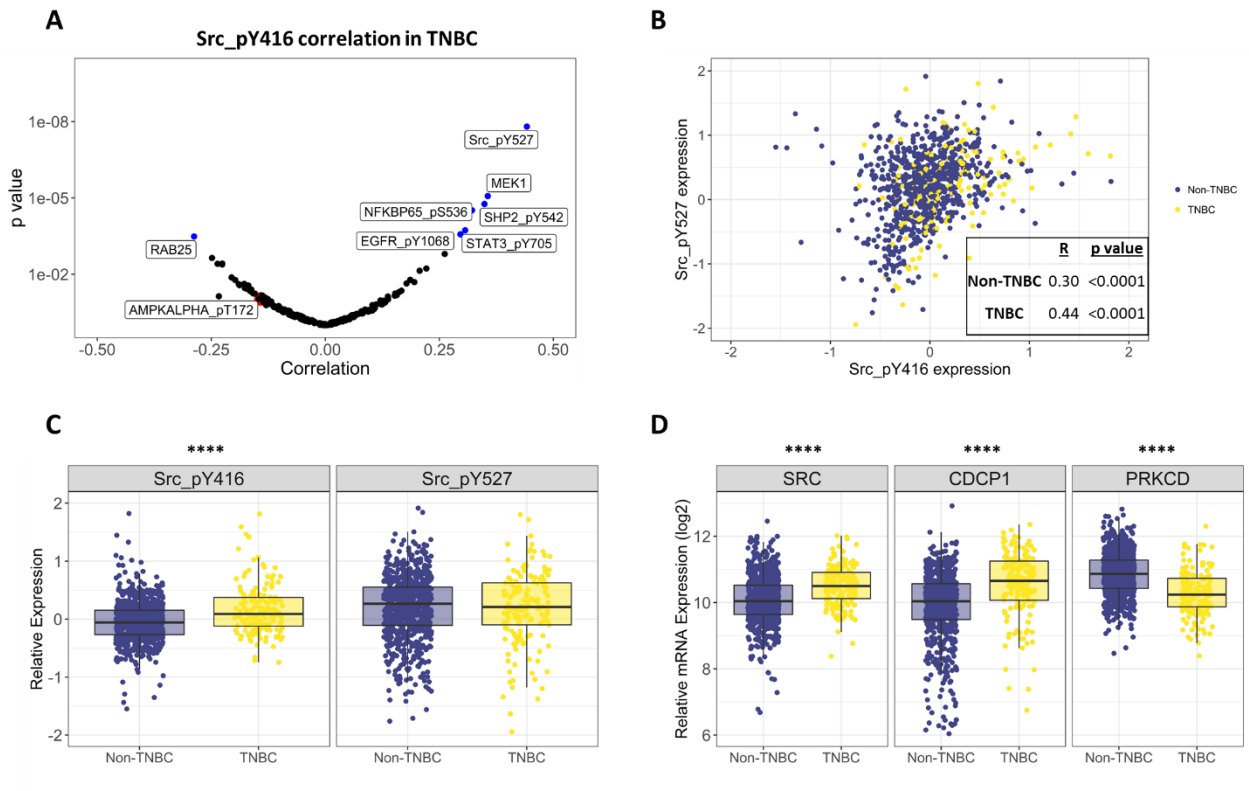

Figure 5.2: *In silico* analysis of Src pathway in TCGA/TCPA public data sets.
(A) Protein expression correlations with Src_pY416 in TCPA dataset. Top 7 proteins are shown in blue and Src_pY527 exhibits the strongest correlation. AMPKα_pT172 (a non-correlative protein used as a control in Figure 5.3) is shown as a larger red point. **(B)** Scatter plot showing correlation between Src_pY416 and Src_pY527 in TNBC samples (yellow) and non-TNBC samples (blue). **(C)** Expression of Src_pY416 is higher in TNBC compared to non-TNBC; expression of Src_pY527 is similar in TNBC compared to non-TNBC. **(D)** mRNA expression of Src, CDCP1, and PKCδ (PRKCD) in TNBC and non-TNBC. Expression of Src and CDCP1 is higher in TNBC compared to non-TNBC, while expression of PKCδ is decreased. Correlations in **(A)** and **(B)** were tested with Pearson's product moment correlation test. p values in **(C)** and **(D)** were derived by unpaired student's t test. **** p<0.0001.

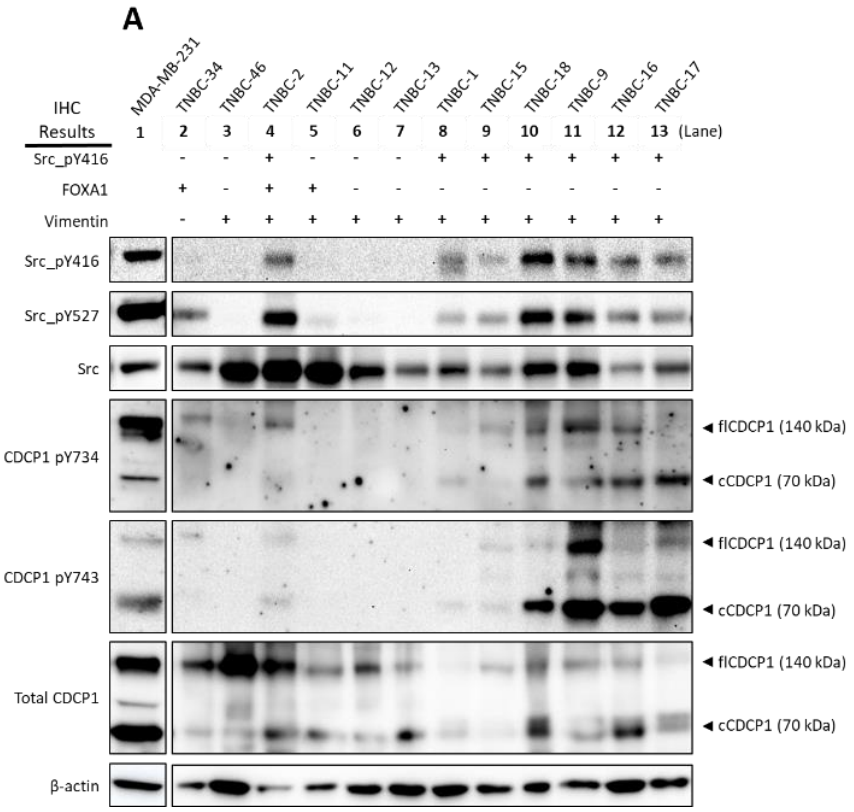
A
MDA-MB-231
TNBC-34
TNBC-46
TNBC-2
TNBC-11
TNBC-12
TNBC-13
TNBC-1
TNBC-15
TNBC-18
TNBC-9
TNBC-16
TNBC-17
IHC Results
1 2 3 4 5 6 7 8 9 10 11 12 13 (Lane)
Src_pY416 - - + - - - + + + + + +
FOXA1 + - + + - - - - - - - -
Vimentin - + + + + + + + + + + +
Src_pY416
Src_pY527
Src
CDCP1 pY734
CDCP1 pY743
Total CDCP1
β-actin
◄ flCDCP1 (140 kDa)
◄ cCDCP1 (70 kDa)

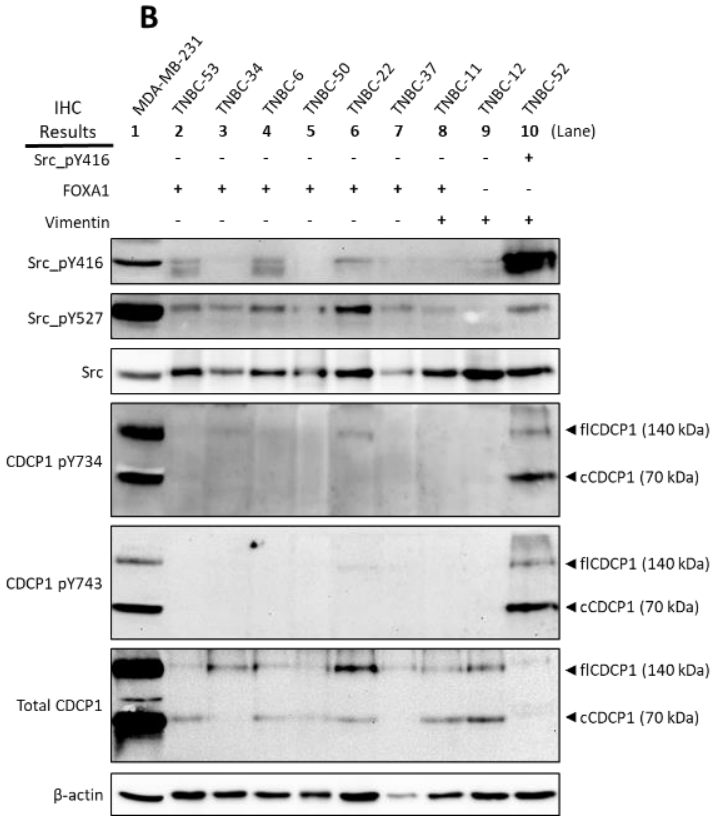
B
MDA-MB-231
TNBC-53
TNBC-34
TNBC-6
TNBC-50
TNBC-22
TNBC-37
TNBC-11
TNBC-12
TNBC-52
IHC Results
1 2 3 4 5 6 7 8 9 10 (Lane)
Src_pY416 - - - - - - - - +
FOXA1 + + + + + + + - -
Vimentin - - - - - - + + +
Src_pY416
Src_pY527
Src
CDCP1 pY734
CDCP1 pY743
Total CDCP1
β-actin
◄ flCDCP1 (140 kDa)
◄ cCDCP1 (70 kDa)

Figure 5.3: Western blot analysis of protein samples extracted from paraffin-embedded TNBC foci for expression and phosphorylation of Src and the Src substrate CDCP1.

FOXA1, vimentin, and Src_pY416 expression was previously assessed by IHC and summarized on top. **(A)** Analysis of vimentin^{+} patient samples showed variable activity of the Src/CDCP1 pathway. All Src_pY416^{+} patient samples as determined by IHC were also positive by western blot. Whole cell lysate from the TNBC cell line MDA-MB-231 was used as a positive control (lane 1). The MDA-MB-231 lysate was run on the same gel (notice similar background of images), but the position was changed manually for presentation purposes. **(B)** Analysis of FOXA1^{+}/vimentin^{-} patient samples showed a trend toward an inactive Src/CDCP1 pathway. Equal amounts of protein were loaded to each lane as quantitated by tryptophan fluorescence spectrometry. β-actin was used as a loading control. flCDCP1 = full-length CDCP1, cCDCP1 = cleaved CDCP1.

Lysate from the TNBC cell line MDA-MB-231, which is known to have an active Src/CDCP1/PKCδ pathway, was used as a positive control (Figure 5.3A, lane 1)[64,194]. Confirming our *in silico* analysis, all tumor foci that were Src_pY416+ were also Src_pY527+ (Figure 5.3A). The Src_pY416 and Src_pY527 antibodies used in this study and in the TCPA dataset may cross-react with multiple SFKs including Src, Yes, Fyn, and Fgr, based on sequence homology[181]. Of the 5 samples in the set analyzed in Figure 5.3A that were Src_pY416-, two showed the classic "inactive" Src phosphorylation pattern of pY416-/pY527+ (Figure 5.3A, lanes 2 and 5) while the others showed little or no staining for Src_pY527 (lanes 3, 6 and 7). Both tumors with the pY416-/pY527+ pattern of phosphorylation were FOXA1+ and therefore presumptively are LAR-TNBC. This prompted us to analyze additional FOXA1+ foci that lack Src_pY416 (Figure 5.3B, lanes 2-8). Src_pY527 was detected in all of these samples. Unexpectedly, a small amount of Src_pY416 was detected in 3 of the samples that were Src_pY416- by IHC (Figure 5.3B, lanes 2, 4, 6), while the other 4 showed the expected "inactive" Src_pY416-/pY527+ pattern (Figure 5.3B, lanes 3, 5, 7-8). Since the tumor cells in the samples represented in lanes 2, 4, and 6 of Figure 5.3B were Src_pY416- by IHC, we considered whether the Src_pY416 seen by western blot in these samples may have originated from non-tumor cells. Indeed, all three of these samples in lanes 2, 4, and 6 contain Src_pY416+ lymphoid cells in the stroma adjacent to the tumor cells; furthermore, the tumor stroma of the samples in lanes 3, 5, and 7-9 is pSrc_pY416- (Supplemental Figure 5.2). For samples without active Src signaling, the data in Figure 5.3A suggest that TNBC without FOXA1 expression are mostly Src_pY527- (Figure 5.3A, lanes 3, 6-7). To confirm this finding, six additional Src_pY416-/FOXA1- foci were evaluated by western blot (Figure 5.4, lanes 2-

7). Five of these tumor samples contained no detectable Src_pY527 (Figure 5.4, lanes 2-3 and 5-7).

In summary, all TNBC samples in this study with active Src contain high levels of both Src_pY416 and Src_pY527 (9/9 samples). In samples with weak or absent Src_pY416 and no detectable Src activity, we saw two different patterns. FOXA1+ samples, i.e. TNBC with luminal differentiation, tend to be Src_pY527+ (7/7 samples, classic "inactive" Src). On the other hand, FOXA1- (non-LAR TNBC) samples that are Src_pY416- tend to be Src_pY527- as well (8/9 samples). Since dephosphorylation of Src Y527 is a critical step in the canonical pathway of Src activation, these samples may represent tumor foci primed for Src activation. This hypothesis suggests that compared with LAR-TNBC, non-LAR TNBC (representing basal and mesenchymal subtypes) contain high levels of Src primed for activation.

CDCP1 is expressed and cleaved in TNBC, but only phosphorylated in samples with active Src

Extracellular proteolytic cleavage of CDCP1 has been implicated in CDCP1 driven activation of Src and is essential for CDCP1-driven metastasis and cell motility[64,66]. To investigate CDCP1 cleavage in primary TNBC tumors, we evaluated CDCP1 isoforms by western blot. CDCP1 was cleaved to varying degrees in all tumor foci analyzed, independent of Src phosphorylation at Y416 (Figures 5.3-5.4). As predicted by our IHC findings, we detected CDCP1_pY743 by western blot almost exclusively in tumors in which Src_pY416 and CDCP1_pY743 were detected by IHC (Figure 5.3A lanes 4 & 8-13, Figure 5.3B lane 10, Figure 5.4 lanes 8-10). The 3 samples that are weakly Src_pY416+ by western blot but have tumor cells that are Src_pY416- by IHC (Figure 5.3B lanes 2, 4, 6) contained no detectable CDCP1_pY743 by western blot, consistent

with the conclusion that the Src_pY416 in these lanes originated from lymphoid cells. As noted above, these samples contain Src_pY416+ lymphoid cells which are not seen in the other samples in Figure 5.3B (Supplemental Figure 5.2). We also analyzed the phosphorylation of CDCP1 at Y734 (CDCP1_pY734) by western blot. Of note, neither the CDCP1_pY743 antibody or the CDCP1_pY734 antibody utilized in this study were validated by the manufacturer for use in paraffin IHC. As it turned out, the CDCP1_pY743 antibody was effective in our IHC procedure while the CDCP1_pY734 antibody was not. Y734 of CDCP1 is reported to be directly phosphorylated by Src and is crucial for Src binding to CDCP1; phosphorylation at Y743 follows phosphorylation at Y734 and is crucial for CDCP1's interaction with other effectors[188,190,209]. Like CDCP1_pY743, CDCP1_pY734 was detected mainly in Src_pY416+ samples, indicating activation of Src/CDCP1 signaling. For both CDCP1_pY734 and CDCP1_pY743, cCDCP1 (~70 kDa) was the dominant phosphorylated isoform, although flCDCP1 (~140 kDa) was also phosphorylated to a varying degree at both sites in samples with activated Src. CDCP1_pY734 of primarily flCDCP1 was detected weakly in some samples with low or absent Src_pY416 (Figure 5.3A lane 2, Figure 5.3B lanes 3 & 6), suggesting that phosphorylation of flCDCP1 at Y734 may occur in the absence of activated Src.

Src/CDCP1/PKCδ coactivation is detected by western blot of TNBC samples

Western blot analysis of Src_pY416+ tumor samples demonstrated co-expression of CDCP1_pY734 and CDCP1_pY743 (Figure 5.3A, lanes 4, 8-13). To further characterize our samples and validate our western blot methods, we analyzed another set of 9 FOXA1-TNBC samples for phosphorylated forms of PKCδ and AMP-activated Protein Kinase Alpha (AMPKα, see below) (Figure 5.4). Three of these samples were Src_pY416+ by IHC; western blot analysis clearly shows that the Src/CDCP1/PKCδ signaling pathway is

only active in these samples (Figure 5.4, lanes 8-10). All samples that were Src_pY416- were also CDCP1_pY734-/pY743- and PKCδ_pY311-. To ensure that the difference in phosphorylation between samples is due to differences in signaling, and not simply differences in sample handling or protein degradation (e.g. cold ischemia time prior to formalin fixation), we also analyzed the expression of AMPKα phosphorylated at Thr172 (pT172), which was not correlated with Src activity in the in silico analysis conducted above (Figure 5.2A). Indeed, we detected AMPKα pT172 across all 9 samples tested, irrespective of Src/CDCP1/PKCδ phosphorylation (Figure 5.4, lanes 2-10), validating the specificity of our method. These data indicate that the Src/CDCP1/PKCδ pathway is active in a subset of TNBC samples.

Src Y416 phosphorylation is associated with expression of immunomodulatory genes

We next asked if Src activation was associated with distinct changes in gene expression. Since our data shows that Src_pY416+ is active independent of Y527 phosphorylation status, we separated TCGA samples into Src_pY416^{hi} and Src_pY416^{lo} groups and looked for differentially regulated genes throughout the transcriptome. The top 100

positively and negatively correlating genes are displayed as a heatmap in Figure 5.5A. The positively correlating genes were analyzed using the STRING database protein-protein interaction (PPI) network and Gene Ontology (GO) analysis[210]. Both analyses showed a strong enrichment for genes and protein networks involved in immune and inflammatory processes as well as cytokine/chemokine signaling (Figure 5.5B-C). Several of these genes have been reported as overexpressed in an “immunomodulatory” (IM) subtype of TNBC[61,157], suggesting that active Src may be a marker for this subset of cases (the full heatmap of positively regulated genes is shown in Supplemental Figure

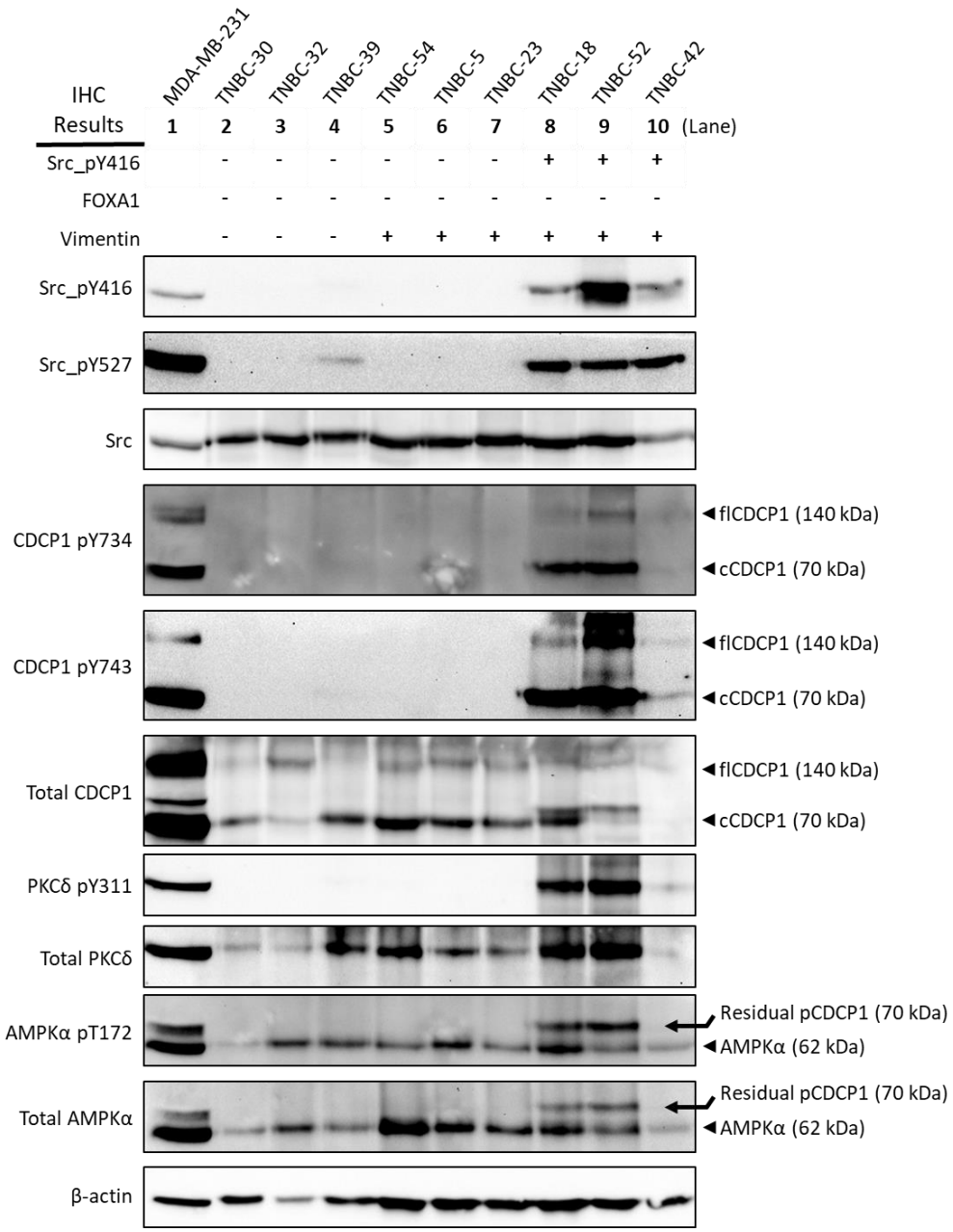

Figure 5.4: Western blot analysis of FOXA1- protein samples extracted from paraffin-embedded TNBC foci for expression and phosphorylation of Src, CDCP1, and PKCδ.

FOXA1, vimentin, and Src_pY416 expression was previously assessed by IHC and summarized on top. All Src_pY416^{+}/pY527^{+} patient samples (lanes 8-10) were CDCP1_pY743^{+}/pY734^{+}, and PKCδ_pY311^{+}. TNBC-42 (lane 10) expresses lower total levels of CDCP1/PKCδ, but still shows the same pattern. Equal amounts of protein were loaded to each lane as quantitated by tryptophan fluorescence spectrometry. β-actin was used as a loading control. flCDCP1 = full-length CDCP1, cCDCP1 = cleaved CDCP1.

5.3). The top negatively correlating genes did not show any significantly enriched GO terms or PPI networks with this method (data not shown). Since an immune signature and expression of immune checkpoint genes may have significance for immunotherapy[211], we analyzed the expression of CTLA-4, PD-1, PD-L1, and PD-L2 in relation to Src_pY416. All 4 genes showed a significant increase in Src_pY416^{hi} samples (Figure 5.5D). Which immune-related genes detected in Src_pY416^{hi} TNBC are intrinsic to the tumor cells themselves and which are expressed by infiltrating immune cells remains to be investigated.

In summary, our data show that Src is co-phosphorylated at Y416/Y527 in a subset of TNBC patient samples and is active in this subset as judged by phosphorylation of its downstream targets CDCP1 and PKCδ. Src activity is positively correlated with expression of the EMT marker vimentin and was seen more often in non-luminal (FOXA1-) tumors. Interestingly, active Src is associated with an immunomodulatory gene expression signature. These findings are relevant to emerging therapies targeting CDCP1 and PKCδ, as well as immunotherapy.

Discussion

The goal of this study was to investigate the activity of the Src/CDCP1/PKCδ pathway in clinical samples of TNBC. Previous studies using fresh tissue detected elevated Src kinase activity in Src immunoprecipitates prepared from clinical samples of triple negative and Her2+ breast cancers[171,172]. Recently various measures of Src activation, including expression of Src_pY416, have been associated with histologic progression of breast cancer[170], latent bone metastasis[212], resistance to targeted hormone therapy[213] and resistance to targeted Her2 therapy[214,215], but the mechanism by which Src activation is

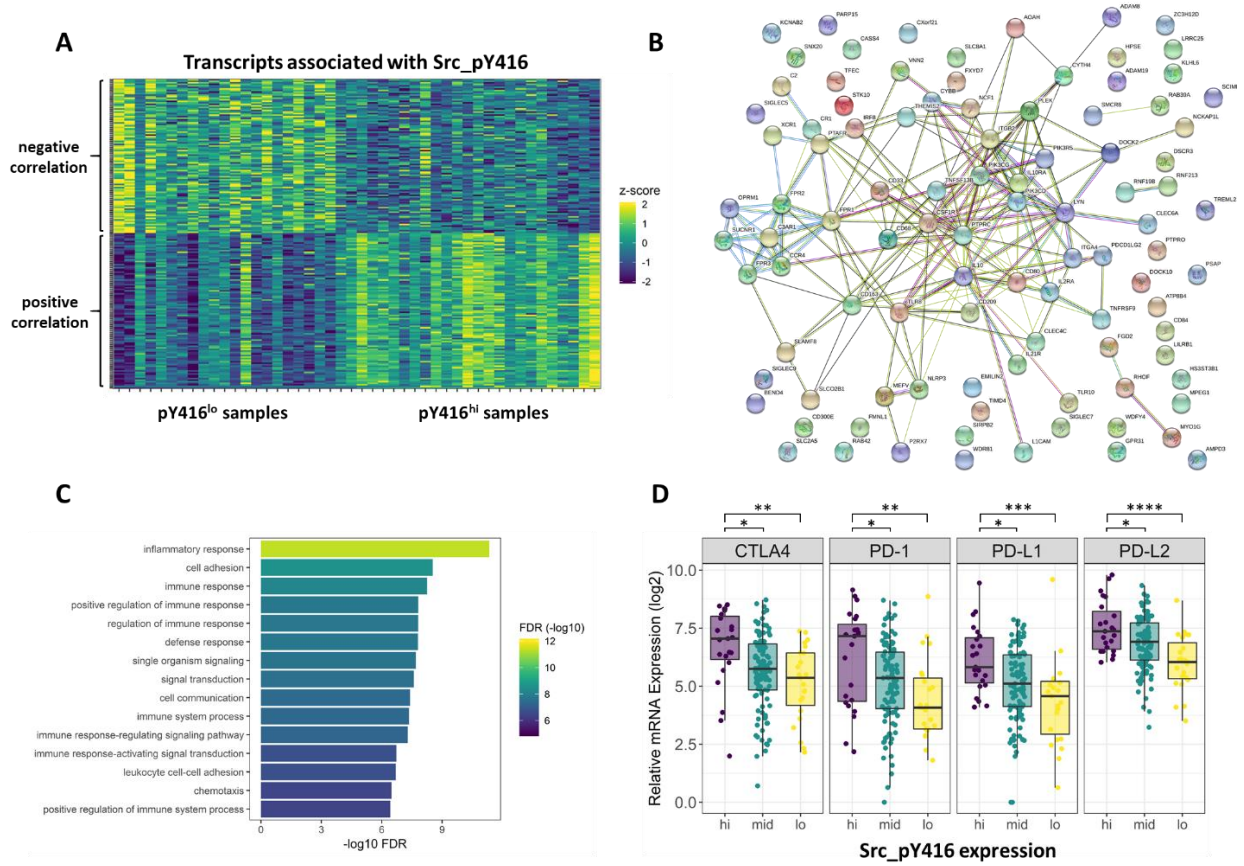

Figure 5.5: Src_pY416 is associated with expression of immunomodulatory genes in TNBC

(A) Heat map showing the top 100 positive/negative gene correlations with Src_pY416 in TNBC. Samples were separated into Src_pY416^{hi} (top 15%) and Src_pY416^{lo} (bottom 15%) to highlight differences in gene expression. **(B)** Protein-protein interaction (PPI) network constructed using the STRING database. **(C)** Gene Ontology analysis of top 100 genes overexpressed in Src_pY416^{hi} samples revealed enrichment in genes involved in immune/inflammatory response. For the top 100 genes underexpressed in Src_pY416^{hi} samples, no significant enrichment terms were discovered (data not shown). **(D)** Comparison of expression levels of cancer-related immunosuppressive genes in TNBC samples separated by Src_pY416 expression. FDR = false discovery rate. p values in **(D)** were derived by unpaired student's t test. *p<0.05, **p<0.01, ***p<0.001, ****p<0.0001.

associated with these phenotypes is not clear. As Src substrates, CDCP1 and PKCδ function downstream of Src. Their activities coordinately promote migration of renal cell carcinoma[194] and TNBC cancer cells[64], and increase anoikis-resistance in lung adenocarcinoma cells[216]. Src activation has been detected in parallel with CDCP1 and PKCδ phosphorylation in a cohort of lung cancer samples[198], and in a set of 8 primary breast cancer samples (with unknown receptor expression status)[68]. This report presents a detailed assessment of the Src/CDCP1/PKCδ pathway in TNBC. Src_pY416, a putative marker of Src activation, was detected by IHC in 40% of TNBC samples analyzed. We found a high degree of correlation ($p < 0.0001$) between the expression of Src_pY416 and the downstream phosphorylation of CDCP1 and PKCδ (Supplemental Table 5.2). These data suggest that immunohistochemical detection of Src_pY416 in resected breast cancer samples indicates activation of Src/CDCP1/PKCδ signaling in the neoplastic cells. No data on clinical outcome are available for the patients whose tumors were analyzed in this study, but expression of Src_pY416 in resected TNBC has been associated with poor prognosis in previous studies[217,218].

Src activation was not associated with any distinct clinical or classical pathologic characteristic in TNBC in this study. However, there was a strong association between Src activation and expression of vimentin, a mesenchymal cytoskeletal protein. This suggests that Src activation in TNBC is associated with epithelial-mesenchymal transition. Previous studies have implicated activation of Src in the progression of ovarian carcinoma cells to an intermediate mesenchymal state associated with anoikis-resistance and spheroidogenesis[219]. We also evaluated FOXA1 expression in our cohort of TNBC samples to investigate Src activation in the context of luminal versus basal differentiation.

FOXA1+ tumors were distinguished by older age at presentation, lower tumor stage and lower proliferative activity. These findings confirm the conclusion of previous studies that LAR-TNBC are clinically and pathologically distinct from the basal-like and mesenchymal subtypes of TNBC[61,156,157,159] and support the use of FOXA1 as a marker of the LAR subtype. We found that Src_pY416 expression was less common in FOXA1+ tumors, but this could potentially be explained by the lower frequency of vimentin+ samples in this group.

Due to the significant sequence homology between Src family kinases[181], the antibodies used in this study may cross-react with several Src family members in addition to c-Src. mRNA expression studies have identified Src and Lyn as highly expressed in breast cancer tissue[220]. Our analysis of TCGA data indicates that Lyn and Yes expression is especially elevated in TNBC compared to other breast cancers, while Src expression is only slightly increased (Supplemental Figure 5.4A). Likewise, Lyn mRNA expression shows the strongest correlation with Src_pY416 expression, suggesting that Lyn expression may be associated with the Src activation seen in this study (Supplemental Figure 5.3B). A recent study focused on Lyn expression found that in breast cancers with high c-Myc expression, Lyn expression was significantly associated with a shorter time to relapse and decreased overall survival, and suggested that patients with high c-Myc expression would benefit from Src inhibitors[221].

The strong correlation between expression of Src_pY416 and phosphorylation of CDCP1 demonstrated here supports the conclusion developed in cancer cell lines that CDCP1 activates Src by serving as a binding partner and platform for Src autophosphorylation, and that active Src, in turn, phosphorylates CDCP1 at multiple sites at its C-

terminus[190,192]. Our observation that Src_pY416 is not detected immunohistochemically in the absence of CDCP1 phosphorylation further supports this signaling relationship. Multiple studies in cell lines and animal models have clearly identified CDCP1 and PKCδ as crucial downstream effectors of Src that directly contribute to aggressive behavior of cancer cells[64,187,189,194,198,216]. Our discovery that this pathway is active in clinical samples of TNBC builds upon these studies and solidifies the rationale for targeting this pathway in TNBC. Due to the prominent role of Src in solid tumor progression[222], efforts have been focused on small molecule discovery for direct targeting of Src. However, Src inhibition as a monotherapy has so far shown minimal efficacy in treating solid tumors, including TNBC[223,224]. Clinical trials of Src inhibitors have also been hampered by drug toxicity and serious adverse side effects[223]. Targeting either CDCP1 or PKCδ directly may be a better therapeutic strategy, since CDCP1 knockout mice are viable with no known pathology[225]. Recently, several strategies for inhibiting CDCP1 and/or PKCδ have been developed: 1) anti-CDCP1 blocking antibodies prevented tissue colonization and caused PARP1-mediated apoptosis in vivo in a mouse metastasis model[66]; 2) a small molecule blocking the interaction between CDCP1 and PKCδ showed promising anti-tumor effects in mouse models of gastric cancer and pancreatic cancer[226]; 3) a CDCP1 blocking fragment that acts extracellularly inhibited CDCP1 dimerization and PKCδ activation and decreased tumor progression and metastasis in two mouse models of TNBC[64,65]. Thus, targeting CDCP1 or PKCδ directly to inhibit this pro-tumorigenic arm of Src signaling may prove to be an effective therapeutic strategy for a subset of TNBC patients.

Most of the FOXA1- (non-LAR) TNBC in this study that lacked detectable Src_pY416 also contained no detectable Src_pY527, whereas TNBC that contained high levels of Src_pY416, also contained Src_pY527. This was unexpected since phosphorylation at Y527 is generally known as negative regulator of Src activity[227]. It is well documented that phosphorylation of Y527 in nascent Src by Csk induces a tight interaction between pY527 and the SH2 domain of Src, locking the catalytic site in an inactive state[179]. Viral Src (v-Src), the oncogenic gene product of the Rous sarcoma virus, lacks the C-terminal region that contains Y527, causing it to be constitutively active[206,228]. It is not clear from our studies whether the phosphorylation of Y527 occurs concurrently with or subsequent to phosphorylation of Y416 during the activation of Src. However, the observation that most FOXA1- TNBC are either doubly phosphorylated or lack phosphate at both sites suggests that these phosphorylation events are linked in some way. Biochemical reconstitution studies using purified recombinant Src and Csk have shown that Csk can phosphorylate Src at Y527 after it is activated by autophosphorylation at Y416, and that this doubly phosphorylated enzyme remains active[229]. On the other hand, concurrent phosphorylation of both sites has been observed in a non-canonical pathway of Src activation stimulated by oxidative stress signaling[230]. Our analysis of TCPA data, further supported by western blot analysis of samples in this study, suggests that activated Src in breast cancer is phosphorylated at both Y416 and Y527. Further analysis of the TCPA dataset indicated that phosphorylation of Y416 and Y527 is correlated in multiple tumor types (data not shown). We suggest that Src is phosphorylated at Y416 and Y527 on the same molecule in tumors with activated Src. However, the possibility that the detection

of Src_pY416 and Src_pY527 in the same sample represents the presence of separate mono-phosphorylated Src molecules is not excluded by the data presented here.

Our *in silico* observation that expression of Src_pY416 by TNBC is associated with high expression of immune-related and inflammatory genes raises some interesting questions. Lehmann et al. used gene expression profiling to classify TNBC into 6 subtypes, one of which was termed the "immunomodulatory" (IM) subtype[61]. This subtype expresses many immune-related genes, including several of the genes that are upregulated in Src_pY416+ TCPA samples (Supplemental Figure 5.3). A refinement of the Lehmann-Bauer TNBC classification using laser microdissected tissue samples concluded that the gene expression profile of the immunomodulatory subgroup primarily reflects genes expressed by infiltrating immune cells[62]. Many of the immune related genes upregulated in Src_pY416+ TCPA samples are also specifically expressed in immune cells (e.g. FPR1, FPR2, and FPR3 are neutrophil-specific chemotactic receptors present in the small leftmost cluster in Figure 5.5B). This interesting finding suggests that cancer cells with active Src signaling modulate their tumor microenvironment to stimulate immune infiltration. Tumor specific factors that result in recruitment of immune cells into the microenvironment of TNBC remain to be determined. However, we note that in certain cellular systems, Src can activate an epigenetic switch associated with increased Interleukin-6 expression[231]. In a recent clinical trial, the anti-PD-L1 antibody atezolizumab combined with nab-paclitaxel chemotherapy has shown promising results in TNBC, especially in patients with high PD-L1 expression[232]. While this manuscript was in preparation, the FDA granted accelerated approval for the use of this combination therapy as frontline therapy for patients with locally advanced or metastatic PD-L1 positive TNBC.

The observation that Src_pY416+ TNBC in TCPA express high levels of PD-L1 (Figure 5.5D) suggests that expression of Src_pY416+ may predict response to immune checkpoint inhibitors.

This study demonstrates the feasibility of western blot analysis of proteins extracted from FFPE tissue to assess signaling pathway activity. Despite the extensive protein chemical modifications and denaturation associated with formalin fixation and paraffin embedding, protein antigens have been analyzed in FFPE tissue by IHC since the advent of antigen retrieval methods[233]. The first successful application of shotgun proteomics to FFPE was reported in 2005[234]. Since then, several reports have indicated that the protein composition of tissue in FFPE material is equivalent to fresh tissue[235,236]. This does not abrogate concerns regarding the effect of cold ischemic time on the biochemical composition of resected tumor samples. The uncontrolled period of hypoxia/ischemia that tissues are exposed to during and after surgical resection and before fixation occurs affects their biochemical composition in ways that are not well defined. The stability of phosphoproteins in particular is unpredictable[237,238]. We addressed this concern early in our study by comparing levels of phosphoproteins in freshly resected tumor samples and cognate samples held at room temperature for an additional period up to 90 minutes before immersion in formalin. These studies indicated that the phosphoproteins evaluated in this study are relatively stable (data not shown).

Complete solubilization of proteins in FFPE is not essential to successful bottom-up proteomic analysis since proteins are fragmented in this approach[234,239,240]. However, complete solubilization is essential for methods such as western blot analysis in which intact proteins are analyzed according to their molecular weight. The solubilization

procedure used in this study was validated by comparison of western blots of extracts prepared from fresh and cognate FFPE tissue samples (data not shown) and is similar to a solubilization procedure validated by mass spectroscopy[236]. We found that solubilization of proteins in FFPE tissue is facilitated by high concentration SDS and high concentration dithiothreitol. SDS interferes with trypsin digestion and reverse phase liquid chromatography but is compatible with direct analysis of FFPE samples by standard western blot techniques. Western blots should be ideal for characterizing proteins in FFPE that are expressed as variable molecular weight isoforms due to proteolysis, as shown here for CDCP1, or isoforms arising from alternate mRNA splicing. The number of antibodies that are validated for use in western blot analysis far exceeds the number of antibodies validated for use in paraffin IHC. The ability to evaluate protein expression in FFPE tissue by western blot expands the catalogue of antibodies that can be used to study archived tissue.

Materials and Methods

Patient sample acquisition

Archival triple negative breast cancer resections were identified by review of pathology records at Hoag Memorial Hospital Presbyterian. Selected slides and blocks from breast cancers reported to be negative for estrogen receptor and progesterone receptor (<1%) and Her2 negative (0-1+) were reviewed. Cases with adequate tumor (>15 mm) were selected for microdissection. Foci of carcinoma were microdissected from the tumor using a punch biopsy tool and re-embedded in a 10 x 10 mm paraffin block with a unique identifier. Areas of tumor that contained a high proportion of tumor cells were chosen for microdissection. Areas of tumor with extensive necrosis or a high percentage of stroma

were avoided. TNBC of special types including lobular carcinoma and low-grade metaplastic carcinoma were excluded. High grade metaplastic carcinomas were included. Standard clinicopathologic data including patient age, tumor size, histologic grade, and node status were linked to the tumor sample identifier. The study design was reviewed by the Western Institutional Review Board (#1-890338-1) and determined to pose less than minimal risk to participants and therefore exempt from the informed consent requirement.

Reagents and Antibodies

The following primary antibodies were used: Src_pY416 #2101, Src_pY527 #2105, Src #2108, CDCP1 pY734 #9050, CDCP1 pY743 #14965, CDCP1 #13794, CDCP1 #4115, PKCδ pY311 #2055, PKCδ #2058, AMPKα pT172 #2535, AMPKα #2532, N-cadherin #13116, Slug #9585 (Cell Signaling Technology, Danvers, MA), PKCδ pY311 #ab76181, FOXA1 #ab173287 (Abcam, Cambridge, MA), Vimentin # MA511883, CK5/6 #180267 (Thermo Fisher Scientific, Waltham, MA), β-Actin #A5441 (Millipore Sigma, St. Louis, MO), Vimentin #M0725 (Agilent, Santa Clara, CA), Sox10 #BSB2583 (Bio SB, Santa Barbara, CA). Antibody dilutions for each method are shown in Supplemental Table 6.3.

Immunohistochemical analysis of samples

Immunohistochemical staining was performed on the Leica Biosystems BOND III automated immunostainer. In brief, 3-micron sections of microdissected tumor foci were mounted on adhesive slides and baked for 60 minutes at 60°C. Up to 8 tumor foci were evaluated per slide. For phosphoprotein staining, and most other antigens, slides were dewaxed and rehydrated offline. Antigen retrieval was performed offline in a pressure cooker for 20 minutes in Leica epitope retrieval solution 2. Covertiles were applied to wet slides and the immunostainer programmed to run with the dewax step turned off. After a

second antigen retrieval step online, slides were stained using a 73-minute protocol that included a 30-minute ambient temperature antibody incubation step. Bound antibody was detected using the Bond Polymer Refine Detection system and the slides were counterstained with hematoxylin. Staining of greater than 1% of tumor cells was considered positive; intensity of staining was not recorded for this study. The percentage of tumor cells staining as well as the localization of the stain (membrane, cytoplasm, nucleus) were recorded.

Extraction of protein and western blotting

Protein extraction from formalin fixed paraffin embedded (FFPE) tissue was performed as follows: 40-micron sections of FFPE were placed in 2 ml screw cap vials. Paraffin was removed by two washes of xylene. Xylene was removed with 2 washes of reagent alcohol and one wash of methanol. The deparaffinized tissue was rehydrated in ultrapure water. The rehydrated tissue sections were suspended in 50 volumes of extraction buffer (4% SDS, 125 mM Tris HCl, 100 mM dithiothreitol, 20% glycerol) and placed in a heating block set at 99°C for 60 minutes. After cooling to room temperature, the samples were centrifuged for 5 minutes at 12,100x g to separate the insoluble material. An aliquot (4 µl) of the supernatant was transferred to 3 ml of 8 M urea/10 mM Tris HCl pH 8.0 to determine protein concentration by fluorescence spectroscopy as previously described[241].

For cell line lysates, cells grown on 10 cm dishes were lysed in ice-cold lysis buffer (20 mM Tris pH 7.5, 1% Triton X-100, 150 mM NaCl, 1 mM EDTA/EGTA, 10 mM Sodium Pyrophosphate, 10 mM β-glycerophosphate, 1 mM Sodium Orthovanadate, 50 mM Sodium Fluoride) and scraped into chilled tubes, then incubated on ice for 10 minutes

with brief vortexing every 2-3 minutes. Samples were centrifuged at 12,000x g for 10 minutes at 4°C to pellet insoluble material. The soluble fraction was mixed with 5x sample buffer (312 mM Tris pH 6.8, 10% SDS, 10% β-mercaptoethanol, 50% glycerol, 0.05% bromophenol blue) and boiled for 5 minutes at 95°C, then cooled on ice. Total protein content of cell line lysates was assessed using BCA assay (Thermo Fisher cat# 23225).

Protein lysates were loaded onto 10% polyacrylamide gels and run for 30 minutes at 90V, then approximately 90 minutes at 120V. Proteins were transferred to 0.2-µM-pore nitrocellulose membranes and blocked for 60 minutes with 5% non-fat milk in PBS/0.05% Tween-20 (PBS-T). Primary antibodies were diluted in 5% BSA/PBS-T and incubations were performed overnight at 4°C with gentle shaking. Secondary antibodies were diluted in blocking buffer and incubations were performed for 1 hour at room temperature. Images were acquired on the Bio-Rad ChemiDoc XRS+ imaging system.

Analysis of public datasets

The Cancer Genome Atlas BRCA data set was downloaded from xenabrowser.net. Samples were separated into “TNBC” and “non-TNBC” subsets based on HER2, ER, and PR expression. RNA expression data is presented as RPKM-UQ values. RPPA protein expression data was obtained from The Cancer Proteome Atlas (tcpaportal.org, MD Anderson Cancer Center). The two data sets were aligned in R version 3.5.1 by matching sample IDs. To confirm matching of samples, we checked that RPPA expression values correlated well with TCGA mRNA expression values for the same gene.

Statistical Analysis

Statistical significance of immunohistochemical staining results was performed using Pearson’s chi-squared test. All correlation tests of TCGA/TCPA data were performed

using Pearson's product moment correlation test. Direct comparisons of 2 sample groups used unpaired student's t-test. All statistical analyses were done in R version 3.5.1.

Chapter 6: Discussion and Future Directions

Opening Statement:

In this dissertation, we have explored several lines of research investigating specific molecular pathways as potential therapeutic targets in human cancer. Here, I plan to discuss some of the future goals for these projects, and how I envision the research moving forward toward novel application of targeted therapies. Furthermore, as most of the work here was done using *in vitro* human cell line culture or mouse models, I will discuss how these studies may be shaped in order to be more translatable to the clinic by focusing on using patient derived samples. Chapter 5 began to address this topic briefly by investigating CDCP1 and Src signaling in primary human breast cancer tissues. Finally, as the library of actionable targets is rapidly increasing in cancer therapeutics, the ability to accurately predict the response of an individual patient to a given therapy will be critical. To that end, future studies investigating targeted therapies should also include extensive characterization of companion biomarkers to identify molecular determinants of drug sensitivity and resistance.

Targeted therapy strategies for CC-RCC

In chapter 2, we discovered that the *VHL* tumor suppressor gene acts as a negative regulator of ROCK activity. Furthermore, pVHL binds directly to Rho small GTPases, the upstream modulators of ROCK signaling. pVHL preferentially binds the inactive, GDP-bound form of Rho, and this interaction is likely the mechanism of ROCK modulation by pVHL, although we were not able to show this definitively. These findings shed some light on the report from our research group[24] that *VHL*-deficient cells are hyper-sensitized

to treatment with multiple ROCK inhibitors, including Y-27632 and RKI-1447. We followed up by testing another ROCK inhibitor, AT-13148, which has better pharmacological properties and is more potent than Y-27632 and RKI-1447. Interestingly, we only found a weak synthetic lethal interaction with AT-13148 treatment and *VHL* deficiency. As discussed in Chapter 2, these results may be complicated by the off-target effects of both Y-27632 and AT-13148.

If pVHL indeed regulates Rho/ROCK signaling by a protein-protein interaction with Rho, this would have broad implications in cancer biology, especially in CC-RCC where *VHL* is inactivated in >80% of patients. Rho GTPases are rarely mutated in human cancers but are often differentially expressed in cancer tissue compared to normal tissue[242,243]. Even more common is the dysregulation of the molecules that modulate Rho activity: Guanine nucleotide exchange factors (GEFs), GTPase activating proteins (GAPs) and Guanine nucleotide dissociation inhibitors (GDIs) [244,245]. It is therefore intriguing that pVHL may regulate Rho/ROCK signaling by direct interaction with Rho, likely acting as an allosteric modulator. A logical question is: does this interaction play any part in pVHL's role as a tumor suppressor? Several studies have argued that the tumor suppressive function of pVHL is mostly dependent on its ability to regulate HIF protein levels[8,80,246]. This brings into question the significance of the pVHL-Rho interaction in tumorigenesis, especially since we found that tumorigenic point mutants of pVHL did not have an altered binding capacity for Rho (Supplemental Figure 2.5). However, as discussed in Chapter 2, the loss of this interaction may be more important in *VHL*-deficient CC-RCC cells that have lost pVHL expression entirely, or other mutations that were not tested in our studies. Alternatively, the pVHL mutants tested in chapter 2 may have altered effects on Rho

activity, even though they retain the ability to bind Rho. Finally, loss of pVHL-mediated regulation of Rho/ROCK signaling may have implications in certain aggressive behaviors of cancer like migration and invasion, since Rho and ROCK are key modulators of the actin cytoskeleton.

Regardless of its importance in cancer, it would be beneficial to further characterize the pVHL/Rho interaction to better understand its consequences in the future. One possibility is that pVHL modulates Rho activity by an allosteric mechanism, either by altering Rho's substrate specificity or competing with another Rho substrate. To test this, we could perform co-immunoprecipitation (Co-IP) of Rho in the presence or absence of pVHL to see if we can identify differential binders. To this end, we have performed two pilot runs of Co-IP followed by mass spectrometry (MS) and identified several Rho interactors that were modulated in response to *VHL* knockout in both runs (Supplemental Figure 6.1). To move forward with this approach, we would need to validate some of the top hits from this screen to confirm the results, especially proteins that are known to have a role in Rho/ROCK signaling or cancer. It would also be interesting to map the physical interface of the pVHL/Rho interaction. This could be done by cross-linking the pVHL/Rho complex using cleavable cross-linkers[247] and analyzing the cross-linked peptides by MS to determine where on each protein the interaction is taking place. This would also further our ability to study the importance of the pVHL/Rho interaction, since knowledge of the binding interface would offer hints to the functional consequence of the interaction based on known domain functions in both pVHL and Rho. This would also allow us to generate point mutants of each protein to disrupt the interaction, something we were unable to do in our studies in Chapter 2.

To move forward with ROCK inhibitors as targeted therapies for CC-RCC, significant effort should be put into clinical investigation to determine which patients are likely to respond to ROCK inhibition. To start, we should analyze commercially available tissue microarrays for ROCK activity by staining for phosphorylation of downstream ROCK targets like Myosin Light Chain and LIM Kinase[32,33]. Based on our results in chapter 2, we expect that *VHL*-deficient tumors will have elevated levels of ROCK activity. We should also attempt to correlate elevated ROCK activity with other molecular determinants of CC-RCC. Besides *VHL*, the most common mutations in CC-RCC involve regulators of chromatin modification: *PBRM1*, *SETD2*, and *BAP1*[99]. Interestingly, all three of these genes are located on the same chromosome as *VHL* (3p), within the same 50-Mb region. These genes are often inactivated in tandem with *VHL* loss, although mutations of *PBRM1* and *BAP1* are reported to be mutually exclusive and define distinct CC-RCC subtypes with unique clinical and histological features[248–250]. It is likely that these newly defined subtypes of CC-RCC may have very different characteristics, including activation of ROCK activity. We should start investigating this by determining the status of these genes in our panel of cell lines that we tested in Chapter 2. For example, it would be very interesting to determine if there is a unique genetic signature in RCC4 cells that would explain why re-expression of pVHL had no effect on ROCK activity (Figure 2.2A-2.2B).

Another approach to targeting the Rho/ROCK pathway is focusing on inhibiting Rho itself. Although Rho GTPases have traditionally been deemed “undruggable”, it is possible to alter Rho activity through modulation of its interaction with GAPs or GEFs[251]. However, this approach is difficult to fully control or characterize, since there are many GEFs (~80)

and GAPs (~65) with the ability to regulate Rho[252]. A secondary approach is to interfere with the posttranslational modifications (PTMs) of Rho. Statins, which inhibit HMG-CoA reductase, a key enzyme in the mevalonate pathway that supplies the geranylgeranyl groups for Rho and other small GTPases, have been shown to have some anti-cancer activity[251]. Our lab has found that statin treatment was also synthetically lethal with *VHL* loss and inhibited the growth of 786-O cells *in vivo* in a subcutaneous model[77]. Retrospective clinical studies have suggested that long-term statin use may protect against CC-RCC or decrease risk of progression after surgery[253–255], but there are some conflicting studies that show no effect[256,257], leading to some debate as to whether statins offer a protective effect[258]. These varying results may be due to the lack of patient stratification in these studies (for example by *VHL* status), or failure to take into account the unique pharmacological properties of different statins.

In chapter 3, we moved on to studying another family of signaling molecules that may be targetable in CC-RCC: Cyclin-dependent kinases. Tumor cells almost invariably have some sort of dysregulation of the cell cycle machinery, making CDK inhibition a very attractive therapeutic option. Our results in chapter 3 showed that inhibition of CDK 1,2,5, and 9 with Dinaciclib had potent anti-tumor effects in a PDX-based model of CC-RCC. Our *in vitro* work suggested that there were multiple mechanisms by which Dinaciclib affected CC-RCC cells. Dinaciclib inhibited the proliferation of all cells, including non-transformed cells, but only induced apoptosis in cancer cells. Interestingly, we found that actively dividing cells underwent apoptosis quickly, staining positive for cleaved caspase 3, cleaved PARP, and cell surface Annexin V within 24 hours of treatment. In contrast, dormant cells that were serum starved or cultured as a monolayer took longer (~48 hours)

to show signs of apoptosis. This is likely due to the effects of multiple CDKs being inhibited by Dinaciclib, with the short term, cell cycle-dependent effects likely mediated through CDK1 and CDK2 (involved in regulation of G2/M and G1/S checkpoints, respectively) and the delayed effects through CDK9 (involved in cell survival through transcription of key proteins like MCL-1). To test this hypothesis, we have acquired specific inhibitors for CDK1 and CDK9, and validated siRNAs to specifically knock down individual CDKs (Figure 3.5). It will be crucial to parse apart the different effects of inhibiting individual CDKs to better understand the biological function of each in CC-RCC cells and identify potential therapeutic vulnerabilities. Importantly, we should repeat these experiments in multiple cell lines, including Dinaciclib-resistant cell lines like TK-10 and RPTEC.

Early in our study of CDK inhibitors, we found that Dinaciclib equally inhibited proliferation of both *VHL*-deficient 786-O cells and *VHL*-expressing 786-O cells (786-O *VHL*, Supplemental Figure 3.2A) and prevented colony formation (data not shown). However, later experiments showed that neither Dinaciclib nor the CDK9 specific inhibitor AZD45743 induced apoptosis in 786-O *VHL* cells (Supplemental Figure 3.2B); a similar effect was seen in the non-transformed renal epithelial cell line RPTEC (Figure 3.6C). It would therefore appear that the inhibition of proliferation is not cell-type specific, but induction of apoptotic cell death is selective to CC-RCC cancer cells *in vitro* and can be reversed by re-expression of *VHL*. This finding is very encouraging and suggests there is a therapeutic window for CDK inhibition. It will be crucial for us to validate these results in other cell lines and determine the mechanism by which *VHL* expression prevents the induction of apoptosis upon CDK inhibition. To determine the HIF-dependence, we

should re-express non-degradable HIFs in 786-O *VHL* cells to see if that re-sensitizes the cells to CDK inhibitors. Furthermore, since HIF-2α may modulate MYC activity, we should overexpress a constitutively active MYC in 786-O VHL cells and RPTEC cells. MYC overexpression has been reported as synthetically lethal with CDK1 or CDK9 inhibition, and we would expect that MYC expression in these cells will sensitize them to the effects of both Dinaciclib and AZD4573.`

Moving forward with this project from a preclinical drug testing perspective, we should focus on the use of more specific CDK inhibitors to minimize the off-target effects seen with Dinaciclib. Based on our current knowledge, an excellent candidate would be CDK9, which is not involved in the cell cycle, but instead phosphorylates RNA Pol II to promote transcription elongation of RNA pol II-dependent genes[259]. Inhibition of CDK9 may have significant promise as a cancer therapeutic, due to its role in stimulating transcription of several short-lived pro-survival proteins, such as MCL-1 and XIAP[260,261]. Small molecule inhibitors specific for CDK9 are a recent development and to date have been most effective against hematological malignancies, with two CDK9-specific inhibitors currently in Phase I clinical trials[102,103]. However, the fact that resistance to apoptosis is a hallmark of both solid cancers and hematological cancers, and the fact that CDK9 inhibition may be synthetically lethal with MYC activation[98], suggests that CDK9 inhibition could be more broadly effective across different cancer types. In our study, we found that knockdown of CDK1 or CDK9 showed the strongest toxic effect in CC-RCC cells *in vitro*, and specific inhibition of CDK9 with AZD4573 (currently in Phase I clinical trials) recapitulated the effects of Dinaciclib *in vitro*. Targeting CDK9 is further supported by the fact that CC-

RCC tumors with elevated CDK9 expression have a significantly worse prognosis (Supplemental Figure 3.5).

In the future, a key question to answer will be: What are the molecular determinants of cell death upon CDK inhibition? It is interesting to note that cells resistant to apoptosis induction by Dinaciclib and AZD4573 had residual MCL-1 expression after treatment, while in sensitive cells MCL-1 expression was almost completely abolished (see Figure 3.2A, Figure 3.4D, and Figure 3.6C). MCL-1 is a short-lived protein and its protein stability is regulated by the proteasome[262]. Some reports have identified GSK-3β mediated phosphorylation as a key stimulator of MCL-1 ubiquitination and degradation[263,264]. This is initially counterintuitive because *VHL* loss was reported to activate Akt and increase the inhibitory phosphorylation of GSK-3B[265]. We would therefore expect *VHL* expression to destabilize MCL-1 expression, and not vice versa; however, regulation of GSK-3β may be more complex than a simple on/off switch and phosphorylation does not necessarily inhibit GSK-3B activity (reviewed in [266]). To investigate this, we should examine GSK-3β and MCL-1 phosphorylation in our sensitive vs. resistant cell lines. We should also see if co-treatment with a GSK-3β inhibitor induces resistance to CDK inhibition, since this should theoretically stabilize MCL-1 protein expression. This should be coupled with a comparison of levels of phosphorylated RNA pol II (which is dependent on CDK9 activity) and MCL-1 transcription by qPCR to ensure that CDK9 inhibition is equally effective in all cells. Finally, we can inhibit MCL-1 activity by small molecule inhibitors and siRNA knockdown to determine the MCL-1 dependence of various cells (e.g. cancer cells vs. normal cells and cancer cells +/- pVHL).

Through our studies of CDK inhibition, we dedicated a lot of effort evaluating *in vitro* culture techniques to study freshly isolated PDX tumor samples. We observed that PDX tumor cells did not grow or survive well in generic 2D cell culture, although growth could be stimulated by culturing at 2% - 5% oxygen (data not shown). We also cultured freshly harvested PDX tumor cells in 3D extracellular matrices and found that 2 out of 3 tumors tested formed “organoid”-like structures in 3D, although they grew very slowly (see Figure 3.1F). Dinaciclib was just as effective at inhibiting proliferation in 3D as it was in 2D (Figure 3.1E). This is important since it has been reported that various 3D culture methods may significantly alter the response of cultured cells to drug treatment *in vitro*[267]. To improve our 3D culture techniques and incorporate hypoxic gradients, we recently began a collaboration with the Gerecht lab at Johns Hopkins University. As a proof of concept, we encapsulated 786-O cells and cells from one PDX tumor in Gelatin-based 3D matrices. These matrices are formed by a polymerization reaction that concurrently depletes oxygen[268], thus creating oxygen gradients dependent on the thickness of the gel (Supplemental Figure 6.2A). In agreement with our observation that hypoxia stimulated the growth of PDX cells, we found that both 786-O cells and “MD0865” PDX tumor cells were stimulated in thicker hydrogels with lower oxygen tension, forming robust 3D structures and even tubular networks (Supplemental Figure 6.2B). In the future, we are excited to implement these hypoxic 3D environments into our research as a standard method for culturing PDX tumor cells *in vitro*, and as a physiologically relevant *in vitro* drug screening platform.

In chapter 4 we began to explore a third and final strategy for targeting CC-RCC: Induction of mitotic catastrophe. Briefly, we showed that ROCK inhibition with Y-27632 caused

gross mitotic errors in *VHL*-deficient cells that were significantly reduced in VHL-expressing cells. These results agree with previous literature identifying VHL as a key regulator of mitotic stability[87,88,139,269]. The concept of mitotic catastrophe as a therapeutic strategy in cancer is based on the observation that cancer cells in general display mitotic abnormalities and execute error-prone mitoses[38,50,52,53]. Therefore, treating with agents that further destabilize mitosis may preferentially affect cancer cells in this weakened mitotic state, while leaving normal cells unaffected. Based on this concept, and the fact that ROCK inhibition preferentially induced abnormal mitoses in VHL-deficient cells (Figure 4.1), we expect that other targeted mitotic agents will be synthetically lethal with VHL loss. To start, we plan to test inhibitors of Aurora Kinase A (AurA) and Checkpoint Kinase 1 (Chk1). AurA is a crucial mitotic kinase responsible for progression through the G2/M checkpoint, centrosome maturation and assembly of the mitotic spindle[270], and treatment with AurA inhibitors causes mitotic abnormalities similar to what we saw with Y-27632 treatment in Figure 4.1[59]. Interestingly, another recent report found that loss of *VHL* could determine sensitivity to AurA inhibitors *in vitro* and *in vivo*[153], although this study did not investigate the role of mitotic catastrophe in cell death. On the other hand, Chk1 is also involved in regulation of the G2/M checkpoint through its indirect regulation of CDK1, and Chk1 inhibition has been shown to induce cell death due to mitotic catastrophe[58]. Since loss of *VHL* weakens the G2/M checkpoint through a decrease in MAD2 expression[88], *VHL*-deficient cells may be especially sensitive to Chk1 inhibition. Importantly, *VHL*'s effect on mitotic stability is expected to be independent of HIF expression[88]. To test this, we should express *VHL* mutants that are defective in microtubule stabilization but retain their ability to regulate HIF expression[139].

As mitotic catastrophe is a dynamic process involving abnormal mitotic events followed by delayed cell death[52], we will need to apply live time lapse imaging to track cells going through mitotic catastrophe. To begin addressing this, we have generated stable cell lines expressing GFP-labeled histone H2B to track DNA in real time with fluorescent imaging. Since VHL regulates microtubules, we should also use fluorescent microtubule markers (e.g. mCherry fused to the microtubule-interacting protein Tau[271]) to follow the dynamics of mitotic spindle formation. We hypothesize that with the proposed mitotic agents (ROCK, AurA, Chk1 inhibitors) we will see mitotic errors (including lagging chromosomes and multipolar spindles, as seen in Chapter 4) followed by generation of aneuploidy and cell death either during mitosis or at the next interphase, as has been shown in other models of mitotic catastrophe[272,273].

With any targeted therapy, tumor cells are likely to eventually develop resistance to the drug through compensatory pathways or mutations[274]. Modern approaches to combinatorial therapy may involve initial treatment with a targeted therapy, followed by addition of one or more agents based on genetic analysis of resistant tumors at the time of disease progression. For example, the ongoing LOGIC-2 clinical trial for advanced BRAF mutant melanoma aims to treat patients with a combination of BRAF/MEK, re-analyze the tumors upon disease progression, and follow up with one of four inhibitors (CDK4/6, PI3K, c-Met, or FGFR) based on the genetic analysis[275]. In accordance with this strategy, moving forward with ROCK inhibitors (Chapter 2), CDK inhibitors (Chapter 3), or mitotic agents (Chapter 4) would require an understanding of potential mechanisms of resistance. To examine this, we plan to first analyze the transcriptome of naïve vs Dinaciclib-treated tumors from chapter 3 (Figure 3.7) by RNA sequencing analysis, to

identify differentially expressed genes in tumors exposed to CDK inhibitors. This study is in progress and we look forward to seeing the results. Since development of resistance will likely include kinase-dependent signaling events, we should also perform phosphoproteomic screens to identify key activated signaling pathways in resistant tumors. This process should also be performed with CDK9 inhibitors, since we expect that specific CDK9 inhibition will be more effective than inhibition of multiple CDKs with Dinaciclib.

In summary, we have presented evidence of 3 pathways that may have therapeutic promise in CC-RCC: 1) Rho/ROCK signaling, 2) Cyclin-dependent kinase signaling, and 3) regulation of mitosis. Moving forward with these projects should involve rigorous preclinical testing and identification of molecular determinants of sensitivity through genomic and/or proteomic analysis of sensitive and resistant cell lines or tumors. The orthotopic PDX model we described in Chapter 3, together with physiologically relevant 3D *in vitro* culturing techniques should prove useful for preclinical drug testing using freshly derived PDX tumors from CC-RCC patients.

Triple Negative Breast Cancer and the Src/CDCP1 pathway

In chapter 5 we discussed some very exciting results investigating CDCP1 and Src signaling in primary TNBC patient specimens. Briefly, we found co-activation of CDCP1 and Src together with PKCδ phosphorylation in a subset of TNBC tumors, which potentially identifies a distinct class of TNBC likely to respond to agents targeting this pathway. This study crucially confirmed the many *in vitro* and animal model studies that have identified the Src/CDCP1 signaling axis as an important player in human cancer, including TNBC[64–67,187,225]. Likewise, it solidifies the rationale of targeting Src/CDCP1

signaling in this subset of TNBC cases. Since Src inhibitors have not been very effective, several other methods of targeting CDCP1 or PKCδ have recently been developed[64–66,226] (see Chapter 5: Discussion). It will be beneficial to see if these treatment strategies are effective against patient-derived tumors with active Src/CDCP1 signaling. To test this, we have recently acquired TNBC PDX specimens and will need to analyze analyze Src, CDCP1, and PKCδ signaling by IHC and western blot, as we did in Chapter 5. Then we can test response to these new treatments utilizing 3D *in vitro* cell culture, and *in vivo* PDX animal studies. We expect that tumors with active Src/CDCP1 signaling will be sensitive to agents targeting this pathway, and successful preclinical studies using patient-derived specimens would greatly strengthen the case for moving forward with drug development and clinical studies.

From a scientific methods perspective, the ability to extract proteins from FFPE tissues for downstream analysis will be quite useful for translational research in the future. For example, this technique allowed us to investigate CDCP1 cleavage in clinical samples by size discrimination in SDS-PAGE gels. This was important since no antibody is available to discriminate cleaved from full-length CDCP1 by IHC. We were also able to apply other biochemical techniques such as immunoprecipitation on these protein extracts (data not shown), opening the possibility to further explore signaling relationships that have been identified *in vitro* in clinical specimens.

In our study of TNBC FFPE specimens, we found that sample heterogeneity played a confounding role in the results. For example, we detected phosphorylated Src by western blots in some samples that were negative in tumor cells by IHC (e.g. Figure 5.3B) and found that this was due to infiltrating immune cells with high levels of activated Src

(Supplemental Figure 5.2). Furthermore, in our analysis of TCGA public data sets, we found that activated Src correlated strongly with the presence of immunomodulatory genes, and many of these genes are expressed specifically in immune cells. This prevented us from focusing on the tumor cell-specific roles of Src in clinical TNBC samples. To circumvent this issue in our future studies, we will need to develop ways to parse out different cell types in our analyses. Microdissection of FFPE tissue prior to protein extraction may be an effective option, although this technique is time and labor-intensive and not amenable to high-throughput studies. Microdissection was crucial for refining the popular gene expression-based TNBC subtyping strategy described by Lehmann et al[61,62]. Alternatively, we could use fluorescence activated cell sorting (FACS) to separate tumor cells from infiltrating immune cells in tumor samples via the leukocyte-specific CD45 marker[276]. Single cell RNA sequencing is emerging as the standard for analyzing heterogeneity of clinical tumor samples, including TNBC[277,278], although this technique does not allow protein-level analysis. Another approach, which would allow us to investigate proteomic events at a single cell level, is to incorporate single cell western blots[279]. Yet another option is to employ Mass Cytometry (CyTOF®) for real time analysis of a large panel of antibodies at a single cell resolution, with concurrent discrimination between immune cells, stromal cells and tumor cells. Importantly, these single-cell methods will require fresh patient tumor tissue, and not be applicable to archived FFPE tissues like our study was.

Closing Statement:

In this body of work, we have demonstrated preclinical analysis of 3 unique signaling pathways that may represent actionable therapeutic targets in CC-RCC (chapters 2-4).

Throughout these studies we have explored emerging methods of improved *in vitro* cell culture and *in vivo* drug testing utilizing patient-derived tumors to increase the relevance of these studies to human disease. We also applied proteomic analysis of archived clinical specimens to solidify the rationale for targeting the Src/CDCP1 pathway in TNBC (chapter 5). These findings contribute to the field of targeted therapy in both CC-RCC and TNBC and help pave the way for more detailed preclinical studies involving the use of freshly derived patient specimens, as well as rigorous investigation of mechanisms of drug response and discovery of relevant biomarkers.

References

1. NCHS Data Visualization Gallery - Mortality Trends in the United States. (2017). Available at: https://www.cdc.gov/nchs/data-visualization/mortality-trends/index.htm. (Accessed: 24th June 2019)
2. Cancer of the Kidney and Renal Pelvis - Cancer Stat Facts. *SEER* Available at: https://seer.cancer.gov/statfacts/html/kidrp.html. (Accessed: 24th June 2019)
3. Moore, L. E. *et al.* Von Hippel-Lindau (VHL) Inactivation in Sporadic Clear Cell Renal Cancer: Associations with Germline VHL Polymorphisms and Etiologic Risk Factors. *PLOS Genet.* **7**, e1002312 (2011).
4. v. Hippel, E. Über eine sehr seltene Erkrankung der Netzhaut. *Albrecht Von Graefes Arch. Für Ophthalmol.* **59**, 83–106 (1904).
5. Lindau, A. ZUR FRAGE DER ANGIOMATOSIS RETINæ UND IHRER HIRNKOMPLIKATIONEN. *Acta Ophthalmol. (Copenh.)* **4**, 193–226 (1926).
6. Von Hippel-Lindau disease | Genetic and Rare Diseases Information Center (GARD) – an NCATS Program. Available at: https://rarediseases.info.nih.gov/diseases/7855/von-hippel-lindau-disease. (Accessed: 9th July 2019)
7. Lonergan, K. M. *et al.* Regulation of hypoxia-inducible mRNAs by the von Hippel-Lindau tumor suppressor protein requires binding to complexes containing elongins B/C and Cul2. *Mol. Cell. Biol.* **18**, 732–741 (1998).
8. Kondo, K., Klco, J., Nakamura, E., Lechpammer, M. & Kaelin, W. G. Inhibition of HIF is necessary for tumor suppression by the von Hippel-Lindau protein. *Cancer Cell* **1**, 237–246 (2002).
9. Lilleby, W. & Fosså, S. D. Chemotherapy in metastatic renal cell cancer. *World J. Urol.* **23**, 175–179 (2005).
10. Rini, B. I. *et al.* Society for Immunotherapy of Cancer consensus statement on immunotherapy for the treatment of renal cell carcinoma. *J. Immunother. Cancer* **4**, 81 (2016).
11. Sternberg, C. N. *et al.* Pazopanib in Locally Advanced or Metastatic Renal Cell Carcinoma: Results of a Randomized Phase III Trial. *J. Clin. Oncol.* (2010). doi:10.1200/JCO.2009.23.9764
12. Motzer, R. J. *et al.* Axitinib versus sorafenib as second-line treatment for advanced renal cell carcinoma: overall survival analysis and updated results from a randomised phase 3 trial. *Lancet Oncol.* **14**, 552–562 (2013).
13. Motzer, R. J. *et al.* Sunitinib versus Interferon Alfa in Metastatic Renal-Cell Carcinoma. *N. Engl. J. Med.* **356**, 115–124 (2007).
14. Escudier, B. *et al.* Sorafenib in Advanced Clear-Cell Renal-Cell Carcinoma. *N. Engl. J. Med.* **356**, 125–134 (2007).
15. Gossage, L., Eisen, T. & Maher, E. R. VHL, the story of a tumour suppressor gene. *Nat. Rev. Cancer* **15**, 55–64 (2015).
16. Choueiri, T. K. *et al.* Cabozantinib Versus Sunitinib As Initial Targeted Therapy for Patients With Metastatic Renal Cell Carcinoma of Poor or Intermediate Risk: The Alliance A031203 CABOSUN Trial. *J. Clin. Oncol.* **35**, 591–597 (2017).
17. Motzer, R. J. *et al.* Efficacy of everolimus in advanced renal cell carcinoma: a double-blind, randomised, placebo-controlled phase III trial. *The Lancet* **372**, 449–456 (2008).

18. Hudes, G. *et al.* Temsirolimus, Interferon Alfa, or Both for Advanced Renal-Cell Carcinoma. *N. Engl. J. Med.* **356**, 2271–2281 (2007).
19. Fingar, D. C. *et al.* mTOR Controls Cell Cycle Progression through Its Cell Growth Effectors S6K1 and 4E-BP1/Eukaryotic Translation Initiation Factor 4E. *Mol. Cell. Biol.* **24**, 200–216 (2004).
20. Hudson, C. C. *et al.* Regulation of Hypoxia-Inducible Factor 1α Expression and Function by the Mammalian Target of Rapamycin. *Mol. Cell. Biol.* **22**, 7004–7014 (2002).
21. Lane, H. A. *et al.* mTOR Inhibitor RAD001 (Everolimus) Has Antiangiogenic/Vascular Properties Distinct from a VEGFR Tyrosine Kinase Inhibitor. *Clin. Cancer Res.* **15**, 1612–1622 (2009).
22. Motzer, R. J. *et al.* Lenvatinib, everolimus, and the combination in patients with metastatic renal cell carcinoma: a randomised, phase 2, open-label, multicentre trial. *Lancet Oncol.* **16**, 1473–1482 (2015).
23. Motzer, R. J. *et al.* Nivolumab plus Ipilimumab versus Sunitinib in Advanced Renal-Cell Carcinoma. *N. Engl. J. Med.* **378**, 1277–1290 (2018).
24. Thompson, J. M. *et al.* Rho-associated kinase 1 inhibition is synthetically lethal with von Hippel-Lindau deficiency in clear cell renal cell carcinoma. *Oncogene* **36**, 1080–1089 (2017).
25. Totsukawa, G. *et al.* Distinct Roles of Rock (Rho-Kinase) and Mlck in Spatial Regulation of Mlc Phosphorylation for Assembly of Stress Fibers and Focal Adhesions in 3t3 Fibroblasts. *J. Cell Biol.* **150**, 797–806 (2000).
26. Croft, D. R. & Olson, M. F. The Rho GTPase Effector ROCK Regulates Cyclin A, Cyclin D1, and p27Kip1 Levels by Distinct Mechanisms. *Mol. Cell. Biol.* **26**, 4612–4627 (2006).
27. Ishizaki, T. *et al.* p160ROCK, a Rho-associated coiled-coil forming protein kinase, works downstream of Rho and induces focal adhesions. *FEBS Lett.* 118–124 (2017). doi:10.1016/S0014-5793(97)00107-5@10.1002/(ISSN)1873-3468.50YEARSFEBSLETTERS
28. Coleman, M. L. *et al.* Membrane blebbing during apoptosis results from caspase-mediated activation of ROCK I. *Nat. Cell Biol.* **3**, 339 (2001).
29. Rath, N. *et al.* Rho Kinase Inhibition by AT13148 Blocks Pancreatic Ductal Adenocarcinoma Invasion and Tumor Growth. *Cancer Res.* **78**, 3321–3336 (2018).
30. Liu, S., Goldstein, R. H., Scepansky, E. M. & Rosenblatt, M. Inhibition of Rho-Associated Kinase Signaling Prevents Breast Cancer Metastasis to Human Bone. *Cancer Res.* **69**, 8742–8751 (2009).
31. Vennin, C. *et al.* Transient tissue priming via ROCK inhibition uncouples pancreatic cancer progression, sensitivity to chemotherapy, and metastasis. *Sci. Transl. Med.* **9**, eaai8504 (2017).
32. Amano, M. *et al.* Phosphorylation and Activation of Myosin by Rho-associated Kinase (Rho-kinase). *J. Biol. Chem.* **271**, 20246–20249 (1996).
33. Ohashi, K. *et al.* Rho-associated Kinase ROCK Activates LIM-kinase 1 by Phosphorylation at Threonine 508 within the Activation Loop. *J. Biol. Chem.* **275**, 3577–3582 (2000).

34. He, M. *et al.* Vascular endothelial growth factor C promotes cervical cancer metastasis via up-regulation and activation of RhoA/ROCK-2/moesin cascade. *BMC Cancer* **10**, 170 (2010).
35. Yang, S. & Kim, H.-M. ROCK Inhibition Activates MCF-7 Cells. *PLOS ONE* **9**, e88489 (2014).
36. Priya, R. *et al.* Feedback regulation through myosin II confers robustness on RhoA signalling at E-cadherin junctions. *Nat. Cell Biol.* **17**, 1282–1293 (2015).
37. Smith, A. L., Dohn, M. R., Brown, M. V., Reynolds, A. B. & Assoian, R. K. Association of Rho-associated protein kinase 1 with E-cadherin complexes is mediated by p120-catenin. *Mol. Biol. Cell* **23**, 99–110 (2011).
38. Hanahan, D. & Weinberg, R. A. Hallmarks of Cancer: The Next Generation. *Cell* **144**, 646–674 (2011).
39. Mitchison, T. J. The proliferation rate paradox in antimitotic chemotherapy. *Mol. Biol. Cell* **23**, 1–6 (2012).
40. Malumbres, M. Cyclin-dependent kinases. *Genome Biol.* **15**, 122 (2014).
41. Asghar, U., Witkiewicz, A. K., Turner, N. C. & Knudsen, E. S. The history and future of targeting cyclin-dependent kinases in cancer therapy. *Nat. Rev. Drug Discov.* **14**, 130 (2015).
42. Le Tourneau, C. *et al.* Phase I evaluation of seliciclib (R-roscovitine), a novel oral cyclin-dependent kinase inhibitor, in patients with advanced malignancies. *Eur. J. Cancer* **46**, 3243–3250 (2010).
43. Ramaswamy, B. *et al.* A dose-finding, pharmacokinetic and pharmacodynamic study of a novel schedule of flavopiridol in patients with advanced solid tumors. *Invest. New Drugs* **30**, 629–638 (2012).
44. Barlaam, B. *et al.* Abstract 1650: Discovery of AZD4573, a potent and selective inhibitor of CDK9 that enables transient target engagement for the treatment of hematologic malignancies. *Cancer Res.* **78**, 1650–1650 (2018).
45. Nemunaitis, J. J. *et al.* A first-in-human, phase 1, dose-escalation study of dinaciclib, a novel cyclin-dependent kinase inhibitor, administered weekly in subjects with advanced malignancies. *J. Transl. Med.* **11**, 259 (2013).
46. Finn, R. S. *et al.* Palbociclib and Letrozole in Advanced Breast Cancer. *N. Engl. J. Med.* **375**, 1925–1936 (2016).
47. Chen, X.-X. *et al.* Cyclin-dependent kinase inhibitor dinaciclib potently synergizes with cisplatin in preclinical models of ovarian cancer. *Oncotarget* **6**, 14926–14939 (2015).
48. Feldmann, G. *et al.* Cyclin-dependent kinase inhibitor Dinaciclib (SCH727965) inhibits pancreatic cancer growth and progression in murine xenograft models. *Cancer Biol. Ther.* **12**, 598–609 (2011).
49. Rajput, S. *et al.* Inhibition of cyclin dependent kinase 9 by dinaciclib suppresses cyclin B1 expression and tumor growth in triple negative breast cancer. *Oncotarget* **7**, 56864–56875 (2016).
50. Boveri, T. *Zur Frage der Entstehung maligner Tumoren.* (Gustav Fischer, 1914).
51. Wang, W. *et al.* Chromosomal instability and acquired drug resistance in multiple myeloma. *Oncotarget* **8**, 78234–78244 (2017).

52. Vitale, I., Galluzzi, L., Castedo, M. & Kroemer, G. Mitotic catastrophe: a mechanism for avoiding genomic instability. *Nat. Rev. Mol. Cell Biol.* **12**, 385–392 (2011).
53. Holland, A. J. & Cleveland, D. W. Boveri revisited: chromosomal instability, aneuploidy and tumorigenesis. *Nat. Rev. Mol. Cell Biol.* **10**, 478–487 (2009).
54. Schiff, P. B., Fant, J. & Horwitz, S. B. Promotion of microtubule assembly in vitro by taxol. *Nature* **277**, 665 (1979).
55. Noble, R. L., Beer, C. T. & Cutts, J. H. Further biological activities of vincaleukoblastine—an alkaloid isolated from Vinca rosea (L.). *Biochem. Pharmacol.* **1**, 347–348 (1959).
56. Jordan, M. A., Thrower, D. & Wilson, L. Mechanism of Inhibition of Cell Proliferation by Vinca Alkaloids. *Cancer Res.* **51**, 2212–2222 (1991).
57. Derry, W. B., Wilson, L. & Jordan, M. A. Substoichiometric Binding of Taxol Suppresses Microtubule Dynamics. *Biochemistry* **34**, 2203–2211 (1995).
58. Niida, H. *et al.* Depletion of Chk1 Leads to Premature Activation of Cdc2-cyclin B and Mitotic Catastrophe. *J. Biol. Chem.* **280**, 39246–39252 (2005).
59. Hoar, K. *et al.* MLN8054, a Small-Molecule Inhibitor of Aurora A, Causes Spindle Pole and Chromosome Congression Defects Leading to Aneuploidy. *Mol. Cell. Biol.* **27**, 4513–4525 (2007).
60. Turner, N. C. & Reis-Filho, J. S. Tackling the Diversity of Triple-Negative Breast Cancer. *Clin. Cancer Res.* **19**, 6380–6388 (2013).
61. Lehmann, B. D. *et al.* Identification of human triple-negative breast cancer subtypes and preclinical models for selection of targeted therapies. *J. Clin. Invest.* **121**, 2750–2767 (2011).
62. Lehmann, B. D. *et al.* Refinement of Triple-Negative Breast Cancer Molecular Subtypes: Implications for Neoadjuvant Chemotherapy Selection. *PLOS ONE* **11**, e0157368 (2016).
63. Turdo, F. *et al.* CDCP1 is a novel marker of the most aggressive human triple-negative breast cancers. *Oncotarget* **7**, 69649–69665 (2016).
64. Wright, H. J. *et al.* CDCP1 cleavage is necessary for homodimerization-induced migration of triple-negative breast cancer. *Oncogene* **35**, 4762–4772 (2016).
65. Wright, H. J. *et al.* CDCP1 drives triple-negative breast cancer metastasis through reduction of lipid-droplet abundance and stimulation of fatty acid oxidation. *Proc. Natl. Acad. Sci. U. S. A.* **114**, E6556–E6565 (2017).
66. Casar, B. *et al.* Blocking of CDCP1 cleavage in vivo prevents Akt-dependent survival and inhibits metastatic colonization through PARP1-mediated apoptosis of cancer cells. *Oncogene* **31**, 3924–3938 (2012).
67. Casar, B. *et al.* In vivo cleaved CDCP1 promotes early tumor dissemination via complexing with activated β1 integrin and induction of FAK/PI3K/Akt motility signaling. *Oncogene* **33**, 255–268 (2014).
68. Leroy, C. *et al.* CUB-domain-containing protein 1 overexpression in solid cancers promotes cancer cell growth by activating Src family kinases. *Oncogene* **34**, 5593–5598 (2015).
69. Wong, C. H. *et al.* Phosphorylation of the SRC epithelial substrate Trask is tightly regulated in normal epithelia but widespread in many human epithelial cancers. *Clin. Cancer Res. Off. J. Am. Assoc. Cancer Res.* **15**, 2311–2322 (2009).

70. Hsieh, J. J. *et al.* Renal cell carcinoma. *Nat. Rev. Dis. Primer* **3**, 17009 (2017).
71. Escudier, B. *et al.* Renal cell carcinoma: ESMO Clinical Practice Guidelines for diagnosis, treatment and follow-up†. *Ann. Oncol.* **30**, 706–720 (2019).
72. Yasui, Y. *et al.* Roles of Rho-associated Kinase in Cytokinesis; Mutations in Rho-associated Kinase Phosphorylation Sites Impair Cytokinetic Segregation of Glial Filaments. *J. Cell Biol.* **143**, 1249–1258 (1998).
73. Tanaka, T. *et al.* Nuclear Rho Kinase, ROCK2, Targets p300 Acetyltransferase. *J. Biol. Chem.* **281**, 15320–15329 (2006).
74. Hartmann, S., Ridley, A. J. & Lutz, S. The Function of Rho-Associated Kinases ROCK1 and ROCK2 in the Pathogenesis of Cardiovascular Disease. *Front. Pharmacol.* **6**, (2015).
75. Wyckoff, J. B., Pinner, S. E., Gschmeissner, S., Condeelis, J. S. & Sahai, E. ROCK- and Myosin-Dependent Matrix Deformation Enables Protease-Independent Tumor-Cell Invasion In Vivo. *Curr. Biol.* **16**, 1515–1523 (2006).
76. Sahai, E. & Marshall, C. J. ROCK and Dia have opposing effects on adherens junctions downstream of Rho. *Nat. Cell Biol.* **4**, 408–415 (2002).
77. Thompson, J. M. *et al.* Targeting the Mevalonate Pathway Suppresses VHL-Deficient CC-RCC through an HIF-Dependent Mechanism. *Mol. Cancer Ther.* **17**, 1781–1792 (2018).
78. Abe, H. *et al.* Possible role of the RhoC/ROCK pathway in progression of clear cell renal cell carcinoma. *Biomed. Res. Tokyo Jpn.* **29**, 155–161 (2008).
79. Bian, D. *et al.* The G 12/13 -RhoA signaling pathway contributes to efficient lysophosphatidic acid-stimulated cell migration. *Oncogene* **25**, 2234 (2006).
80. Ohh, M. Ubiquitin Pathway in VHL Cancer Syndrome. *Neoplasia N. Y. N* **8**, 623–629 (2006).
81. Ewing, R. M. *et al.* Large-scale mapping of human protein–protein interactions by mass spectrometry. *Mol. Syst. Biol.* **3**, 89 (2007).
82. Knauth, K., Cartwright, E., Freund, S., Bycroft, M. & Buchberger, A. VHL Mutations Linked to Type 2C von Hippel-Lindau Disease Cause Extensive Structural Perturbations in pVHL. *J. Biol. Chem.* **284**, 10514–10522 (2009).
83. Diaz, A. A. *et al.* Prediction of protein solubility in *Escherichia coli* using logistic regression. *Biotechnol. Bioeng.* **105**, 374–383 (2010).
84. Ishizaki, T. *et al.* Pharmacological properties of Y-27632, a specific inhibitor of rho-associated kinases. *Mol. Pharmacol.* **57**, 976–983 (2000).
85. Yap, T. A. *et al.* AT13148 Is a Novel, Oral Multi-AGC Kinase Inhibitor with Potent Pharmacodynamic and Antitumor Activity. *Am. Assoc. Cancer Res.* **18**, 3912–3923 (2012).
86. Gilkes, D. M. *et al.* Hypoxia-inducible factors mediate coordinated RhoA-ROCK1 expression and signaling in breast cancer cells. *Proc. Natl. Acad. Sci.* 201321510 (2013). doi:10.1073/pnas.1321510111
87. Thoma, C. R. *et al.* Quantitative image analysis identifies pVHL as a key regulator of microtubule dynamic instability. *J. Cell Biol.* **190**, 991–1003 (2010).
88. Thoma, C. R. *et al.* VHL loss causes spindle misorientation and chromosome instability. *Nat. Cell Biol.* **11**, 994–1001 (2009).

89. Fujisawa, K., Fujita, A., Ishizaki, T., Saito, Y. & Narumiya, S. Identification of the Rho-binding Domain of p160ROCK, a Rho-associated Coiled-coil Containing Protein Kinase. *J. Biol. Chem.* **271**, 23022–23028 (1996).
90. Priya, R., Yap, A. S. & Gomez, G. A. E-cadherin supports steady-state Rho signaling at the epithelial zonula adherens. *Differentiation* **86**, 133–140 (2013).
91. Frew, I. J. *et al.* pVHL and PTEN tumour suppressor proteins cooperatively suppress kidney cyst formation. *EMBO J.* **27**, 1747–1757 (2008).
92. Uehata, M. *et al.* Calcium sensitization of smooth muscle mediated by a Rho-associated protein kinase in hypertension. *Nature* **389**, 990 (1997).
93. Motzer, R. J. *et al.* IMmotion151: A Randomized Phase III Study of Atezolizumab Plus Bevacizumab vs Sunitinib in Untreated Metastatic Renal Cell Carcinoma (mRCC). *J. Clin. Oncol.* **36**, 578–578 (2018).
94. Parry, D. *et al.* Dinaciclib (SCH 727965), a Novel and Potent Cyclin-Dependent Kinase Inhibitor. *Mol. Cancer Ther.* **9**, 2344–2353 (2010).
95. Kumar, S. K. *et al.* Phase 1/2 Trial of a Novel CDK Inhibitor Dinaciclib (SCH727965) in Patients with Relapsed Multiple Myeloma Demonstrates Encouraging Single Agent Activity. *Blood* **120**, 76–76 (2012).
96. Gojo, I. *et al.* Phase II Study of the Cyclin-Dependent Kinase (CDK) Inhibitor Dinaciclib (SCH 727965) In Patients with Advanced Acute Leukemias. *Blood* **116**, 3287–3287 (2010).
97. Kang, J., Sergio, C. M., Sutherland, R. L. & Musgrove, E. A. Targeting cyclin-dependent kinase 1 (CDK1) but not CDK4/6 or CDK2 is selectively lethal to MYC-dependent human breast cancer cells. *BMC Cancer* **14**, 32 (2014).
98. Huang, C.-H. *et al.* CDK9-mediated transcription elongation is required for MYC addiction in hepatocellular carcinoma. *Genes Dev.* **28**, 1800–1814 (2014).
99. The Cancer Genome Atlas Research Network. Comprehensive molecular characterization of clear cell renal cell carcinoma. *Nature* **499**, 43–49 (2013).
100. Beroukhim, R. *et al.* Patterns of Gene Expression and Copy-Number Alterations in von-Hippel Lindau Disease-Associated and Sporadic Clear Cell Carcinoma of the Kidney. *Cancer Res.* **69**, 4674–4681 (2009).
101. Gordan, J. D., Bertovrt, J. A., Hu, C.-J., Diehl, J. A. & Simon, M. C. HIF-2α promotes hypoxic cell proliferation by enhancing c-Myc transcriptional activity. *Cancer Cell* **11**, 335–347 (2007).
102. Open Label Phase I Dose Escalation Study With BAY1143572 in Patients With Advanced Cancer - Full Text View - ClinicalTrials.gov. Available at: https://clinicaltrials.gov/ct2/show/NCT01938638. (Accessed: 9th July 2019)
103. Study to Assess Safety, Tolerability, Pharmacokinetics and Antitumor Activity of AZD4573 in Relapsed/Refractory Haematological Malignancies - Full Text View - ClinicalTrials.gov. Available at: https://clinicaltrials.gov/ct2/show/NCT03263637. (Accessed: 9th July 2019)
104. Diril, M. K. *et al.* Cyclin-dependent kinase 1 (Cdk1) is essential for cell division and suppression of DNA re-replication but not for liver regeneration. *Proc. Natl. Acad. Sci.* **109**, 3826–3831 (2012).
105. Zarkowska, T. & Mittnacht, S. Differential Phosphorylation of the Retinoblastoma Protein by G1/S Cyclin-dependent Kinases. *J. Biol. Chem.* **272**, 12738–12746 (1997).

106. Futatsugi, A. *et al.* Cyclin-dependent kinase 5 regulates E2F transcription factor through phosphorylation of Rb protein in neurons. *Cell Cycle* **11**, 1603–1610 (2012).
107. Paparidis, N. F. dos S., Durvale, M. C. & Canduri, F. The emerging picture of CDK9/P-TEFb: more than 20 years of advances since PITALRE. *Mol. Biosyst.* **13**, 246–276 (2017).
108. Boffo, S., Damato, A., Alfano, L. & Giordano, A. CDK9 inhibitors in acute myeloid leukemia. *J. Exp. Clin. Cancer Res.* **37**, 36 (2018).
109. Horiuchi, D. *et al.* MYC pathway activation in triple-negative breast cancer is synthetic lethal with CDK inhibition. *J. Exp. Med.* **209**, 679–696 (2012).
110. Pongtornpipat, P., Puvvada, S. D. & Schatz, J. H. Targeting MYC Expression With CDK Inhibitors Shows Potency In Preclinical Models Of High-Risk Diffuse Large B-Cell Lymphom. *Blood* **122**, 1831–1831 (2013).
111. Moharram, S. A. *et al.* Efficacy of the CDK inhibitor dinaciclib in vitro and in vivo in T-cell acute lymphoblastic leukemia. *Cancer Lett.* **405**, 73–78 (2017).
112. Brägelmann, J. *et al.* Systematic Kinase Inhibitor Profiling Identifies CDK9 as a Synthetic Lethal Target in NUT Midline Carcinoma. *Cell Rep.* **20**, 2833–2845 (2017).
113. Prevo, R. *et al.* CDK1 inhibition sensitizes normal cells to DNA damage in a cell cycle dependent manner. *Cell Cycle Georget. Tex* **17**, 1513–1523 (2018).
114. Rowland, T. *et al.* Selective Targeting Cyclin-Dependent Kinase-9 (CDK9) Downmodulates c-MYC and Induces Apoptosis in Diffuse Large B-Cell Lymphoma (DLBCL) Cells. *Blood* **128**, 289–289 (2016).
115. Sonawane, Y. A. *et al.* Cyclin Dependent Kinase 9 Inhibitors for Cancer Therapy. *J. Med. Chem.* **59**, 8667–8684 (2016).
116. Wang, S. & Fischer, P. M. Cyclin-dependent kinase 9: a key transcriptional regulator and potential drug target in oncology, virology and cardiology. *Trends Pharmacol. Sci.* **29**, 302–313 (2008).
117. Bussolati, B., Bruno, S., Grange, C., Ferrando, U. & Camussi, G. Identification of a tumor-initiating stem cell population in human renal carcinomas. *FASEB J.* **22**, 3696–3705 (2008).
118. Hu, J. *et al.* Endoglin Is Essential for the Maintenance of Self-Renewal and Chemoresistance in Renal Cancer Stem Cells. *Stem Cell Rep.* **9**, 464–477 (2017).
119. Peired, A. J., Sisti, A. & Romagnani, P. Renal Cancer Stem Cells: Characterization and Targeted Therapies. *Stem Cells Int.* **2016**, (2016).
120. Zhong, Y. *et al.* Spheres derived from the human SK-RC-42 renal cell carcinoma cell line are enriched in cancer stem cells. *Cancer Lett.* **299**, 150–160 (2010).
121. Hu, J. *et al.* Cancer Stem Cell Marker Endoglin (CD105) Induces Epithelial Mesenchymal Transition (EMT) but Not Metastasis in Clear Cell Renal Cell Carcinoma. *Stem Cells Int.* **2019**, (2019).
122. Mita, M. M. *et al.* Randomized Phase II Trial of the Cyclin-Dependent Kinase Inhibitor Dinaciclib (MK-7965) Versus Capecitabine in Patients With Advanced Breast Cancer. *Clin. Breast Cancer* **14**, 169–176 (2014).
123. Stephenson, J. J. *et al.* Randomized phase 2 study of the cyclin-dependent kinase inhibitor dinaciclib (MK-7965) versus erlotinib in patients with non-small cell lung cancer. *Lung Cancer* **83**, 219–223 (2014).
124. Xiao, H. *et al.* miR-206 functions as a novel cell cycle regulator and tumor suppressor in clear-cell renal cell carcinoma. *Cancer Lett.* **374**, 107–116 (2016).

125. Li, Y. *et al.* MiR-31-5p acts as a tumor suppressor in renal cell carcinoma by targeting cyclin-dependent kinase 1 (CDK1). *Biomed. Pharmacother.* **111**, 517–526 (2019).
126. Tang, J. *et al.* Wilms' tumor 1-associating protein promotes renal cell carcinoma proliferation by regulating CDK2 mRNA stability. *J. Exp. Clin. Cancer Res.* **37**, 40 (2018).
127. Juengel, E. *et al.* HDAC-inhibition counteracts everolimus resistance in renal cell carcinoma in vitro by diminishing cdk2 and cyclin A. *Mol. Cancer* **13**, 152 (2014).
128. Tadesse, S., Caldon, E. C., Tilley, W. & Wang, S. Cyclin-Dependent Kinase 2 Inhibitors in Cancer Therapy: An Update. *J. Med. Chem.* **62**, 4233–4251 (2019).
129. Bindra, R. S., Vasselli, J. R., Stearman, R., Linehan, W. M. & Klausner, R. D. VHL-mediated Hypoxia Regulation of Cyclin D1 in Renal Carcinoma Cells. *Cancer Res.* **62**, 3014–3019 (2002).
130. GDC. Available at: https://portal.gdc.cancer.gov/. (Accessed: 16th July 2019)
131. R2 Genomics Analysis and Visualization Platform. Available at: http://hgserver1.amc.nl/cgi-bin/r2/main.cgi. (Accessed: 19th July 2019)
132. Timaner, M. *et al.* Therapy-Educated Mesenchymal Stem Cells Enrich for Tumor-Initiating Cells. *Cancer Res.* **78**, 1253–1265 (2018).
133. Chen, X., Liao, R., Li, D. & Sun, J. Induced cancer stem cells generated by radiochemotherapy and their therapeutic implications. *Oncotarget* **8**, 17301–17312 (2016).
134. Coschi, C. H. *et al.* Mitotic chromosome condensation mediated by the retinoblastoma protein is tumor-suppressive. *Genes Dev.* **24**, 1351–1363 (2010).
135. Storchova, Z. & Kuffer, C. The consequences of tetraploidy and aneuploidy. *J. Cell Sci.* **121**, 3859–3866 (2008).
136. Li, R. *et al.* Aneuploidy correlated 100% with chemical transformation of Chinese hamster cells. *Proc. Natl. Acad. Sci.* **94**, 14506–14511 (1997).
137. Johnson, I. S., Wright, H. F., Svoboda, G. H. & Vlantis, J. Antitumor Principles Derived from Vinca rosea Linn: I. Vincaleukoblastine and Leurosine. *Cancer Res.* **20**, 1016–1022 (1960).
138. Steinmetz, M. O. & Prota, A. E. Microtubule-Targeting Agents: Strategies To Hijack the Cytoskeleton. *Trends Cell Biol.* **28**, 776–792 (2018).
139. Hergovich, A., Lisztwan, J., Barry, R., Ballschmieter, P. & Krek, W. Regulation of microtubule stability by the von Hippel-Lindau tumour suppressor protein pVHL. *Nat. Cell Biol.* **5**, 64–70 (2003).
140. Oku, Y. *et al.* Multimodal Effects of Small Molecule ROCK and LIMK Inhibitors on Mitosis, and Their Implication as Anti-Leukemia Agents. *PLOS ONE* **9**, e92402 (2014).
141. Thompson, S. L. & Compton, D. A. Chromosome missegregation in human cells arises through specific types of kinetochore–microtubule attachment errors. *Proc. Natl. Acad. Sci. U. S. A.* **108**, 17974–17978 (2011).
142. Huang, Y. *et al.* Lagging chromosomes entrapped in micronuclei are not 'lost' by cells. *Cell Res.* **22**, 932–935 (2012).
143. Chan, J. Y. A Clinical Overview of Centrosome Amplification in Human Cancers. *Int. J. Biol. Sci.* **7**, 1122–1144 (2011).

144. Schofield, A. V., Steel, R. & Bernard, O. Rho-associated Coiled-coil Kinase (ROCK) Protein Controls Microtubule Dynamics in a Novel Signaling Pathway That Regulates Cell Migration. *J. Biol. Chem.* **287**, 43620–43629 (2012).
145. Kosako, H. *et al.* Rho-kinase/ROCK is involved in cytokinesis through the phosphorylation of myosin light chain and not ezrin/radixin/moesin proteins at the cleavage furrow. *Oncogene* **19**, 6059 (2000).
146. Kanai, M., Crowe, M. S., Zheng, Y., Vande Woude, G. F. & Fukasawa, K. RhoA and RhoC Are Both Required for the ROCK II-Dependent Promotion of Centrosome Duplication. *Oncogene* **29**, 6040–6050 (2010).
147. Ma, Z. *et al.* Interaction between ROCK II and Nucleophosmin/B23 in the Regulation of Centrosome Duplication. *Mol. Cell. Biol.* **26**, 9016–9034 (2006).
148. Ganem, N. J., Godinho, S. A. & Pellman, D. A mechanism linking extra centrosomes to chromosomal instability. *Nature* **460**, 278–282 (2009).
149. Navarro-Serer, B., Childers, E. P., Hermance, N. M., Mercadante, D. & Manning, A. L. Aurora A inhibition limits centrosome clustering and promotes mitotic catastrophe in cells with supernumerary centrosomes. *Oncotarget* **10**, 1649–1659 (2019).
150. Leber, B. *et al.* Proteins Required for Centrosome Clustering in Cancer Cells. *Sci. Transl. Med.* **2**, 33ra38-33ra38 (2010).
151. dos Santos, E. O., Carneiro-Lobo, T. C., Aoki, M. N., Levantini, E. & Bassères, D. S. Aurora kinase targeting in lung cancer reduces KRAS-induced transformation. *Mol. Cancer* **15**, 12 (2016).
152. Opyrchal, M. *et al.* Molecular targeting of the Aurora-A/SMAD5 oncogenic axis restores chemosensitivity in human breast cancer cells. *Oncotarget* **8**, 91803–91816 (2017).
153. Ding, X.-F. *et al.* VHL loss predicts response to Aurora kinase A inhibitor in renal cell carcinoma cells. *Mol. Med. Rep.* **18**, 1206–1210 (2018).
154. Foulkes, W. D., Smith, I. E. & Reis-Filho, J. S. Triple-Negative Breast Cancer. *N. Engl. J. Med.* **363**, 1938–1948 (2010).
155. Carey, L., Winer, E., Viale, G., Cameron, D. & Gianni, L. Triple-negative breast cancer: disease entity or title of convenience? *Nat. Rev. Clin. Oncol.* **7**, 683–692 (2010).
156. Doane, A. S. *et al.* An estrogen receptor-negative breast cancer subset characterized by a hormonally regulated transcriptional program and response to androgen. *Oncogene* **25**, 3994–4008 (2006).
157. Bareche, Y. *et al.* Unravelling triple-negative breast cancer molecular heterogeneity using an integrative multiomic analysis. *Ann. Oncol.* **29**, 895–902 (2018).
158. Dieci, M. V., Orvieto, E., Dominici, M., Conte, P. & Guarneri, V. Rare Breast Cancer Subtypes: Histological, Molecular, and Clinical Peculiarities. *The Oncologist* **19**, 805–813 (2014).
159. Burstein, M. D. *et al.* Comprehensive Genomic Analysis Identifies Novel Subtypes and Targets of Triple-Negative Breast Cancer. *Clin. Cancer Res.* **21**, 1688–1698 (2015).
160. Neve, R. M. *et al.* A collection of breast cancer cell lines for the study of functionally distinct cancer subtypes. *Cancer Cell* **10**, 515–527 (2006).

161. Hennessy, B. T. *et al.* Characterization of a Naturally Occurring Breast Cancer Subset Enriched in Epithelial-to-Mesenchymal Transition and Stem Cell Characteristics. *Cancer Res.* **69**, 4116–4124 (2009).
162. Taube, J. H. *et al.* Core epithelial-to-mesenchymal transition interactome gene-expression signature is associated with claudin-low and metaplastic breast cancer subtypes. *Proc. Natl. Acad. Sci.* **107**, 15449–15454 (2010).
163. Sarrió, D. *et al.* Epithelial-Mesenchymal Transition in Breast Cancer Relates to the Basal-like Phenotype. *Cancer Res.* **68**, 989–997 (2008).
164. Hunter, T. & Sefton, B. M. Transforming gene product of Rous sarcoma virus phosphorylates tyrosine. *Proc. Natl. Acad. Sci. U. S. A.* **77**, 1311–1315 (1980).
165. Irby, R. B. & Yeatman, T. J. Role of Src expression and activation in human cancer. *Oncogene* **19**, 5636–5642 (2000).
166. Summy, J. M. & Gallick, G. E. Src family kinases in tumor progression and metastasis. *Cancer Metastasis Rev.* **22**, 337–358 (2003).
167. Yeatman, T. J. A renaissance for SRC. *Nat. Rev. Cancer* **4**, 470–480 (2004).
168. Finn, R. S. Targeting Src in breast cancer. *Ann. Oncol.* **19**, 1379–1386 (2008).
169. Wheeler, D. L., Iida, M. & Dunn, E. F. The Role of Src in Solid Tumors. *The Oncologist* **14**, 667–678 (2009).
170. Elsberger, B. Translational evidence on the role of Src kinase and activated Src kinase in invasive breast cancer. *Crit. Rev. Oncol. Hematol.* **89**, 343–351 (2014).
171. Verbeek, B. S. *et al.* c-Src PROTEIN EXPRESSION IS INCREASED IN HUMAN BREAST CANCER. AN IMMUNOHISTOCHEMICAL AND BIOCHEMICAL ANALYSIS. *J. Pathol.* **180**, 383–388
172. Rosen, N. *et al.* Analysis of pp60c-src protein kinase activity in human tumor cell lines and tissues. *J. Biol. Chem.* **261**, 13754–13759 (1986).
173. Bolen, J. B., Veillette, A., Schwartz, A. M., DeSeau, V. & Rosen, N. Activation of pp60c-src protein kinase activity in human colon carcinoma. *Proc. Natl. Acad. Sci.* **84**, 2251–2255 (1987).
174. Talamonti, M. S., Roh, M. S., Curley, S. A. & Gallick, G. E. Increase in activity and level of pp60c-src in progressive stages of human colorectal cancer. *J. Clin. Invest.* **91**, 53–60 (1993).
175. Muthuswamy, S. K., Siegel, P. M., Dankort, D. L., Webster, M. A. & Muller, W. J. Mammary tumors expressing the neu proto-oncogene possess elevated c-Src tyrosine kinase activity. *Mol. Cell. Biol.* **14**, 735–743 (1994).
176. Curtis, C. *et al.* The genomic and transcriptomic architecture of 2,000 breast tumours reveals novel subgroups. *Nature* **486**, 346–352 (2012).
177. Network, T. C. G. A. Comprehensive molecular portraits of human breast tumours. *Nature* **490**, 61–70 (2012).
178. Bailey, M. H. *et al.* Comprehensive Characterization of Cancer Driver Genes and Mutations. *Cell* **173**, 371-385.e18 (2018).
179. Roskoski, R. Src kinase regulation by phosphorylation and dephosphorylation. *Biochem. Biophys. Res. Commun.* **331**, 1–14 (2005).
180. Taylor, S. S., Keshwani, M. M., Steichen, J. M. & Kornev, A. P. Evolution of the eukaryotic protein kinases as dynamic molecular switches. *Philos. Trans. R. Soc. Lond. B. Biol. Sci.* **367**, 2517–2528 (2012).

181. Okada, M. Regulation of the SRC family kinases by Csk. *Int. J. Biol. Sci.* **8**, 1385–1397 (2012).
182. Meng, Y. & Roux, B. Locking the active conformation of c-Src kinase through the phosphorylation of the activation loop. *J. Mol. Biol.* **426**, 423–435 (2014).
183. Porter, M., Schindler, T., Kuriyan, J. & Miller, W. T. Reciprocal Regulation of Hck Activity by Phosphorylation of Tyr527 and Tyr416 EFFECT OF INTRODUCING A HIGH AFFINITY INTRAMOLECULAR SH2 LIGAND. *J. Biol. Chem.* **275**, 2721–2726 (2000).
184. Bromann, P. A., Korkaya, H. & Courtneidge, S. A. The interplay between Src family kinases and receptor tyrosine kinases. *Oncogene* **23**, 7957–7968 (2004).
185. Thomas, S. M. & Brugge, J. S. Cellular functions regulated by Src family kinases. *Annu. Rev. Cell Dev. Biol.* **13**, 513–609 (1997).
186. Mader, C. C. *et al.* An EGFR–Src–Arg–Cortactin Pathway Mediates Functional Maturation of Invadopodia and Breast Cancer Cell Invasion. *Cancer Res.* **71**, 1730–1741 (2011).
187. Kollmorgen, G., Bossenmaier, B., Niederfellner, G., Häring, H.-U. & Lammers, R. Structural Requirements for Cub Domain Containing Protein 1 (CDCP1) and Src Dependent Cell Transformation. *PLOS ONE* **7**, e53050 (2012).
188. Brown, T. A. *et al.* Adhesion or Plasmin Regulates Tyrosine Phosphorylation of a Novel Membrane Glycoprotein p80/gp140/CUB Domain-containing Protein 1 in Epithelia. *J. Biol. Chem.* **279**, 14772–14783 (2004).
189. Liu, H. *et al.* CUB-domain-containing protein 1 (CDCP1) activates Src to promote melanoma metastasis. *Proc. Natl. Acad. Sci. U. S. A.* **108**, 1379–1384 (2011).
190. Benes, C. H. *et al.* The C2 domain of PKCdelta is a phosphotyrosine binding domain. *Cell* **121**, 271–280 (2005).
191. Uekita, T. & Sakai, R. Roles of CUB domain-containing protein 1 signaling in cancer invasion and metastasis. *Cancer Sci.* **102**, 1943–1948 (2011).
192. Bhatt, A. S., Erdjument-Bromage, H., Tempst, P., Craik, C. S. & Moasser, M. M. Adhesion signaling by a novel mitotic substrate of src kinases. *Oncogene* **24**, 5333–5343 (2005).
193. Benes, C. & Soltoff, S. P. Modulation of PKCdelta tyrosine phosphorylation and activity in salivary and PC-12 cells by Src kinases. *Am. J. Physiol. Cell Physiol.* **280**, C1498-1510 (2001).
194. Razorenova, O. V. *et al.* VHL loss in renal cell carcinoma leads to up-regulation of CUB domain-containing protein 1 to stimulate PKC{delta}-driven migration. *Proc. Natl. Acad. Sci. U. S. A.* **108**, 1931–1936 (2011).
195. Isakov, N. Protein kinase C (PKC) isoforms in cancer, tumor promotion and tumor suppression. *Semin. Cancer Biol.* **48**, 36–52 (2018).
196. Allen-Petersen, B. L., Carter, C. J., Ohm, A. M. & Reyland, M. E. Protein kinase Cδ is required for ErbB2-driven mammary gland tumorigenesis and negatively correlates with prognosis in human breast cancer. *Oncogene* **33**, 1306–1315 (2014).
197. Garg, R. *et al.* Protein kinase C and cancer: what we know and what we do not. *Oncogene* **33**, 5225–5237 (2014).
198. Benes, C., Poulogiannis, G., Cantley, L. & Soltoff, S. The SRC-associated protein CUB Domain-Containing Protein-1 regulates adhesion and motility. *Oncogene* **31**, 653–663 (2012).

199. Boyer, B., Tucker, G. C., Vallés, A. M., Gavrilovic, J. & Thiery, J. P. Reversible transition towards a fibroblastic phenotype in a rat carcinoma cell line. *Int. J. Cancer Suppl. J. Int. Cancer Suppl.* **4**, 69–75 (1989).
200. Cimino-Mathews, A. *et al.* Neural crest transcription factor Sox10 is preferentially expressed in triple-negative and metaplastic breast carcinomas. *Hum. Pathol.* **44**, 959–965 (2013).
201. Nielsen, T. O. *et al.* Immunohistochemical and Clinical Characterization of the Basal-Like Subtype of Invasive Breast Carcinoma. *Clin. Cancer Res.* **10**, 5367–5374 (2004).
202. Bhargava, R., Beriwal, S., McManus, K. & Dabbs, D. J. CK5 is more sensitive than CK5/6 in identifying the 'basal-like' phenotype of breast carcinoma. *Am. J. Clin. Pathol.* **130**, 724–730 (2008).
203. Smart, J. E. *et al.* Characterization of sites for tyrosine phosphorylation in the transforming protein of Rous sarcoma virus (pp60v-src) and its normal cellular homologue (pp60c-src). *Proc. Natl. Acad. Sci. U. S. A.* **78**, 6013–6017 (1981).
204. Anbalagan, M. *et al.* Subcellular localization of total and activated Src kinase in African American and Caucasian breast cancer. *PloS One* **7**, e33017 (2012).
205. Li, J. *et al.* TCPA: a resource for cancer functional proteomics data. *Nat. Methods* **10**, 1046–1047 (2013).
206. Cooper, J. A., Gould, K. L., Cartwright, C. A. & Hunter, T. Tyr527 is phosphorylated in pp60c-src: implications for regulation. *Science* **231**, 1431–1434 (1986).
207. Sausgruber, N. *et al.* Tyrosine phosphatase SHP2 increases cell motility in triple-negative breast cancer through the activation of SRC-family kinases. *Oncogene* **34**, 2272–2278 (2015).
208. Laird, A. D. *et al.* Src Family Kinase Activity Is Required for Signal Tranducer and Activator of Transcription 3 and Focal Adhesion Kinase Phosphorylation and Vascular Endothelial Growth Factor Signaling in Vivo and for Anchorage-dependent and -independent Growth of Human Tumor Cells. *Mol. Cancer Ther.* **2**, 461–469 (2003).
209. Gandji, L. Y., Proust, R., Larue, L. & Gesbert, F. The Tyrosine Phosphatase SHP2 Associates with CUB Domain-Containing Protein-1 (CDCP1), Regulating Its Expression at the Cell Surface in a Phosphorylation-Dependent Manner. *PLOS ONE* **10**, e0123472 (2015).
210. Szklarczyk, D. *et al.* The STRING database in 2017: quality-controlled protein–protein association networks, made broadly accessible. *Nucleic Acids Res.* **45**, D362–D368 (2017).
211. Voorwerk, L., Kat, M. & Kok, M. Towards predictive biomarkers for immunotherapy response in breast cancer patients. *Breast Cancer Manag.* **7**, BMT05 (2018).
212. Zhang, X. H.-F. *et al.* Latent bone metastasis in breast cancer tied to Src-dependent survival signals. *Cancer Cell* **16**, 67–78 (2009).
213. Guest, S. K. *et al.* Src Is a Potential Therapeutic Target in Endocrine-Resistant Breast Cancer Exhibiting Low Estrogen Receptor-Mediated Transactivation. *PloS One* **11**, e0157397 (2016).
214. Zhang, S. *et al.* Combating trastuzumab resistance by targeting SRC, a common node downstream of multiple resistance pathways. *Nat. Med.* **17**, 461–469 (2011).

215. de Melo Gagliato, D., Jardim, D. L. F., Marchesi, M. S. P. & Hortobagyi, G. N. Mechanisms of resistance and sensitivity to anti-HER2 therapies in HER2+ breast cancer. *Oncotarget* **7**, 64431–64446 (2016).
216. Uekita, T. *et al.* CUB domain-containing protein 1 is a novel regulator of anoikis resistance in lung adenocarcinoma. *Mol. Cell. Biol.* **27**, 7649–7660 (2007).
217. Elsberger, B. *et al.* Is expression or activation of Src kinase associated with cancer-specific survival in ER-, PR- and HER2-negative breast cancer patients? *Am. J. Pathol.* **175**, 1389–1397 (2009).
218. Kanomata, N., Kurebayashi, J., Kozuka, Y., Sonoo, H. & Moriya, T. Clinicopathological significance of Y416Src and Y527Src expression in breast cancer. *J. Clin. Pathol.* **64**, 578–586 (2011).
219. Huang, R. Y.-J. *et al.* An EMT spectrum defines an anoikis-resistant and spheroidogenic intermediate mesenchymal state that is sensitive to e-cadherin restoration by a src-kinase inhibitor, saracatinib (AZD0530). *Cell Death Dis.* **4**, e915 (2013).
220. Elsberger, B. *et al.* Breast cancer patients' clinical outcome measures are associated with Src kinase family member expression. *Br. J. Cancer* **103**, 899–909 (2010).
221. Martins, M. M. *et al.* Linking Tumor Mutations to Drug Responses via a Quantitative Chemical–Genetic Interaction Map. *Cancer Discov.* **5**, 154–167 (2015).
222. Aleshin, A. & Finn, R. S. SRC: A Century of Science Brought to the Clinic. *Neoplasia* **12**, 599–607 (2010).
223. Woodcock, V. K. *et al.* A first-in-human phase I study to determine the maximum tolerated dose of the oral Src/ABL inhibitor AZD0424. *Br. J. Cancer* **118**, 770–776 (2018).
224. Finn, R. S. *et al.* Dasatinib as a Single Agent in Triple-Negative Breast Cancer: Results of an Open-Label Phase 2 Study. *Clin. Cancer Res.* **17**, 6905–6913 (2011).
225. Spassov, D. S., Wong, C. H., Wong, S. Y., Reiter, J. F. & Moasser, M. M. Trask Loss Enhances Tumorigenic Growth by Liberating Integrin Signaling and Growth Factor Receptor Cross-Talk in Unanchored Cells. *Cancer Res.* **73**, 1168–1179 (2013).
226. Nakashima, K. *et al.* Novel small molecule inhibiting CDCP1-PKCδ pathway reduces tumor metastasis and proliferation. *Cancer Sci.* **108**, 1049–1057 (2017).
227. Roskoski, R. Src protein–tyrosine kinase structure and regulation. *Biochem. Biophys. Res. Commun.* **324**, 1155–1164 (2004).
228. Martin, G. S. The hunting of the Src. *Nat. Rev. Mol. Cell Biol.* **2**, 467–475 (2001).
229. Sun, G., Sharma, A. K. & Budde, R. J. Autophosphorylation of Src and Yes blocks their inactivation by Csk phosphorylation. *Oncogene* **17**, 1587–1595 (1998).
230. Zhang, H., Davies, K. J. A. & Forman, H. J. TGFβ1 rapidly activates Src through a non-canonical redox signaling mechanism. *Arch. Biochem. Biophys.* **568**, 1–7 (2015).
231. Iliopoulos, D., Hirsch, H. A. & Struhl, K. An Epigenetic Switch Involving NF-κB, Lin28, Let-7 MicroRNA, and IL6 Links Inflammation to Cell Transformation. *Cell* **139**, 693–706 (2009).
232. Schmid, P. *et al.* Atezolizumab and Nab-Paclitaxel in Advanced Triple-Negative Breast Cancer. *N. Engl. J. Med.* **379**, 2108–2121 (2018).
233. Shi, S. R., Key, M. E. & Kalra, K. L. Antigen retrieval in formalin-fixed, paraffin-embedded tissues: an enhancement method for immunohistochemical staining based

on microwave oven heating of tissue sections. *J. Histochem. Cytochem. Off. J. Histochem. Soc.* **39**, 741–748 (1991).
234. Hood, B. L. *et al.* Proteomic analysis of formalin-fixed prostate cancer tissue. *Mol. Cell. Proteomics MCP* **4**, 1741–1753 (2005).
235. Sprung, R. W. *et al.* Equivalence of protein inventories obtained from formalin-fixed paraffin-embedded and frozen tissue in multidimensional liquid chromatography-tandem mass spectrometry shotgun proteomic analysis. *Mol. Cell. Proteomics MCP* **8**, 1988–1998 (2009).
236. Ostasiewicz, P., Zielinska, D. F., Mann, M. & Wiśniewski, J. R. Proteome, phosphoproteome, and N-glycoproteome are quantitatively preserved in formalin-fixed paraffin-embedded tissue and analyzable by high-resolution mass spectrometry. *J. Proteome Res.* **9**, 3688–3700 (2010).
237. Baker, A. F. *et al.* Stability of Phosphoprotein as a Biological Marker of Tumor Signaling. *Clin. Cancer Res.* **11**, 4338–4340 (2005).
238. Gündisch, S. *et al.* Critical roles of specimen type and temperature before and during fixation in the detection of phosphoproteins in breast cancer tissues. *Lab. Invest.* **95**, 561–571 (2015).
239. Shi, S.-R., Taylor, C. R., Fowler, C. B. & Mason, J. T. Complete solubilization of formalin-fixed, paraffin-embedded tissue may improve proteomic studies. *PROTEOMICS – Clin. Appl.* **7**, 264–272
240. Pedersen, M. H. *et al.* Downregulation of antigen presentation-associated pathway proteins is linked to poor outcome in triple-negative breast cancer patient tumors. *Oncoimmunology* **6**, e1305531 (2017).
241. Wiśniewski, J. R. & Gaugaz, F. Z. Fast and Sensitive Total Protein and Peptide Assays for Proteomic Analysis. *Anal. Chem.* **87**, 4110–4116 (2015).
242. Faried, A., Faried, L. S., Usman, N., Kato, H. & Kuwano, H. Clinical and Prognostic Significance of RhoA and RhoC Gene Expression in Esophageal Squamous Cell Carcinoma. *Ann. Surg. Oncol.* **14**, 3593–3601 (2007).
243. Kamai, T. *et al.* Overexpression of RhoA, Rac1, and Cdc42 GTPases Is Associated with Progression in Testicular Cancer. *Clin. Cancer Res.* **10**, 4799–4805 (2004).
244. Barrio-Real, L. & Kazanietz, M. G. Rho GEFs and Cancer: Linking Gene Expression and Metastatic Dissemination. *Sci. Signal.* **5**, pe43–pe43 (2012).
245. Vigil, D., Cherfils, J., Rossman, K. L. & Der, C. J. Ras superfamily GEFs and GAPs: validated and tractable targets for cancer therapy? *Nat. Rev. Cancer* **10**, 842–857 (2010).
246. Maranchie, J. K. *et al.* The contribution of VHL substrate binding and HIF1-α to the phenotype of VHL loss in renal cell carcinoma. *Cancer Cell* **1**, 247–255 (2002).
247. Kao, A. *et al.* Development of a Novel Cross-linking Strategy for Fast and Accurate Identification of Cross-linked Peptides of Protein Complexes. *Mol. Cell. Proteomics MCP* **10**, (2011).
248. Joseph, R. W. *et al.* Loss of BAP1 and PBRM1 protein expression and its association with clear cell renal cell carcinoma-specific survival. *J. Clin. Oncol.* **32**, 414–414 (2014).
249. Wang, S.-S. *et al.* Bap1 is essential for kidney function and cooperates with Vhl in renal tumorigenesis. *Proc. Natl. Acad. Sci.* **111**, 16538–16543 (2014).

250. Peña-Llopis, S. *et al.* BAP1 loss defines a new class of renal cell carcinoma. *Nat. Genet.* **44**, 751–759 (2012).
251. Altwairgi, A. K. Statins are potential anticancerous agents (Review). *Oncol. Rep.* **33**, 1019–1039 (2015).
252. van Buul, J. D., Geerts, D. & Huveneers, S. Rho GAPs and GEFs. *Cell Adhes. Migr.* **8**, 108–124 (2014).
253. Khurana, V., Caldito, G. & Ankem, M. Statins Might Reduce Risk of Renal Cell Carcinoma in Humans: Case-Control Study of 500,000 Veterans. *Urology* **71**, 118–122 (2008).
254. Kaffenberger, S. D. *et al.* Statin Use is Associated with Improved Survival in Patients Undergoing Surgery for Renal Cell Carcinoma. *Urol. Oncol.* **33**, 21.e11-21.e17 (2015).
255. Hamilton, R. J. *et al.* The association between statin medication and progression after surgery for localized renal cell carcinoma. *J. Urol.* **191**, 914–919 (2014).
256. Choi, S.-K. *et al.* Effects of statins on the prognosis of local and locally advanced renal cell carcinoma following nephrectomy. *Mol. Clin. Oncol.* **1**, 365–368 (2013).
257. Viers, B. R. *et al.* The association of statin therapy with clinicopathologic outcomes and survival among patients with localized renal cell carcinoma undergoing nephrectomy. *Urol. Oncol.* **33**, 388.e11–18 (2015).
258. Abdullah, M. I., de Wolf, E., Jawad, M. J. & Richardson, A. The poor design of clinical trials of statins in oncology may explain their failure – Lessons for drug repurposing. *Cancer Treat. Rev.* **69**, 84–89 (2018).
259. Hirose, Y. & Ohkuma, Y. Phosphorylation of the C-terminal Domain of RNA Polymerase II Plays Central Roles in the Integrated Events of Eucaryotic Gene Expression. *J. Biochem. (Tokyo)* **141**, 601–608 (2007).
260. Walsby, E. *et al.* A novel Cdk9 inhibitor preferentially targets tumor cells and synergizes with fludarabine. *Oncotarget* **5**, 375–385 (2013).
261. MacCallum, D. E. *et al.* Seliciclib (CYC202, R-Roscovitine) Induces Cell Death in Multiple Myeloma Cells by Inhibition of RNA Polymerase II–Dependent Transcription and Down-regulation of Mcl-1. *Cancer Res.* **65**, 5399–5407 (2005).
262. Xiang, W., Yang, C.-Y. & Bai, L. MCL-1 inhibition in cancer treatment. *OncoTargets Ther.* **11**, 7301–7314 (2018).
263. Wang, R., Xia, L., Gabrilove, J., Waxman, S. & Jing, Y. Down-regulation of Mcl-1 through GSK-3β activation contributes to arsenic trioxide-induced apoptosis in acute myeloid leukemia cells. *Leukemia* **27**, 315–324 (2013).
264. Wakatsuki, S., Tokunaga, S., Shibata, M. & Araki, T. GSK3B-mediated phosphorylation of MCL1 regulates axonal autophagy to promote Wallerian degeneration. *J. Cell Biol.* **216**, 477–493 (2017).
265. Guo, J. *et al.* pVHL suppresses kinase activity of Akt in a proline-hydroxylation–dependent manner. *Science* **353**, 929–932 (2016).
266. Beurel, E., Grieco, S. F. & Jope, R. S. Glycogen synthase kinase-3 (GSK3): Regulation, actions, and diseases. *Pharmacol. Ther.* **148**, 114–131 (2015).
267. Stock, K. *et al.* Capturing tumor complexity *in vitro*: Comparative analysis of 2D and 3D tumor models for drug discovery. *Sci. Rep.* **6**, 28951 (2016).

268. Lewis, D. M., Blatchley, M. R., Park, K. M. & Gerecht, S. O_2-controllable hydrogels for studying cellular responses to hypoxic gradients in three dimensions *in vitro* and *in vivo*. *Nat. Protoc.* **12**, 1620–1638 (2017).
269. Hell, M. P., Duda, M., Weber, T. C., Moch, H. & Krek, W. Tumor Suppressor VHL Functions in the Control of Mitotic Fidelity. *Cancer Res.* **74**, 2422–2431 (2014).
270. Willems, E. *et al.* The functional diversity of Aurora kinases: a comprehensive review. *Cell Div.* **13**, (2018).
271. Mooney, P. *et al.* Tau-based fluorescent protein fusions to visualize microtubules. *Cytoskelet. Hoboken NJ* **74**, 221–232 (2017).
272. Weaver, B. A. A. & Cleveland, D. W. Decoding the links between mitosis, cancer, and chemotherapy: The mitotic checkpoint, adaptation, and cell death. *Cancer Cell* **8**, 7–12 (2005).
273. Bekier, M. E., Fischbach, R., Lee, J. & Taylor, W. R. Length of mitotic arrest induced by microtubule-stabilizing drugs determines cell death after mitotic exit. *Mol. Cancer Ther.* **8**, 1646–1654 (2009).
274. Sabnis, A. J. & Bivona, T. G. Principles of Resistance to Targeted Cancer Therapy: Lessons from Basic and Translational Cancer Biology. *Trends Mol. Med.* **25**, 185–197 (2019).
275. LGX818 and MEK162 in Combination With a Third Agent (BKM120, LEE011, BGJ398 or INC280) in Advanced BRAF Melanoma - Full Text View - ClinicalTrials.gov. Available at: https://clinicaltrials.gov/ct2/show/NCT02159066. (Accessed: 21st July 2019)
276. Ashraf, Y. *et al.* Immunotherapy of triple-negative breast cancer with cathepsin D-targeting antibodies. *J. Immunother. Cancer* **7**, (2019).
277. Karaayvaz, M. *et al.* Unravelling subclonal heterogeneity and aggressive disease states in TNBC through single-cell RNA-seq. *Nat. Commun.* **9**, 3588 (2018).
278. Kim, C. *et al.* Chemoresistance Evolution in Triple-Negative Breast Cancer Delineated by Single-Cell Sequencing. *Cell* **173**, 879-893.e13 (2018).
279. Hughes, A. J. *et al.* Single-cell western blotting. *Nat. Methods* **11**, 749–755 (2014).

Supplemental Figures and Tables

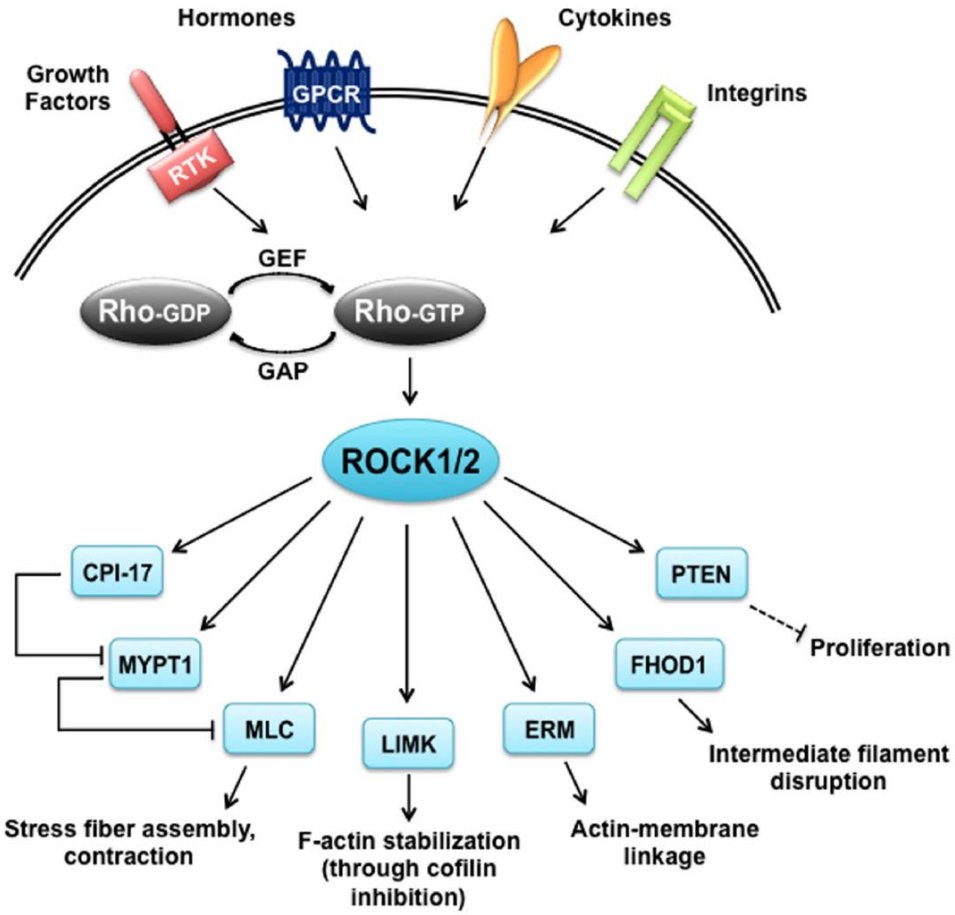

Supplemental Figure 2.1: Overview of ROCK signaling pathway
ROCK activation downstream of Rho small GTPases is stimulated by a variety of stimuli. Active ROCK phosphorylates a myriad of targets to regulate various functions within the cell, most notably actomyosin contraction and cytoskeletal processes. Adapted from Hartmann et al, 2015[74]

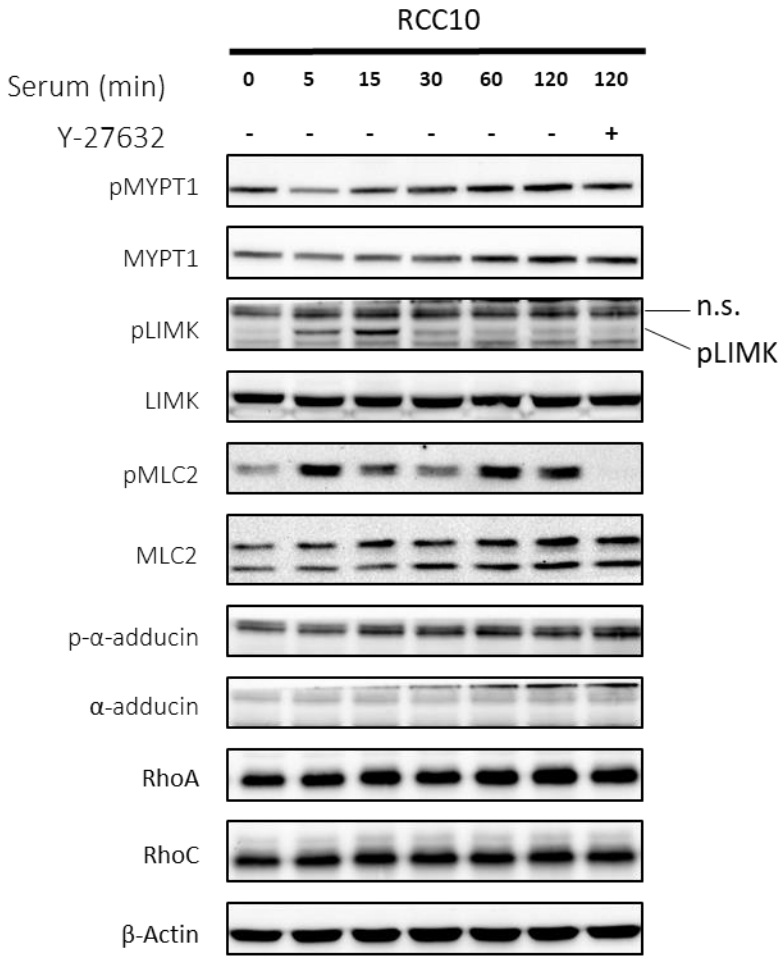

Supplemental Figure 2.2: MLC2 phosphorylation is a good readout of ROCK activity.

Western blot analysis of putative ROCK targets in RCC10 cells. Cells were serum starved overnight and then stimulated with serum-containing medium for the indicated time points, with and without the ROCK inhibitor Y-27632 (40μM), then analyzed by western blot. MLC2 was the only target that showed a marked decrease in phosphorylation upon ROCK inhibition.

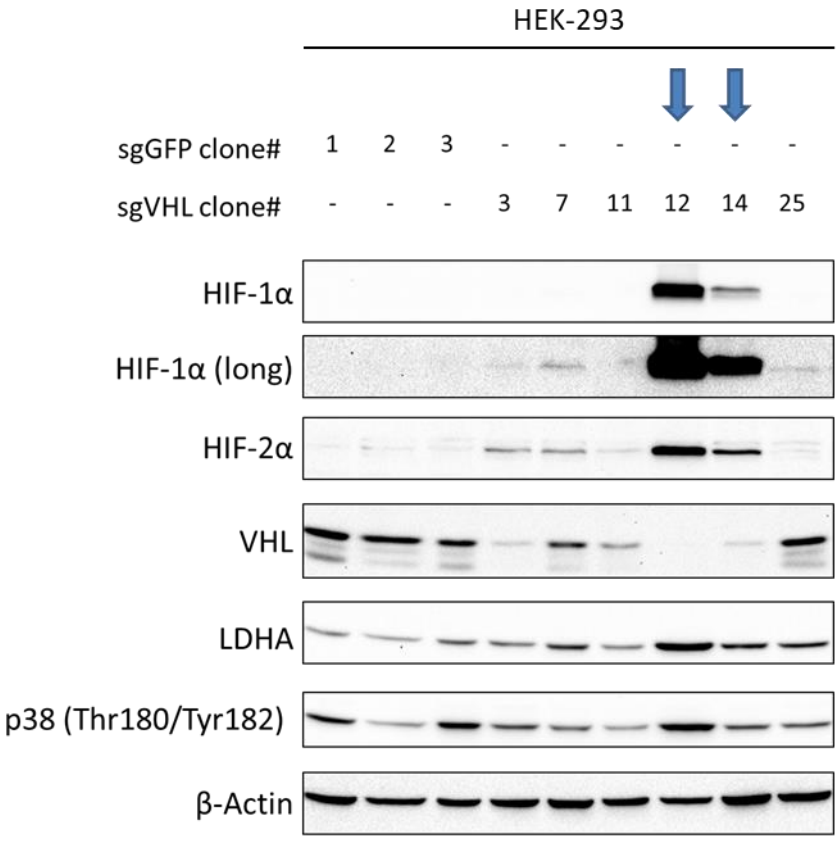

Supplemental Figure 2.3: Validation of VHL knockout lines.
Western blot analysis of selected VHL knockout HEK-293 clonal cell lines. HEK-293 cells were infected with Cas9 and VHL gRNA expressing pooled lentivirus, then plated at low density to isolate clones arising from single cells. Blue arrows indicate clones with low VHL expression and induction of HIF-1α and HIF-2α overexpression.

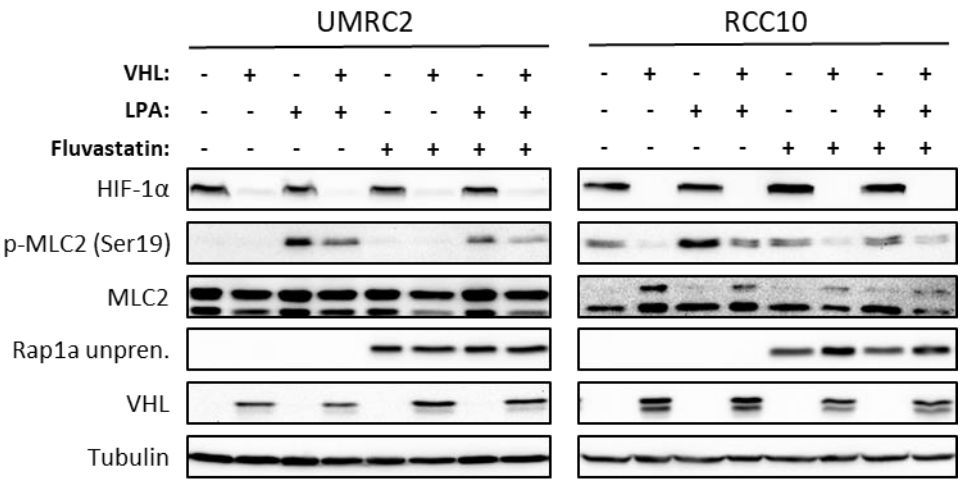

Supplemental Figure 2.4: Fluvastatin treatment decreases MLC2 phosphorylation but does not abrogate the difference between *VHL*-positive and *VHL*-negative cells. Western blot analysis of UMRC2 and RCC10 matched cell lines serum starved overnight and then treated with the indicated combination of agents. Activity of Fluvastatin was confirmed by the increase in unprenylated Rap1a after Fluvastatin treatment.

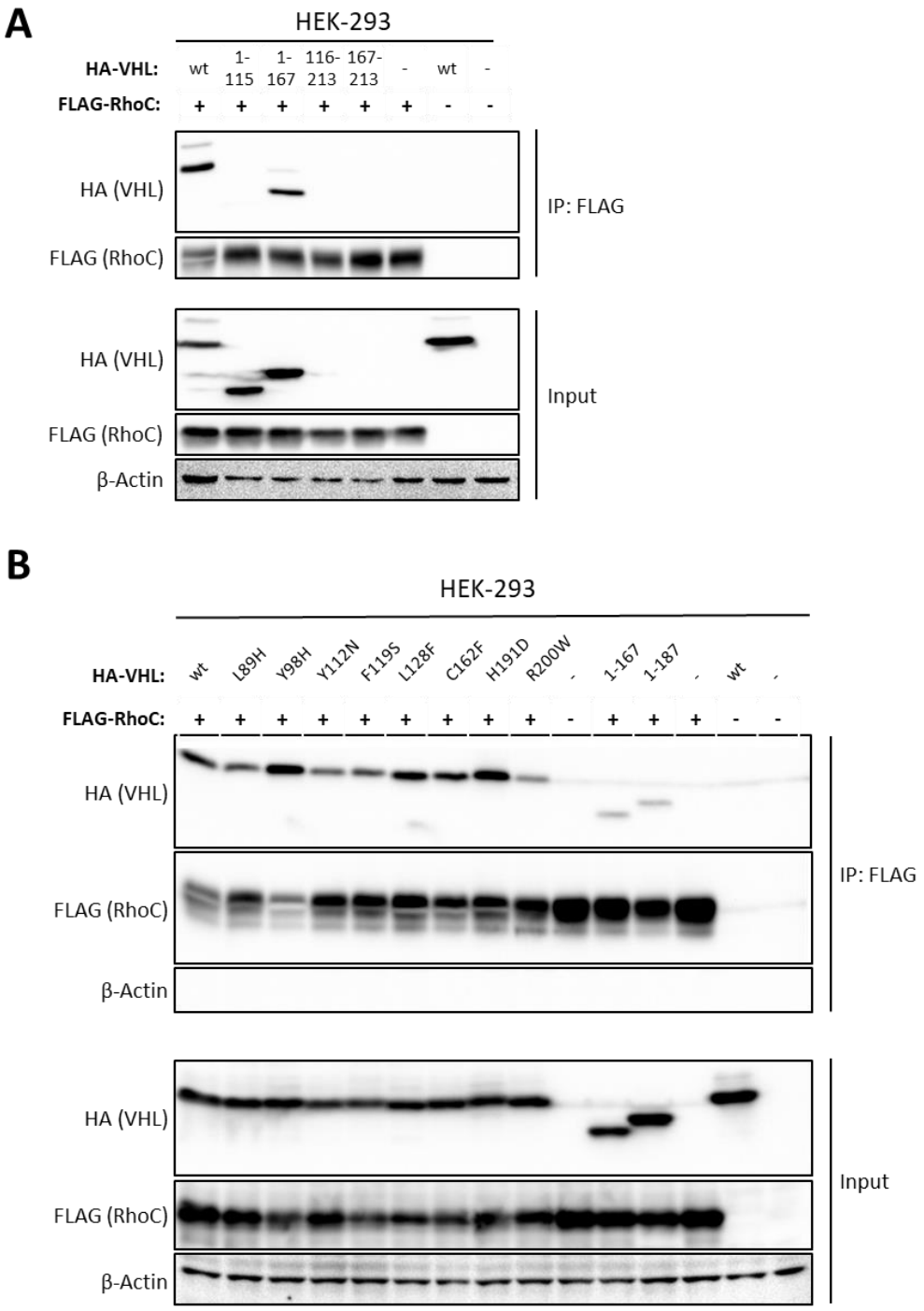

Supplemental Figure 2.5: Characterization of VHL's interaction with RhoC.
(A) VHL(1-115) truncation mutant loses the ability to bind RhoC, indicating that the alpha domain is necessary for the interaction. Alpha-domain only mutants 116-213 and 167-213 were not expressed in HEK-293 cells. **(B)** disease associated VHL mutants do not lose the ability to interact with RhoC. Tagged constructs encoding HA-VHL and FLAG-RhoC were co-transfected in HEK-293 cells, then harvested for FLAG co-immunoprecipitation (co-IP).

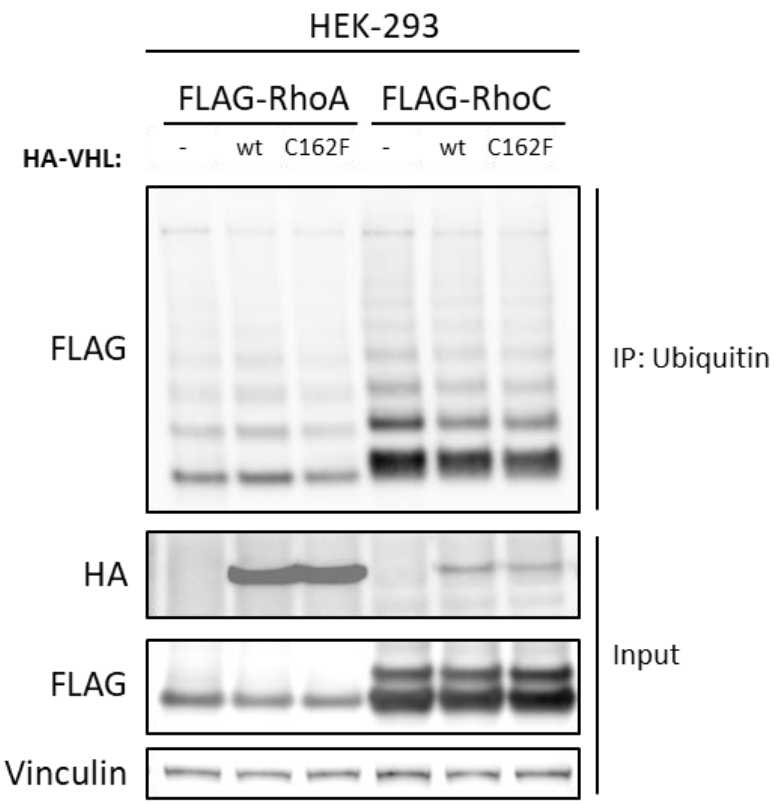

Supplemental Figure 2.6: VHL expression does not alter Rho ubiquitination in HEK-293 cells.

Overexpression of wt or C162F VHL does not alter the levels of RhoA or RhoC ubiquitination. Cells were transfected with the indicated plasmids for 24 hours, then subjected to immunoprecipitation of ubiquitinated proteins and western blot analysis.

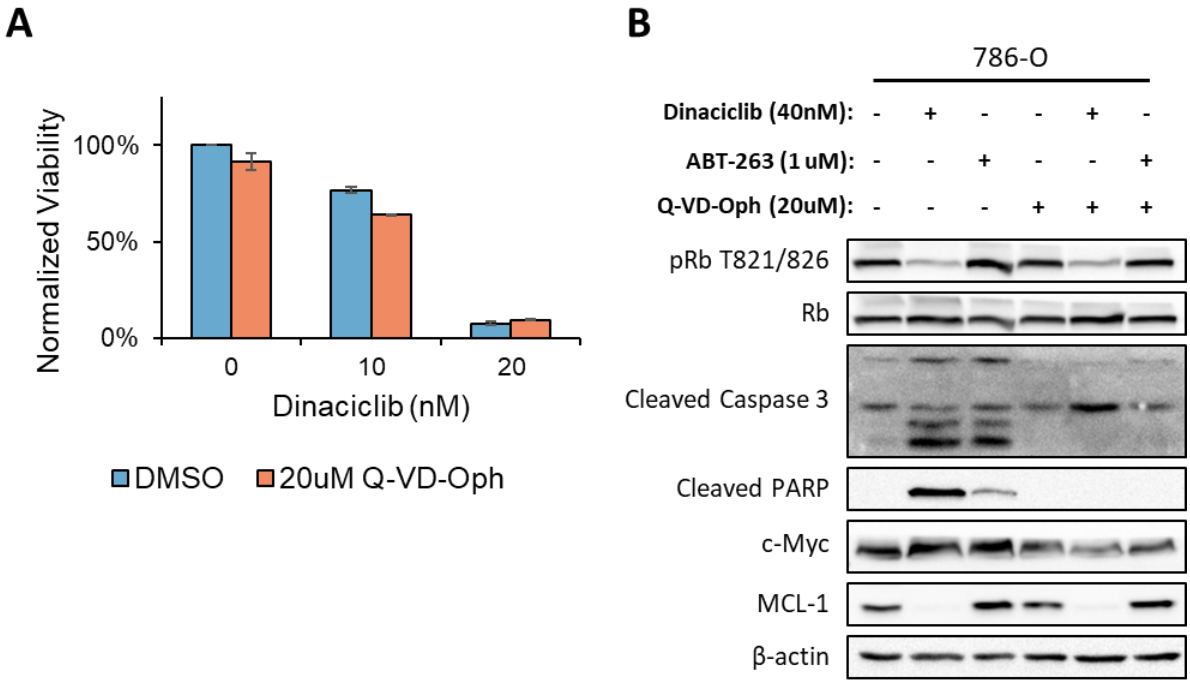

Supplemental Figure 3.1: Inhibition of apoptosis does not rescue proliferation inhibition by Dinaciclib in 786-O cells.

(A) Inhibition of apoptosis with Q-VD-OPh does not alter Dinaciclib's ability to inhibit proliferation in 786-O cells. Cells were plated in 96 well plates and treated for 5 days with Dinaciclib or vehicle, with or without 20μM Q-VD-OPh, then analyzed using CTG assay. (**B)** Q-VD-OPh efficiently inhibits expression of apoptosis markers. Cells were treated with the indicated compounds for 24 hours and analyzed by western blot. ABT-263 was included as a positive control for the induction of apoptosis. Each experiment was repeated 3 times, and error bars represent the standard error of the mean. Significance was calculated using unpaired student's t test.

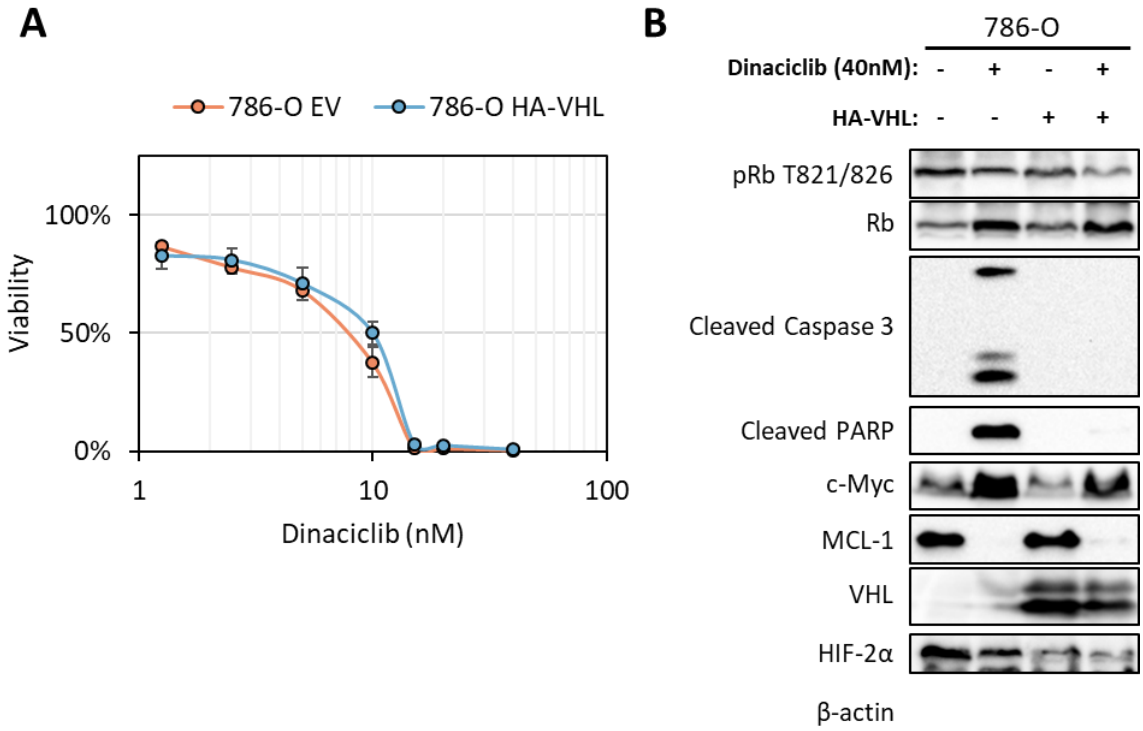

Supplemental Figure 3.2: pVHL re-expression does not rescue proliferation inhibition by Dinaciclib in 786-O cells.

A) Expression of pVHL does not alter Dinaciclib's ability to inhibit proliferation in 786-O cells. 786-O cells were infected with a lentivirus expressing HA-VHL or an empty vector (EV) to produce stable cell lines. Cells were plated in 96 well plates and treated for 5 days with Dinaciclib or vehicle, then analyzed using CTG assay. **B)** pVHL expression decreases expression of apoptosis markers cleaved caspase 3 and cleaved PARP after treatment with Dinaciclib. Cells were treated with Dinaciclib or vehicle (DMSO) for 24 hours and analyzed by western blot. Each experiment was repeated 2-3 times, and error bars represent the standard error of the mean. Significance was calculated using unpaired student's t test.

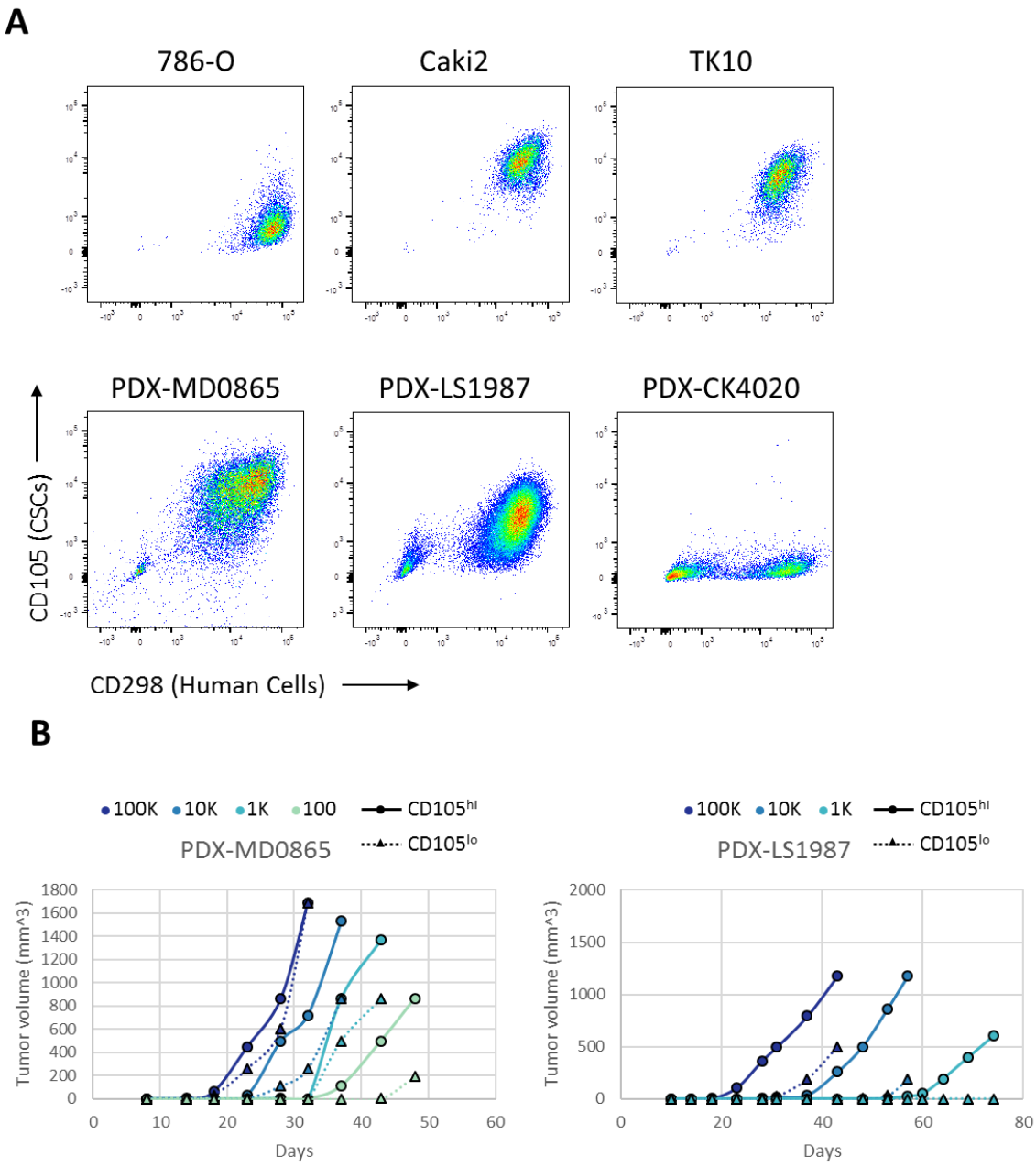

Supplemental Figure 3.3: The CD105^{hi} population in CC-RCC PDX tumors has enhanced tumor initiating potential.

(A) CD105 is expressed in 2/3 CC-RCC cell lines and 2/3 CC-RCC PDX tumors. Cells were trypsinized (cell lines) or digested to single cells from freshly harvested tumors (PDX tumors) and analyzed by flow cytometry for CD298 (human cell-specific marker) and CD105. **(B)** CD105^{hi} cells have enhanced tumor initiating potential. Cells sorted for CD105^{hi} and CD105^{lo} populations from freshly harvested PDX-MD0865 and PDX-LS1987 tumors were serially diluted and injected subcutaneously in each flank of NSG mice (one mouse per condition), and the growth was monitored by measuring the tumor volume with calipers.

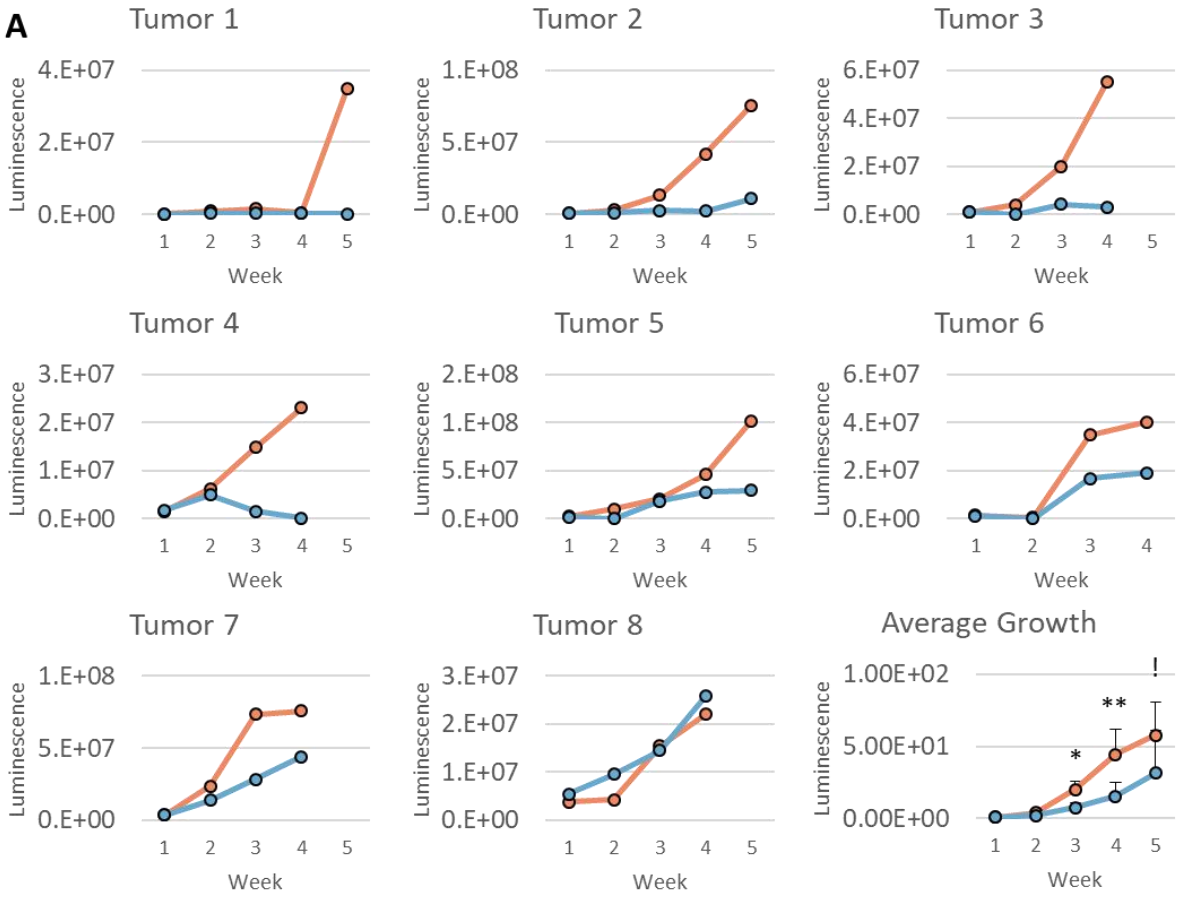
A
Tumor 1
Tumor 2
Tumor 3
Tumor 4
Tumor 5
Tumor 6
Tumor 7
Tumor 8
Average Growth
Luminescence
Week
4.E+07
2.E+07
0.E+00
1.E+08
5.E+07
6.E+07
3.E+07
1.E+07
2.E+08
1.00E+02
5.00E+01
0.00E+00
1 2 3 4 5
1 2 3 4
*
**
!

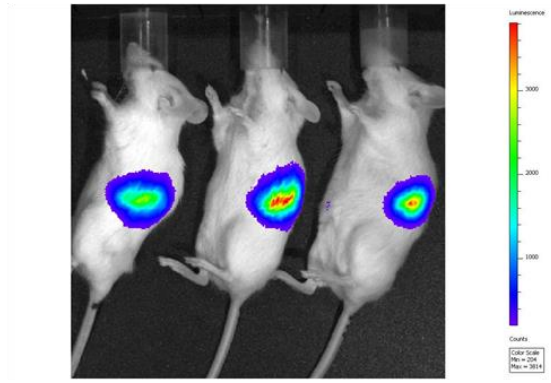
B

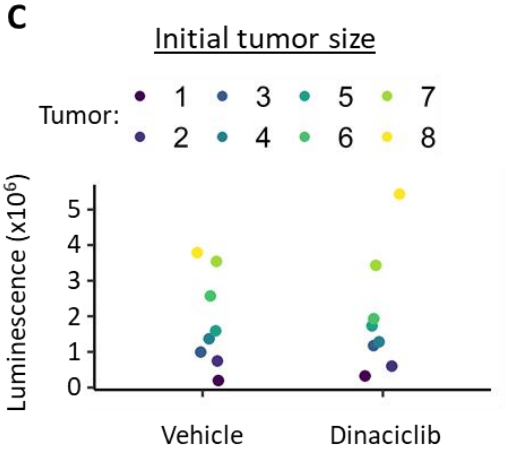
C
Initial tumor size
Tumor:
1 3 5 7
2 4 6 8
Luminescence (x10⁶)
0 1 2 3 4 5
Vehicle
Dinaciclib

Supplemental Figure 3.4: Bioluminescent imaging of matched tumor pairs.
A) Paired sets of tumors in vehicle/Dinaciclib treatment group were analyzed weekly with bioluminescent imaging. Mice were injected i.p. with D-luciferin and imaged after 15 minutes. At week 5, some tumors saturated the luminescent signal, and this data was not used. (**B)** Representative image of tumor-bearing mice showing luminescent signal from tumor in the kidney. (**C)** At the start of the treatment regimen, the initial tumor size was estimated by bioluminescent signal quantification, and mice were separated into vehicle/Dinaciclib treatment groups based on initial tumor size. Significance was calculated using paired student's t test at each time point. *p<0.05, **p<0.01, !unable to calculate due to signal saturation.

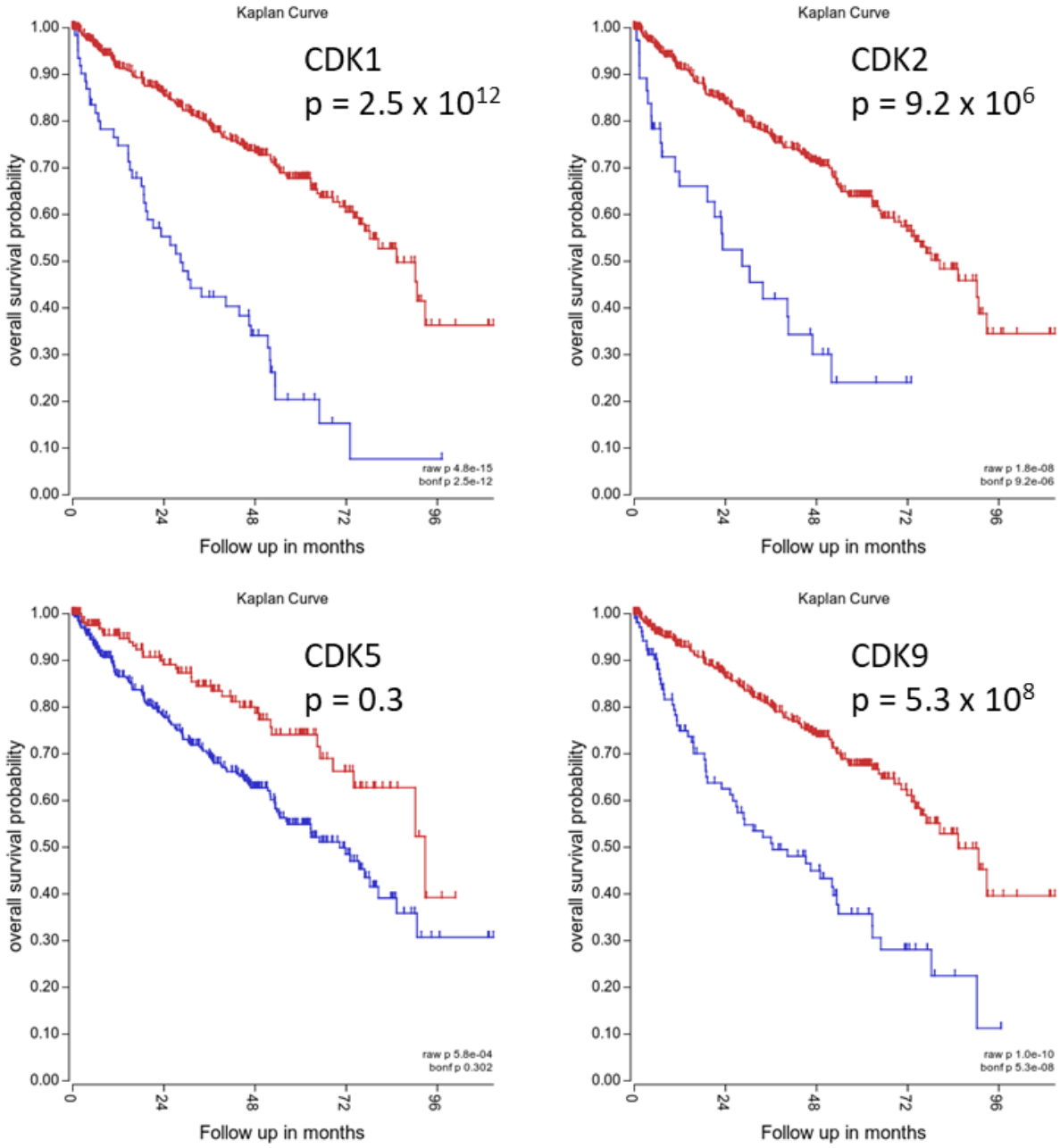

Supplemental Figure 3.5: TCGA Kaplan Meier survival curves for select CDKs in CC-RCC.

CDK1 (p = 2.5e-12) and CDK9 (p = 5.3e-8) correlate most strongly with a negative survival prognosis in CC-RCC. Kaplan Meier Survival analysis of CDK 1, 2, 5, and 9 in CC-RCC TCGA database (KIRC dataset) were generating using R2: Genomics Analysis and visualization Platform (http://r2.amc.nl).

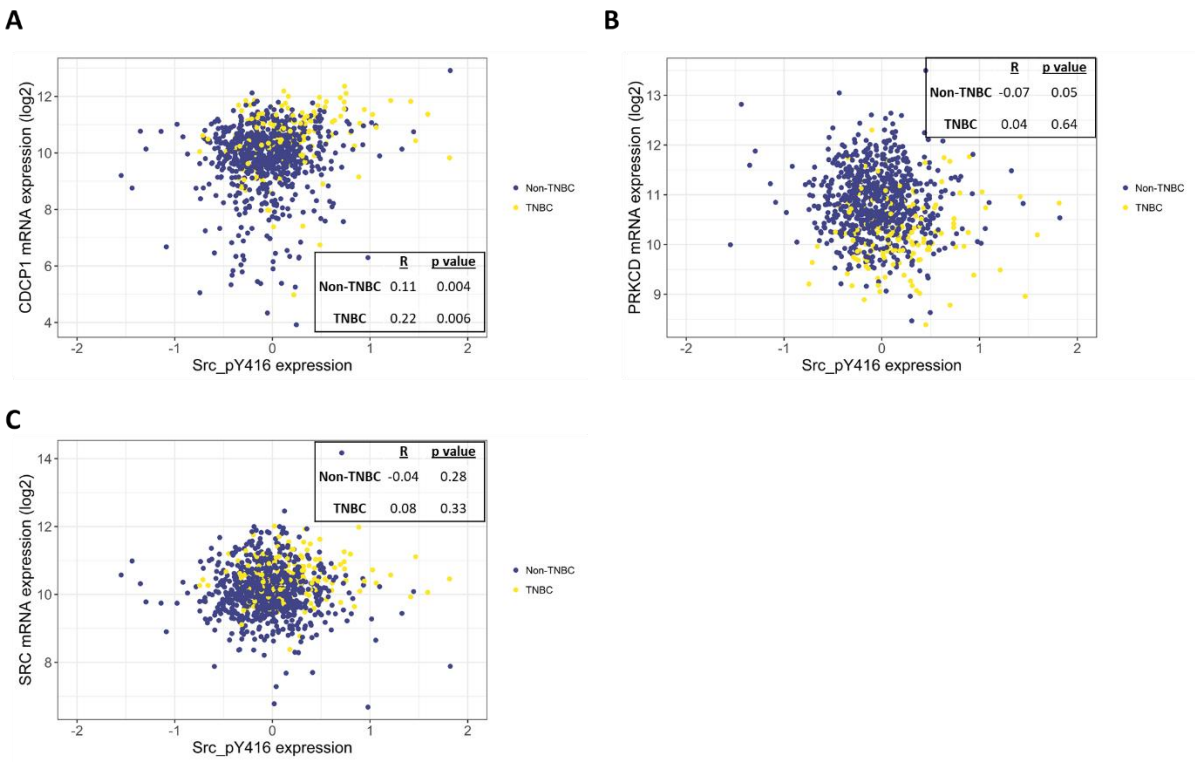

Supplemental Figure 5.1: Correlation between Src_pY416 and mRNA expression of select genes in TCGA breast cancer samples.

Scatter plot analysis of Src_pY416 expression levels from TCPA in relation to mRNA expression levels from TCGA for 3 genes in this study: **(A)** CDCP1; **(B)** PKCδ; **(C)** Src. Correlations were tested with Pearson's product moment correlation test.

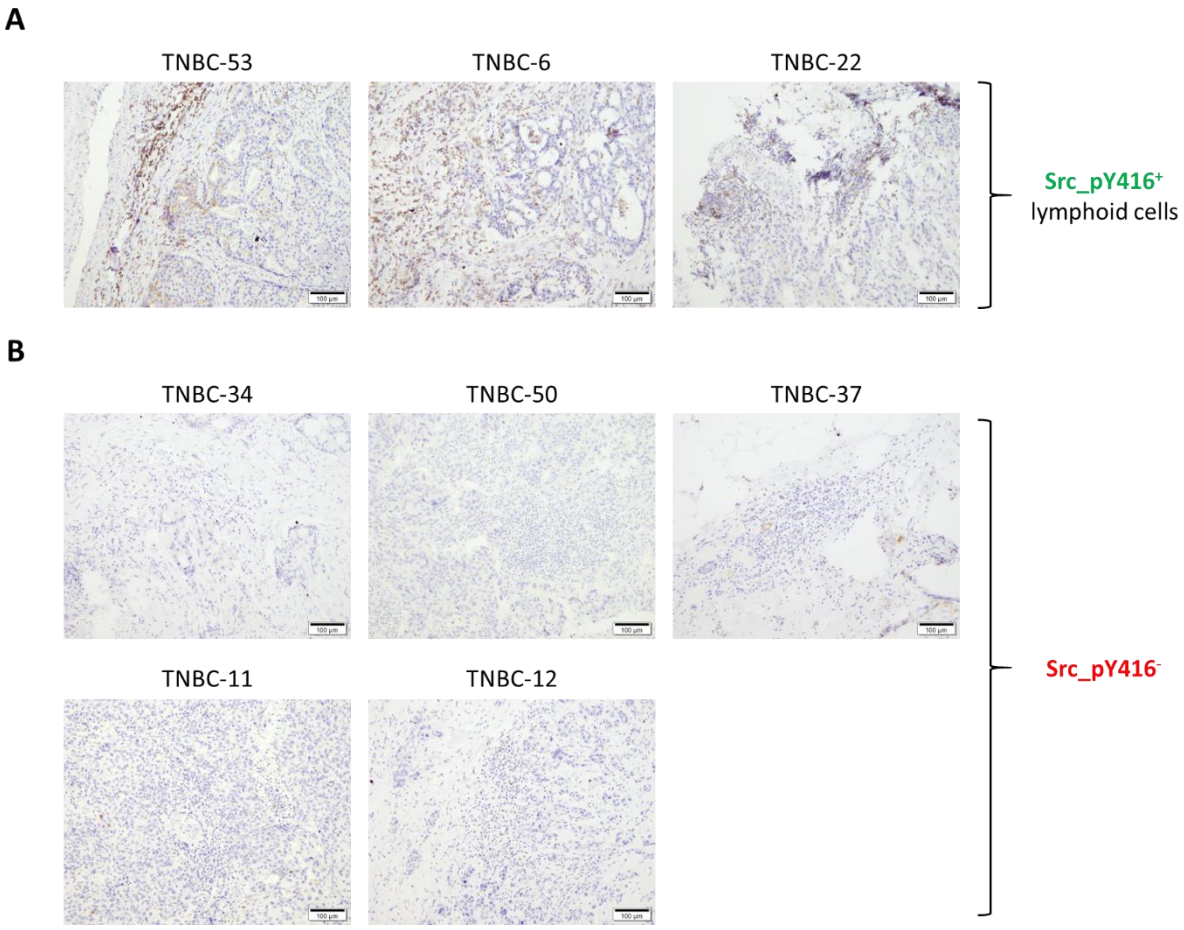

Supplemental Figure 5.2: Src_pY416 is detected by IHC in non-cancer lymphoid cells in some TNBC samples.

(A) 3 TNBC tumors with Src_pY416^{-} tumors cells and some Src_pY416^{+} lymphoid cells (corresponding to Figure 3B lanes 2, 4, 6). **(B)** Representative TNBC tumors with no Src_pY416 staining (corresponding to Figure 3B lanes 3, 5, 7-9).

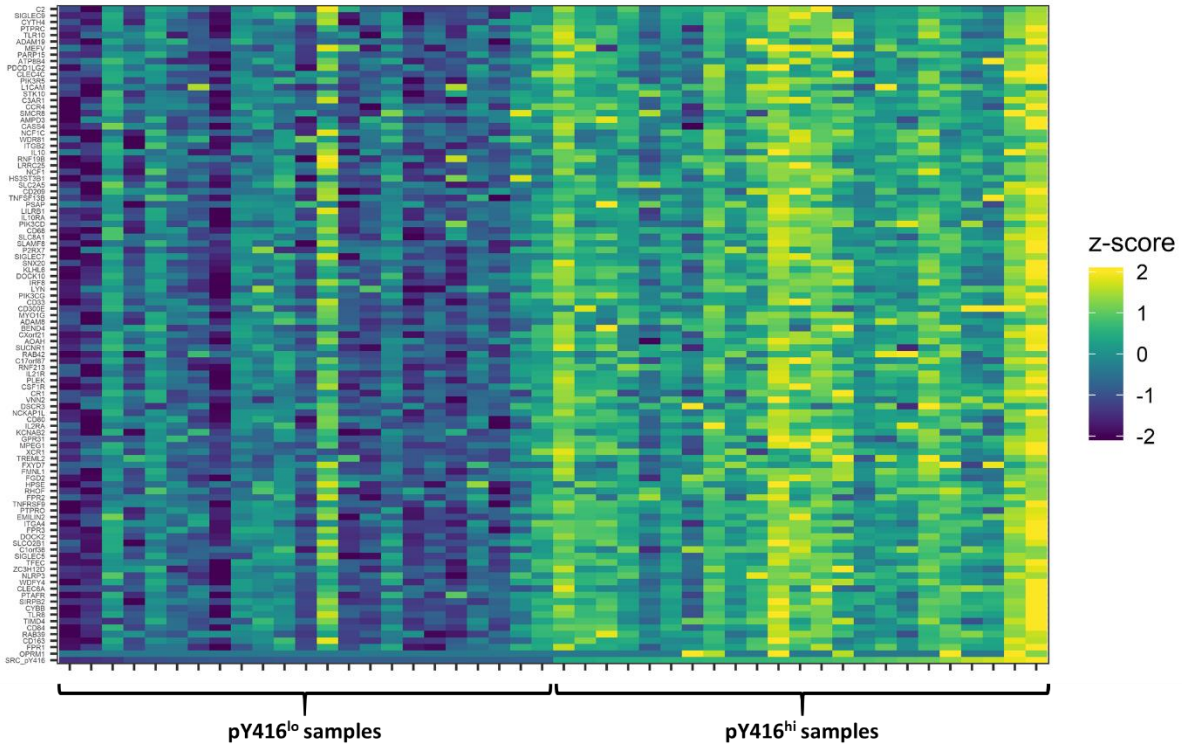

Supplemental Figure 5.3: Full heatmap of top genes positively correlated with Src_pY416 expression.

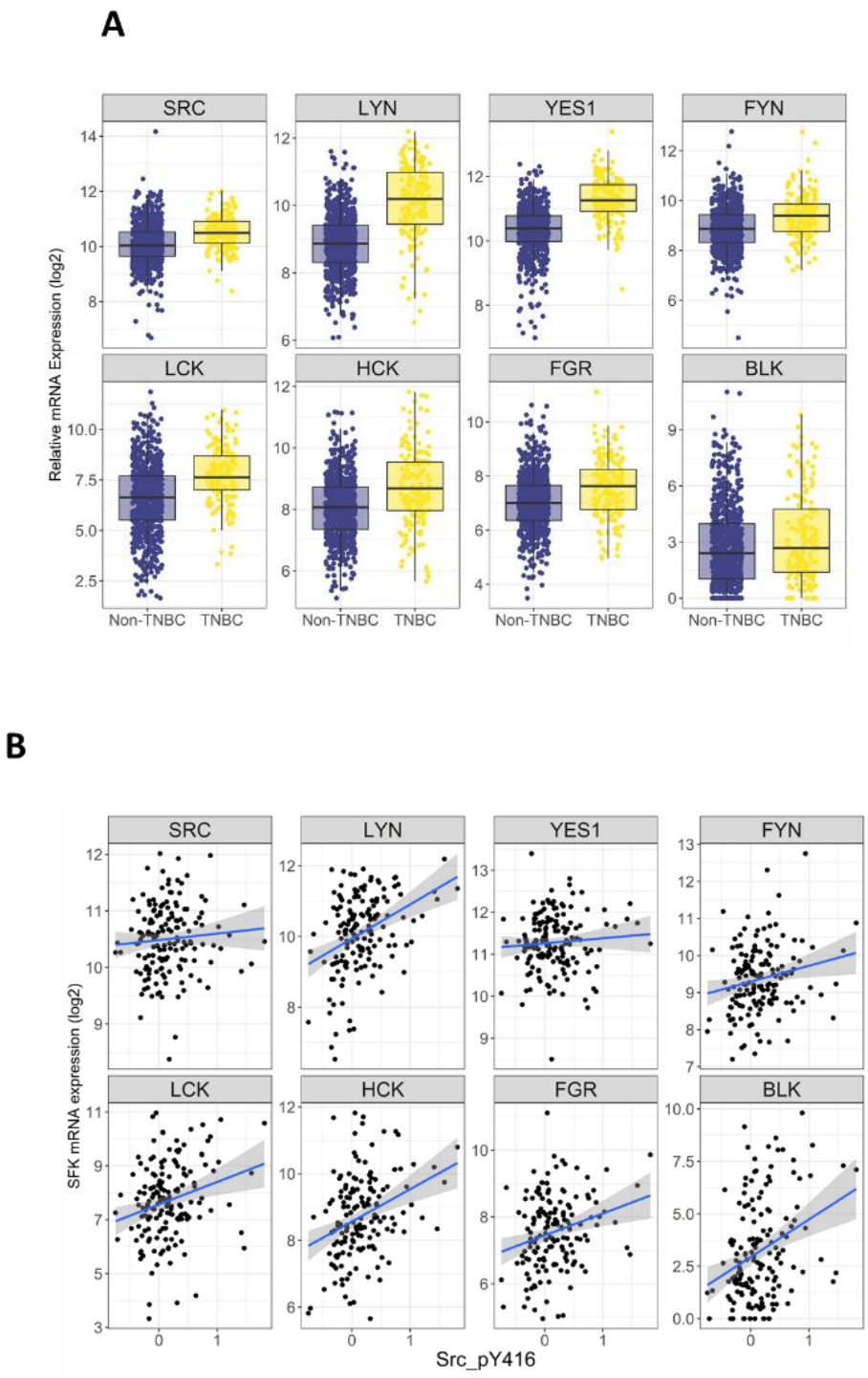

Supplemental Figure 5.4: Expression patterns of other SFKs in TNBC.
(A) The mRNA expression levels of 8 SFKs in the TCGA BRCA data set, compared between TNBC and Non-TNBC. **(B)** Scatter plots showing correlation between Src family member mRNA expression (y axis) and Src_Y416 phosphorylation (x axis) in TCGA BRCA data set (TNBC only).

Supplemental Table 5.1. Clinical and pathologic features of TNBC patient samples in relation to FOXA1 expression.

Characteristic	Total		FOXA1 negative		FOXA1 positive		p value*
	Value	%	Value	%	Value	%	
# Patients	56	-	32	57%	24	43%	
Age							
<50	11	20%	10	31%	1	4%	
50-70	25	45%	16	50%	9	38%	**0.0008**
>70	20	36%	6	19%	14	58%	
T stage							
1	15	27%	7	22%	8	33%	
2	36	64%	20	63%	16	67%	**0.04**
3/4	5	9%	5	16%	0	0%	
N Stage							
n/a	7		2		5		
0	33	67%	23	77%	10	53%	
1	10	20%	4	13%	6	32%	**n.s.**
2/3	6	12%	3	10%	3	16%	
Nottingham histologic grade							
1	0	0%	0	0%	0	0	
2	6	11%	1	3%	5	21%	**0.03**
3	50	89%	31	97%	19	79%	
Ki67							
≤30	8	14%	1	3%	7	29%	**0.006**
>30	48	86%	31	97%	17	71%	

Mesenchymal and myoepithelial markers

Vimentin							
Negative	18	32%	5	16%	13	54%	**0.002**
Positive	38	68%	27	84%	11	46%	
Sox10							
Negative	14	41%	2	11%	12	75%	**0.0002**
Positive	20	59%	16	89%	4	25%	
CK5/6							
Negative	10	48%	6	46%	4	50%	**n.s.**
Positive	11	52%	7	54%	4	50%	
Src_pY416							
Negative	33	59%	17	53%	16	67%	
Positive, 5-20%	10	18%	5	16%	5	21%	**0.1**
Positive, >20%	13	23%	10	31%	3	13%	

**p values calculated using Pearson's Chi Square test*

Supplemental Table 5.2. Clinical and pathologic features of TNBC patient samples in relation to Src_pY416 expression.

Characteristic	Total		Src_pY416 negative		Src_pY416 positive		p value*
	Value	%	Value	%	Value	%	
# Patients	56	-	43	77%	13	23%	
Age							
<50	11	20%	9	21%	2	15%	
50-70	25	45%	20	47%	5	38%	**n.s**
>70	20	36%	14	33%	6	46%	
T stage							
1	15	27%	12	28%	3	23%	
2	36	64%	27	63%	9	69%	**n.s**
3/4	5	9%	4	9%	1	8%	
N Stage							
n/a	7		5		2		
0	33	67%	27	63%	6	46%	
1	10	20%	7	16%	3	23%	**n.s**
2/3	6	12%	4	9%	2	15%	
Nottingham histologic grade							
1	0	0%	0	0%	0	0	
2	6	11%	5	12%	1	8%	**n.s**
3	50	89%	38	88%	12	92%	
Ki67							
≤30	8	14%	6	14%	2	15%	**n.s**
>30	48	86%	37	86%	11	85%	

Vimentin							
Negative	18	14%	17	40%	1	8%	**0.03**
Positive	38	86%	26	60%	12	92%	
FOXA1							
Negative	18	14%	22	51%	10	77%	**n.s.**
Positive	38	86%	21	49%	3	23%	
Src substrates							
CDCP1 pY743							
Negative	40	71%	40	93%	0	0%	**<0.0001**
Positive	16	29%	3	7%	13	100%	
PKCδ pY311							
Negative	44	79%	40	93%	4	31%	**<0.0001**
Positive	12	21%	3	7%	9	69%	

**p values calculated using Pearson's Chi Square test*

Supplemental Table 5.3. Antibodies and dilutions used for IHC and Western Blot.

Antigen	Antibody Info	Western Blot Dilution	IHC Dilution	Antigen Retrieval*
FOXA1	Abcam #ab173287	n/a	1:4,000	1
Vimentin	Dako #M0725	n/a	1:2,000	2
Sox10	Bio SB #BSB2583	n/a	1:100	1
CK5/6	Life Technologies #180267	n/a	1:50	2
CDCP1	Cell Signaling Technology #4115	1:1,000	1:100	1
CDCP1_pY743	Cell Signaling Technology #14965	1:1,000	1:800	1
CDCP1_pY734	Cell Signaling Technology #9050	1:1,000	n/a	n/a
Src	Cell Signaling Technology #2108	1:1,000	n/a	n/a
Src_pY416	Cell Signaling Technology #2101	1:1,000	1:200	1
Src_pY527	Cell Signaling Technology #2105	1:1,000	n/a	n/a
PKCδ	Cell Signaling Technology #2058	1:1,000	n/a	n/a
PKCδ_pY311	Abcam #ab76181	1:2,500	1:3,000	1
N-Cadherin	Cell Signaling Technology #13116	n/a	1:200	1
Slug	Cell Signaling Technology #9585	n/a	1:100	1
AMPKα	Cell Signaling Technology #2532	1:1,000	n/a	n/a
AMPKα_pT172	Cell Signaling Technology #2535	1:1,000	n/a	n/a
β-Actin	Millipore Sigma #A5441	1:5,000	n/a	n/a

**Antigen Retrieval 1: Heat 20 minutes offline in Leica ER2 buffer in steamer; repeat online with Leica ER2 buffer for 20 minutes*

**Antigen Retrieval 2: Dewax and antigen retrieval online in Leica ER2 buffer for 20 minutes*

Supplemental Table 5.4. Complete list of TNBC samples used in the study.

Sample	Patient Age	T Stage	N Stage	Grade	CDCP1 _pY743 (%)	Src _pY416 (%)	PKCδ _pY311 (%)	FOXA1 (%)	Vimentin (%)
TNBC-1	77	1	0	3	90	90	0	0	100
TNBC-2	62	2	n/a	3	0	0	0	60	30
TNBC-3	55	2	n/a	3	60	60	60	0	70
TNBC-4	83	2	n/a	3	0	0	0	30	50
TNBC-5	66	2	0	3	0	0	0	0	100
TNBC-6	90	1	n/a	2	0	0	0	100	0
TNBC-7	61	2	0	3	0	0	0	0	100
TNBC-8	85	2	0	3	0	0	0	30	100
TNBC-9	75	2	0	3	50	70	0	0	100
TNBC-10	37	1	0	3	0	20	0	0	50
TNBC-11	34	2	1	3	0	0	0	100	100
TNBC-12	45	1	0	3	0	0	0	0	100
TNBC-13	69	2	0	3	0	0	0	0	100
TNBC-14	45	1	0	2	0	0	0	0	100
TNBC-15	58	2	0	3	90	90	90	0	50
TNBC-16	77	2	1	3	100	100	80	0	90
TNBC-17	30	2	0	3	60	20	60	0	100
TNBC-18	92	2	n/a	3	80	50	80	0	100
TNBC-19	80	2	n/a	3	0	0	0	100	0
TNBC-20	85	1	0	3	0	0	0	0	100
TNBC-21	63	1	0	3	5	0	0	50	50
TNBC-22	93	2	0	2	0	0	0	100	0
TNBC-23	53	4b	1	3	0	0	0	0	100
TNBC-24	31	2	0	3	20	30	0	0	100
TNBC-25	66	2	0	3	20	20	20	0	100
TNBC-26	57	1	1	3	0	0	0	0	70

TNBC-27	60	1	0	3	100	100	70	100	100
TNBC-28	62	3	0	3	0	0	0	0	100
TNBC-29	50	2	0	3	0	0	0	0	50
TNBC-30	44	2	0	3	0	0	0	0	0
TNBC-31	58	2	0	3	50	20	50	0	100
TNBC-32	45	2	1	3	0	0	0	0	0
TNBC-33	58	2	0	3	0	0	0	0	0
TNBC-34	91	2	1	2	0	0	0	100	0
TNBC-35	93	2	n/a	3	10	0	30	50	0
TNBC-36	50	2	2	3	20	20	0	100	0
TNBC-37	50	2	1	2	0	0	0	100	0
TNBC-38	43	2	0	3	10	20	20	0	0
TNBC-39	66	1	0	3	0	0	0	0	0
TNBC-40	60	1	0	3	0	0	0	100	80
TNBC-41	49	2	0	3	0	0	0	0	100
TNBC-42	37	2	0	3	80	50	0	0	100
TNBC-43	55	4	3	3	80	80	50	0	50
TNBC-44	60	1	0	3	40	20	50	100	0
TNBC-45	82	2	0	3	10	10	20	100	0
TNBC-46	58	3	0	3	0	0	0	0	100
TNBC-47	73	1	1	2	80	80	70	100	0
TNBC-48	61	1	0	3	0	0	0	100	95
TNBC-49	84	2	0	3	5	5	0	90	95
TNBC-50	78	2	0	3	0	0	0	100	0
TNBC-51	53	1	2	3	20	20	20	100	0
TNBC-52	53	2	2	3	80	90	90	0	100
TNBC-53	76	2	2	3	0	0	0	100	0
TNBC-54	75	3	2	3	0	0	0	0	50
TNBC-55	82	2	1	3	100	100	100	100	100
TNBC-56	82	2	1	3	0	0	0	20	100

% indicates percentage of positively stained cells by IHC. 0 indicates 0% or <1% positive cells.

RhoC: less binding with VHL expression

Protein ID	Description
PAK4	Serine/threonine-protein kinase PAK 4
mp2k1	Dual specificity mitogen-activated protein kinase kinase 1 (MEK1)
TES	Testin

RhoC: more binding with VHL expression

Protein ID	Description
G3BP1	Ras GTPase-activating protein-binding protein 1
eif2A	Eukaryotic translation initiation factor 2A
MAP4K4	Mitogen-activated protein kinase kinase kinase kinase 4
SYIM	Isoleucine--tRNA ligase, mitochondrial
rrp44	Exosome complex exonuclease RRP44
rfa2	Replication protein A 32 kDa subunit
mp2k2	Dual specificity mitogen-activated protein kinase kinase 2 (MEK2)

Supplemental Figure 6.1: List of proteins differentially interacting with RhoC dependent on VHL expression.

Proteins with peptides that were decreased (top table) or increased (bottom table) in FLAG-RhoC pulldown fraction upon VHL overexpression. Table includes only peptides that were changed in two independent experiments.

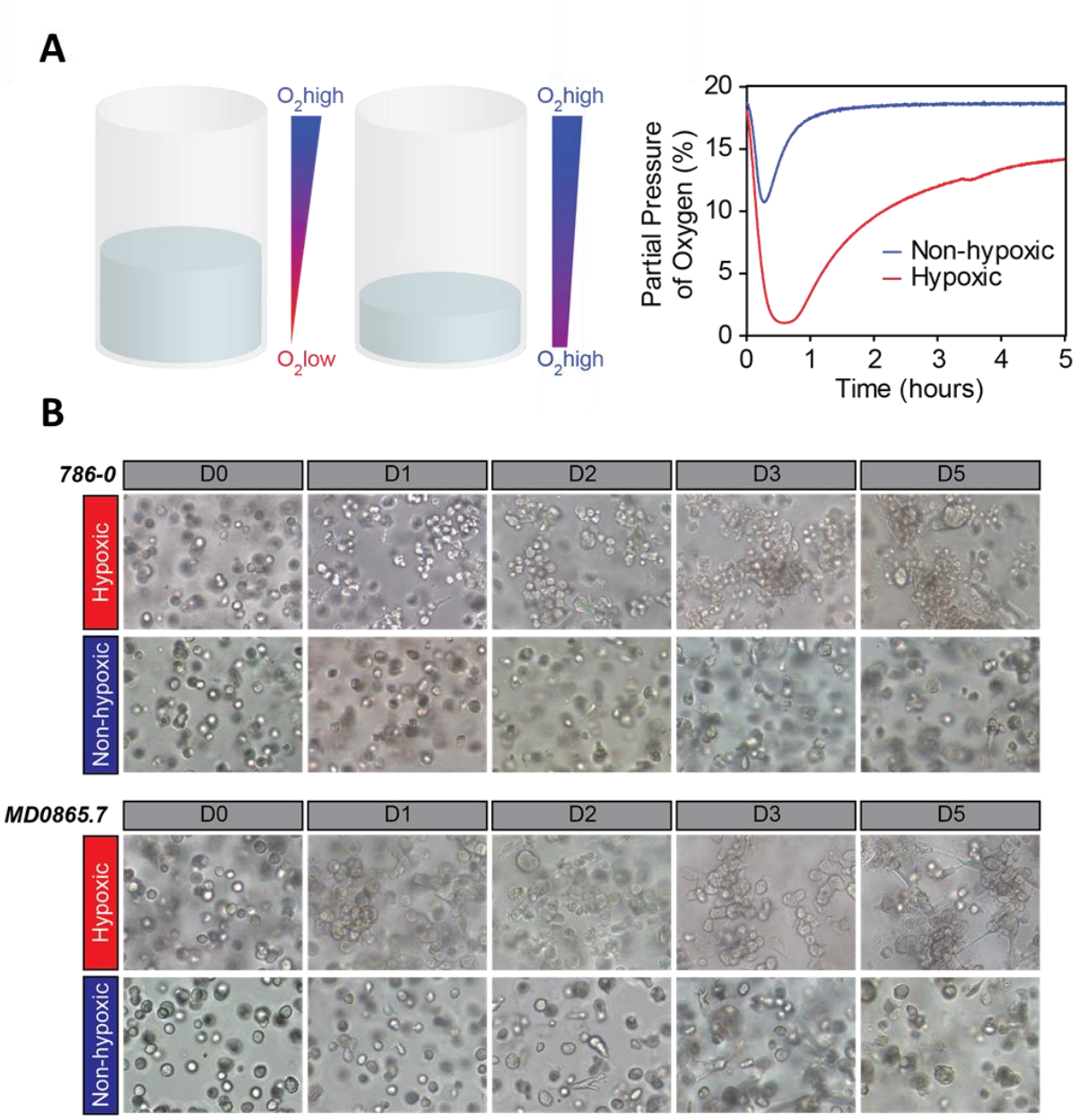
A
O2high
O2low
O2high
O2high
Partial Pressure of Oxygen (%)
Time (hours)
Non-hypoxic
Hypoxic
B
786-0
D0
D1
D2
D3
D5
Hypoxic
Non-hypoxic
MD0865.7
C
786-O
MD0865.7
Partial Pressure of Oxygen (%)
Time (days)
Hypoxic
Non-hypoxic

Supplemental Figure 6.2: 3D *in vitro* culture of 786-O cells and PDX tumor cells in hypoxic hydrogels.

(A) Visual depiction of the formation of hypoxic hydrogels and modulation of oxygen tension through thickness. **(B)** 786-O cells and PDX-MD0865 cells in hypoxic hydrogels proliferated more rapidly than in non-hypoxic hydrogels and formed 3D tube-like structures. 786-O cells and PDX-MD0865 PDX tumors cells were encapsulated into "hypoxic" vs. "non-hypoxic" hydrogels and images were acquired every day for 5 days. **(C)** Hypoxic hydrogels attain a lower oxygen tension than non-hypoxic hydrogels.